Exploring novel aspects of choline phospholipid metabolism in cancer using metabolomics

Thesis submitted by

Chung Ho Lau

To

Imperial College London

For the degree of Doctor of Philosophy (PhD)

Department of Chemistry

2014

Copyright Declaration

Declaration of originality

I declare this thesis is my own work, except where duly acknowledged

Abstract

Abnormal metabolic phenotypes can be a powerful resource for drug and biomarker discoveries. In this thesis, a metabolomic approach was used to examine several aspects of tumour metabolism with potential clinical applications. In the first part, the metabolic consequences of *PIK3CA* mutation in MCF10A breast cells were assessed. *PIK3CA* mutation is oncogenic, and is important for disease progression in many breast tumours. Increased glutaminolysis, fatty acid synthesis, pyruvate entry into the TCA cycle, and decreased glycerophosphocholine (GPC) were identified to be the most prominent phenotypes following knock-in *PIK3CA* mutation in MCF10A cells. GPC has long been reported as a potential marker for disease progression; however, its functional role in cancer remains unclear. Glycerophosphodiester phosphodiesterase is responsible for the hydrolysis of GPC into choline and glycerol-3 phosphate (G3P), and EDI3 is a member of the glycerophosphodiester phosphodiesterase family associated with metastasis in endometrial cancer patients. Through metabolomic analysis of tumour cell models, EDI3 silencing was found to increase GPC levels and the GPC: phosphocholine ratio. Also, it was demonstrated that EDI3 had an impact on a broader spectrum of metabolic phenotypes, and effects on glycolysis and fatty acid synthesis were also observed. Finally, using ^{1}H HR-MAS-NMR, changes in levels of choline phospholipid metabolites following Colony stimulating factor 1 receptor (CSF1R) inhibitor treatment were investigated in a mouse pancreatic tumour model. CSF1R is important for growth signalling of macrophages in tumours. Phosphocholine levels were found to be associated with disease progression and CSF1R inhibitor treatment. Collectively, these findings highlight a number of novel factors in choline phospholipid metabolism that may be important to tumourigenesis and the development of cancer biomarkers, including the role of glycerophosphodiester phosphodiesterase and macrophage-tumour interaction.

Acknowledgement

I would like to thank my supervisors Dr Hector Keun, Prof Eric W-F Lam, Dr Rudiger Woscholski, and Dr Laura Barter for their advice, and the time and effort they have put in to facilitate my study. Also, I would like to thank the post-doctoral researchers and students in Hector's group for their help, particularly Dr James Ellis and Dr Gregory Tredwell, who have respectively coached me to perform cell culture and GC-MS analysis. In addition, I would also like to acknowledge the help and support I have received from the Computational and System Biology section at the Department of Surgery and Cancer, and I am especially grateful to Dr Olaf Beckonert and Dr Toby Athersuch for helping me to learn about NMR spectroscopy.

Many of the studies presented here were done in collaboration, and I would like to acknowledge Dr. Juliana Candido, Prof. Thorsten Hagemann (Barts Cancer Institute, London) and Dr. Rosemarie Marchan and Prof. Jan Hengstler (Leibniz Research Centre for Working Environment and Human Factors, Dortmund) for making the KPC mouse and the EDI3 studies possible.

Also, I am grateful to my PhD examiners, Dr Geoffrey Payne (Institute of Cancer Research, London) and Prof Eric Aboagye (Imperial College London), for providing valuable feedback, and to Gabriel Valbuena (Imperial College London) for proofreading the thesis.

Furthermore, I would like to thank the Department of Chemistry and the Institute of Chemical Biology for funding the project and for the many transferable skill courses/workshops that I have attended.

Finally, I would like to thank my family and my girlfriend for their love and support, and for their help in completing my PhD study.

Table of contents

Table of figures

Chapter 1 Introduction

1.1 Cancer

Cancer is frequently described as a disease of abnormal and uncontrolled cellular proliferation, which leads to the formation of a tumour 'mass'. If it is left untreated, the tumour may invade and destroy neighbouring healthy tissues. Primary tumours can also metastasise by spreading into other parts of the body through the lymphatic system, causing the loss of function of critical organs, widespread health complications, and often death. Cancer occurs in a spectrum of different organs and tissue types, and over two hundred disease subtypes have been identified. As cancer is the leading cause of mortality in economically developed countries (Jemal *et al.* 2011), affecting about half of all men and one-third of all women in the US and UK, the impact of cancer is extensive. There are around 13 million new cases globally every year and cancer accounts for approximately 15 per cent of all human deaths. According to the 2014 WHO World Cancer Report, the financial burden of cancer has been estimated at over 1.16 trillion USD per year, which is equivalent to 1.5% of the global GDP. This makes cancer disease management one of the biggest challenges in society today.

1.1.1 Cancer treatment and management

Cancer can be treated with surgery, radiotherapy and chemical drugs. According to a 2003 report from the Royal College of Radiologists, surgery, radiotherapy and chemotherapy contribute towards approximately 49%, 40% and 11% of the successful treatment outcomes respectively (Tobias 2010). The choice of treatment is very specific to both the tissue location and the staging of the tumours. Surgical removal of the tumour mass is in many cases a very effective method, but this is not always feasible. Radiotherapy is a treatment for cancer in which high-energy beams such as gamma rays are focused on the cancerous tissues. The resulting ionising radiation leads to controlled and targeted destruction of the tumour tissues. Radiotherapy has also proven to be very effective for controlling the symptoms of incurable cancers.

The third broad treatment modality in cancer involves the use of chemical drugs and biologics. Many classes of drugs are currently in use for cancer treatment, and these include conventional chemotherapy drugs such as platinum analogues and taxoids, which target cell division by preventing the synthesis and binding of DNA or the formation of mitotic spindle. However, as chemotherapy targets all rapidly dividing cells that include non-cancerous tissues, patients may suffer from significant side effects (Kelland 2007). Another popular class of chemical drugs is hormone therapy, which targets hormone responsive tumours. For example, Tamoxifen is frequently used in treating estrogen-receptor positive breast cancer. With many initially responsive patients developing resistance to drugs, formulating and managing treatment plans have also proven to be challenging (Hammond *et al.* 2010). More recently, therapeutic agents that target specific biomolecules by utilising natural substances of the living organisms have become gradually more popular and these are generally referred to as biologics. Monoclonal antibodies, cytokines, and vaccines are all examples of biological therapies (Sathish *et al.* 2013), and Trastuzumab (Herceptin) is a monoclonal antibody that has been demonstrated to be effective against HER2-positive breast cancer (Nelson and Gallagher 2014).

There are many challenges to finding new effective treatments for cancer, and many pharmaceutical companies now focus their drug development efforts on targeting specific genetic mutations and deregulated proteins in patient populations. This has led to the development of drugs such as Imatinib and Gefitinib, which target tyrosine kinases; these first became available in the late 1990s. Many new drugs currently in development specifically target signalling deregulation in the GPCR, (Lappano and Maggiolini 2011), EGFR (Lurje and Lenz 2009), PI3K (Workman *et al.* 2010) and the WNT pathways (Anastas and Moon 2013).

1.1.2 Diagnostic and therapeutic biomarkers

Normally in clinics, the extent and the severity of the tumour are decided largely on the anatomical spread of the disease (Ludwig and Weinstein 2005). In many countries including the US and the UK, the staging of tumour is standardised using the TNM system, based on the size and depth of the tumour (T), lymph node spread (N) and the presence of metastases. Together with tumour grade and histological

subtype, the TNM system often forms the basis of formulating a treatment plan and estimating the patient's prognosis. However, tumour biology is a lot more complex than can be captured through the TNM system alone, for example the fate and spread of the disease may also be influenced by lifestyle factors and genetic predisposition of the patient. Biomarkers may provide extra information when predicting survival and therapeutic outcomes. This is of particular importance because as molecular targeted therapeutics become more common, there will exist a greater need to effectively predict and assess the specific therapeutic responses of patients in the clinical setting. Finding effective biomarker is a major challenge (Sawyers 2008); the ideal biomarker must be sensitive, specific, cost-effective, fast and robust, while being able to demonstrate value beyond information already available. For example, EGFR in colon cancer and HER2/NEU (ERBB2) in breast cancer are both biomarkers approved for therapy selection in the US. Advances in genomics, proteomics and other assay method development may also in future aid biomarker discovery (Ludwig and Weinstein 2005).

1.2 Metabolism and health

Metabolism is the active chemical transformation of molecules within cells, and is a very broad discipline in biochemistry. Metabolism is essential for life to exist as we know it. It helps maintain normal physiology by regulating our nutritional requirements, and when we need to adapt to external changes or internal demands such as development, aging and reproduction, metabolism specifies both the chemical library and the defined molecular pathways for biotransformation. Many everyday biological events, from doing exercise or catching a fever to dealing with the stress and demand of pregnancy, are accompanied by metabolic changes. Metabolic substrates and products, more generally known as metabolites, can travel throughout the body at the molecular level, with our diet being an important contributor to the metabolite pool. Many tissue types have distinct metabolic functions and characteristics, and such division of labour is essential in enabling physiological functioning to be coordinated across the body. Furthermore, mechanisms of metabolic feedback are dynamic and complex as metabolism can interact with the signalling circuits of hormones, proteins as well as metabolites. Many diseases are directly related to deficiencies in metabolic regulation; the best-

known example is diabetes, where blood glucose regulation is dysfunctional. Given this central role of metabolism in living systems, the use of metabolic phenotyping has the potential to help inform disease management and treatment.

1.2.1 Metabolic pathways

At the molecular level, metabolism can be characterised through a series of reactions that are catalysed by specific enzymes, each with very specific substrates and products. The products of one reaction often become the substrates of another, setting off a chain of reactions that are interdependent on one another. The sequences of enzymatic reactions are summarised using metabolic pathways, which can be regulated directly by substrate availability, allosteric regulation, enzyme phosphorylation, membrane permeability or transport. Also, substrates like ATP and other co-factors such as NAD^+, FAD, and $NADP^+$ are involved in numerous reactions; the relative metabolic pathway activities are likely to be dependent on their availabilities. The functions of different pathways are diverse: some are involved in ATP generation, while some are involved in the synthesis of nucleotides and membrane lipids for supporting growth. Glycolysis, the citric acid cycle and glutaminolysis are particularly important for energy metabolism, and fatty acid synthesis and phosphatidylcholine metabolism are important for lipid biosynthesis in rapidly proliferating cells. As these pathways are frequently deregulated in cancer, a brief description of each is given below (Mathews *et al.* 2000, Appleton 2013).

Glycolysis

Glucose is broken down into pyruvate through glycolysis in the cytoplasm. It can occur under aerobic or anaerobic conditions (Figure 1.1). The total potential ATP yield from glycolysis alone (2 ATP) is relatively low compared to the subsequent entry of pyruvate into the tricarboxylic acid cycle (TCA) and oxidative phosphorylation (total of 36 ATP). Normally, glucose transporters facilitate the import of glucose through the membrane. The end-product pyruvate could either be converted into lactate via lactate dehydrogenase activity; or it can enter the TCA cycle via pyruvate dehydrogenase or pyruvate carboxylase activities (Mathews *et al.* 2000, Appleton 2013).

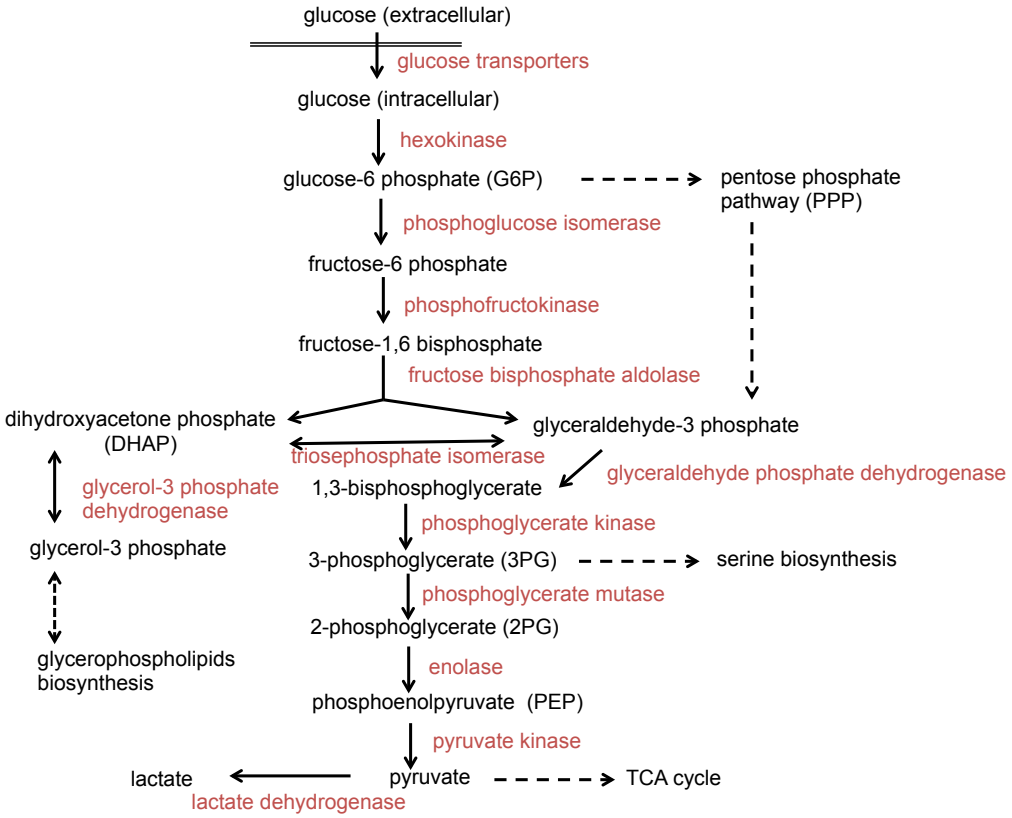

Figure 1.1 Schematic diagram of the glycolytic pathway

The diagram above is redrawn from concepts and figures shown in (Mathews *et al.* 2000, Appleton 2013). Metabolites and enzymes are respectively shown in black and red.

Tricarboxylic acid cycle (TCA)

The tricarboxylic acid cycle (TCA) is an important pathway for generating ATP and other precursor molecules. The TCA cycle requires oxygen and is a cyclical sequence of oxidation reactions that occur in the mitochondrial matrix. Pyruvate is the major precursor to TCA cycle intermediates and can contribute towards the TCA cycle via two separate entry points. The main pathway into the cycle is through pyruvate dehydrogenase activity, where acetyl-CoA is produced and is then combined with oxaloacetate, forming citrate. Alternatively, pyruvate can also enter the TCA cycle through conversion into oxaloacetate via pyruvate carboxylase activity (Figure 1.2). Acetyl-CoA can be derived from the catabolism of carbohydrate, fatty acids or amino acids.

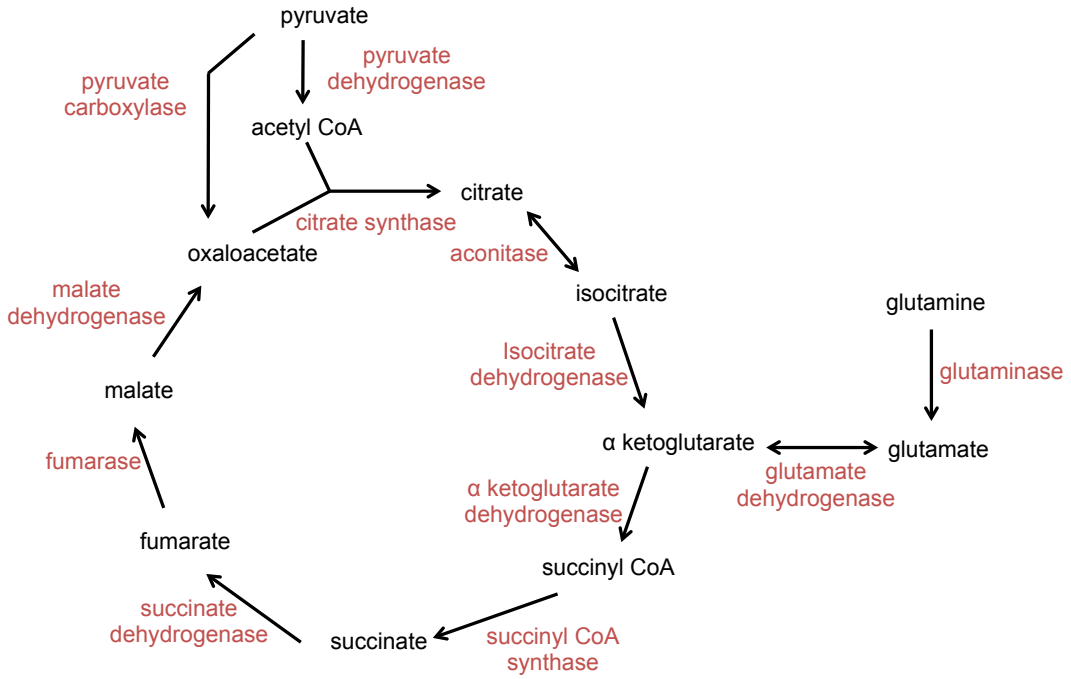

Figure 1.2 Schematic diagram of the TCA cycle

The above diagram is redrawn from concepts and figures shown in (Mathews *et al.* 2000, Appleton 2013). Metabolites and enzymes are respectively shown in black and red.

Glutaminolysis

Glutamine is the most abundant amino acid in the blood plasma. It can be converted to α-ketoglutarate and incorporated into the TCA cycle. Glutaminolysis is a major anaplerotic reaction in rapidly growing cells, supplying cells with high-energy substrates and other biosynthetic precursors. Glutaminolysis consists of two deamination steps: glutamine is first converted into glutamate through glutaminase (GLS), and then into α-ketoglutarate via glutamate dehydrogenase (Gao *et al.* 1999).

Fatty acid synthesis

Fatty acids are the basic building blocks of cellular lipids, which serve a variety of structural and signalling functions. The capacity to turnover lipids is especially important to meet the anabolic requirements of rapidly proliferating cells, such as tumour cells. *De novo* synthesis of fatty acid is a major pathway supplying additional precursor substrates for growth and acetyl-CoA, NADPH and H^+ are essential for fatty acid synthesis. The lipogenic acetyl-CoA units are often derived from carbohydrates such as glucose (Mathews *et al.* 2000, Appleton 2013).

De novo fatty acid synthesis requires a complex sequence of events and processes to occur in the cytoplasm:

1) First, mitochondrial citrate is transported into the cytoplasm, where ATP citrate lyase catalyses the conversion of citrate into acetyl-CoA and oxaloacetate;
2) Acetyl-CoA carboxylase converts acetyl-CoA into malonyl-CoA;
3) Acetyl-CoA and malonyl-CoA separately bind to fatty acid synthase, and their CoA groups are then removed through transacylase activities;
4) A saturated four-carbon chain is formed via condensation, reduction and dehydration;
5) The chain is lengthened as additional malonyl-CoA units cycle through the same transacylation, condensation, reduction and dehydration processes; and when the chain is 16-carbon units long, the chain is cleaved off forming palmitate (C16:0).

Further elongation of fatty acid chain beyond 16 carbons is possible via elongase activity; while the synthesis of unsaturated fatty acid chain would require fatty acyl-CoA desaturase. Dysregulation of fatty acid synthesis has long been associated with cancer. For example, upregulations of ATP citrate lyase (ACLY) (Berwick *et al.* 2002), fatty acid synthase (FASN) (Pizer *et al.* 1996), long chain fatty acid elongase (ELOVL7) (Tamura *et al.* 2009), and stearoyl-CoA desaturase (SCD1) (Tamura *et al.* 2009) have all previously been reported to be important for tumour development.

Choline and phosphatidylcholine metabolism

Phosphatidylcholine (PtdCho) is an important class of phospholipids, which form part of the characteristic bilayer cell membrane structure of the cell membrane. It is typically the most abundant membrane phospholipid in mammalian cells. Thus, PtdCho plays a critical role in maintaining membrane structural integrity. PtdCho and PtdEtn (phosphatidylethanolamine) are normally synthesised *de novo* through the Kennedy pathway (Kennedy and Weiss 1956) (Figure 1.3). Choline is a constituent part of the PtdCho molecule, therefore its uptake is important for the biosynthesis of PtdCho. Choline is an essential nutrient for normal physiology, and its deficiency in diet can lead to liver disease and neurological disorders (Zeisel *et al.* 1991, Zeisel and da Costa 2009). Also, tumour cells exhibit a high level of choline uptake (Katz-Brull *et al.* 2002), with choline and PtdCho metabolism being vital to sustaining tumour cell proliferation (Glunde *et al.* 2011). Furthermore, hydrolysis of PtdCho mediates mitogenic signal transduction, as products of choline phospholipid metabolism such as diacylglycerol and arachidonic acid can also function as second messengers, with downstream signalling implications. The regulation of choline phospholipid metabolism can be affected by growth factors, cytokines, oncogenes or metabolite feedback (Glunde *et al.* 2011).

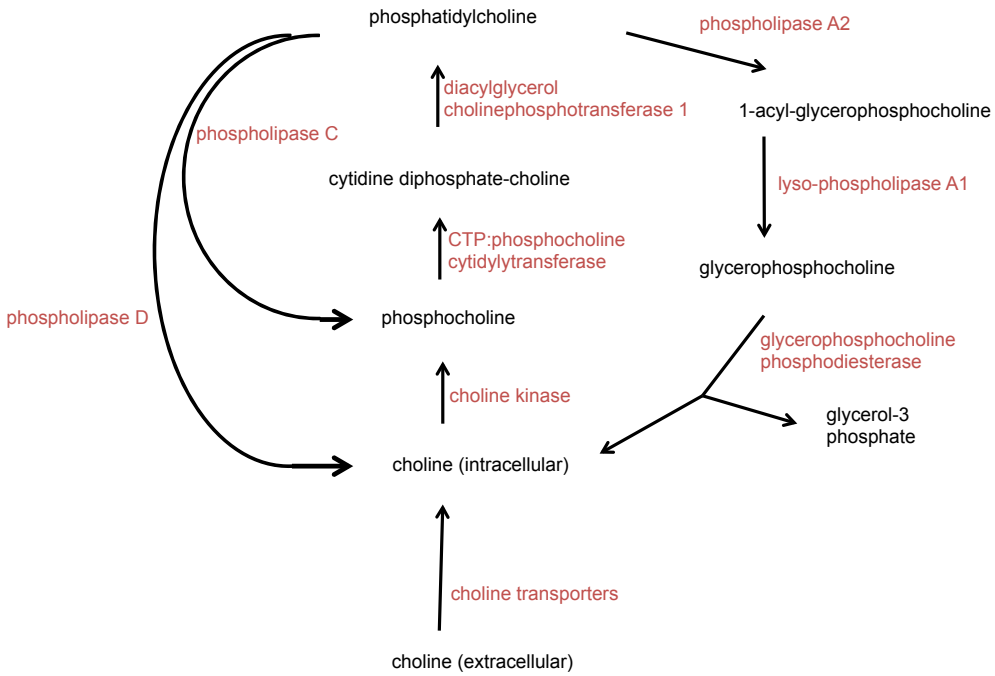

Figure 1.3 Schematic diagram of choline and phosphatidylcholine metabolism

The above diagram is redrawn from a figure shown in (Glunde *et al.* 2011). Metabolites and enzymes are respectively shown in black and red.

1.3 Tumour metabolism

Metabolic alteration is one of the fundamental hallmarks of cancer, and the links between metabolism and cancer are multifaceted (Dang 2012). For example, there is evidence that large mammals with low metabolic rates tend to have a lower incidence of cancer (Caulin and Maley 2011). Cancer risk is also known to be associated with environmental exposures such as smoking, carcinogens, and excessive caloric intake. The metabolic requirement for continuing cell growth and proliferation means that tumour cells have strong demands towards biomass accumulation and anabolism - the metabolic construction of smaller substrates into larger products. Tumour cells are required to increase the synthesis of all biomolecules, from membrane lipids, amino acids, structural proteins to DNA and RNA nucleotides, and this in turn also raises the demand for common metabolic co-factors such as NADPH and ATP. Furthermore, tumour cells need to mitigate the impact of oxidative stress resulting from the build up of radical oxygen species in rapidly proliferating cells. To adjust to all these needs, the metabolic network must be rewired in tumour cells. For example, tumour cells heavily rely on glycolysis for ATP production under aerobic conditions, a phenomenon referred to as the Warburg effect (Warburg 1956). Glucose and glutamine are known to be the major anabolic substrates in supporting energy metabolism and biogenesis in tumour cells (Dang 2012). Other metabolites can also play active roles in the development and the fate of tumour cells (Yang *et al.* 2013). Oxygen radicals can contribute to oncogenic mutations, while nutrient deprivation can feed back to regulate the cell cycle through nutrient sensing signalling modules such as mTOR or AMPK. In addition, the oncometabolite D-2-hydroxyglutarate which results from IDH1/IDH2 mutations can directly diminish hypoxia-inducible factor (HIF) responses. Metabolism and tumour development are intertwined at many levels, and there is renewed optimism that better understanding of tumour metabolism can lead to further innovations in cancer treatments. Recently, metabolomics has played a key role in advancing our understanding in tumour metabolism (Jain *et al.* 2012), and has contributed to therapeutic biomarker and drug discoveries in cancer (Dang *et al.* 2009).

1.3.1 Oncogenic signalling and metabolic regulation

Metabolic reprogramming can occur as a result of genetic and signalling changes in tumours. One of the major signalling nodes where growth and metabolic signalling regulations are integrated is the PI3K/Akt/mTORC1 pathway. This pathway is normally stimulated by growth factors such as IGF-1, EGF, or PDGF, but in tumour cells this can be achieved through oncogenic or tumour suppressor mutations. In addition, mTORC1 is also stimulated by amino acid availability (Sancak *et al.* 2008, Zoncu *et al.* 2011). A number of metabolic enzymes are also regulated in turn through this pathway: Akt stimulates hexokinase, glucose transporters and thus glycolysis; and mTORC1 regulates transcriptional factors PGC-1α and SREBP, which promote mitochondrial biogenesis and *de novo* lipogenesis respectively (Ward and Thompson 2012). Furthermore, reciprocal interactions have been found between choline kinase expression and PI3K/Akt signalling (de Molina *et al.* 2002, Yalcin *et al.* 2010, Glunde *et al.* 2011). Myc is another very important oncogenic master transcriptional factor, which is also involved in the regulation of lactate dehydrogenase A (LDHA) and glutaminase (GLS). In tumour cells, Myc has been shown to activate glycolysis and glutaminolysis (Wise *et al.* 2008).

1.3.2 Exploiting metabolism to detect and treat tumours

There are already imaging modalities used in clinics that exploit metabolic phenotypes unique to tumour cells for monitoring therapeutic responses and for diagnostic purposes. Positron emission tomography (PET) and magnetic resonance spectroscopy (MRS) are the best examples, providing clinicians with functional and biochemical information on the tumour (Spratlin *et al.* 2009). PET is the non-invasive imaging of gamma rays from positron-emitting radioisotopes, with radiotracer labelled compounds that are preferentially taken up by the tumour body being administered to patients (Gambhir 2002). ^{18}F is the most practical isotope for clinical use, and the use of fluorine 18-fluorodeoxyglucose (FDG) has been routinely applied in almost all types of cancers for diagnosis, staging, restaging, and assessing treatment responses. FDG is a glucose analogue, and it exploits the fact that tumour cells have a higher rate of glucose uptake (Zhu *et al.* 2011). Other radiotracer labelled compounds in development include amino acid analogues and choline, and

these may be particularly useful in organ sites where glucose and FDG uptake between tumour cells and non-cancerous tissues cannot be easily differentiated (Zhu *et al.* 2011). Magnetic resonance spectroscopy (MRS) is the other technique that has the capability of imaging metabolite concentration. Whilst both MRS and magnetic resonance imaging (MRI) data can be acquired inside the same scanner, MRS offers more detailed compositional information about the tumour (Bruhn *et al.* 1989). A large range of metabolites can be detected using MRS, and total choline, phosphocholine, glycerophosphocholine, lactate, citrate, have all been proposed as potential markers for disease progression and therapeutic response in preclinical studies (Glunde and Bhujwalla 2011). Nuclear magnetic resonance spectroscopy offers a potential opportunity for translational research, as insights obtained from *ex vivo* tissue analysis can be applied directly *in vivo* using instruments already available in clinics.

Besides its diagnostic value, knowledge of tumour metabolism can also directly contribute in the drug discovery process. Several compounds currently in clinical development directly target metabolic enzymes and pathways. These include compounds that target phospholipid synthesis through choline kinase (e.g. CK37, TCD-717) (Clem *et al.* 2011), and lactate export through monocarboxylate transporter 1 (e.g. AZD3965 (Polanski *et al.* 2014)). Other metabolic targets that have shown promise in preclinical studies include compounds against glucose transporter 1 (GLUT1) (Yun *et al.* 2009), glutaminase 1 (GLS1) (DeLaBarre *et al.* 2011), and isocitrate dehydrogenase (IDH) (Tönjes *et al.* 2013). In addition, there is a resurgent interest in assessing the anticancer benefits of compounds that are already available as prescription drugs, such as statins, metformin and dichloroacetates. Statins are normally used to treat hypercholestrolaemia by targeting the mevalonate pathway, while metformin and dichloroacetates both target mitochondrial metabolism (Galluzzi *et al.* 2013).

1.4 Metabolomics

Metabolomics is the measurement of multiple metabolites in biochemical samples, with the aim of providing a total description of the system metabolite make-up. The comprehensive description of metabolite composition is sometimes referred to as the 'metabolome' (Oliver *et al.* 1998), and often contains valuable information about the metabolic processes that take place inside the bio-system. Applications of metabolomics often involve the comparison of the quantitative and dynamic response of the metabolome upon a specific biological stimulus (Nicholson *et al.* 1999). The examples of metabolomics applications are diverse, and can be found across the subfields in biological and biomedical sciences: from discovering the metabolic function of an unknown enzyme, assessing the toxicity of a drug treatment in cells, to differentiating ill and healthy conditions in patients (Fiehn 2002, Robertson 2005, Kell 2006, Griffiths 2007, Ward *et al.* 2007, Bundy *et al.* 2009).

1.4.1 Analytical techniques

Metabolomics is a platform for both understanding metabolic processes and metabolic biomarker discovery. The metabolome incorporates information arising from interactions with the bio-system environment and contains phenotypic observations that cannot be captured through genetics alone; thus it is complementary to both genome and proteome analysis. Metabolomics in its current form is made possible by the many advances in modern technology and the increase in computational power. In metabolomics, the analytes are molecules that are typically less than 1500Da, and the measurements rely on high-resolution analytical instruments to provide the metabolite coverage necessary. Mass spectrometry, chromatography, and NMR spectroscopy are the principal detection and separation technologies employed in metabolomics. In addition, the semi-automated analysis of high-content data and the use of multivariate statistics are routine and important for efficient information retrieval.

1.4.2 NMR spectroscopy and mass spectrometry

While the aim of metabolomics is to provide a comprehensive description of all metabolites in the sample, in practice, each detection technique and separation method has its own advantages and limitations. The metabolite coverage and threshold of detection are instrument and method dependent; there may be over 4000 metabolites in the human systems, however, only a subset of the metabolome can be captured in any single analysis. For example, NMR is relatively insensitive to metabolites of low concentration and often has lower metabolite coverage. In contrast, mass spectrometry based methods can often detect many more metabolite features, however, metabolites may need to be chemically modified and separated prior to detection. Thus, metabolites detected are pre-selected through column chemistry, and may decompose in the sample preparation stages. Samples analysed using mass spectrometry based methods are subjected to additional sample handling, which could introduce an extra layer of uncertainties and potential errors. Both the range and volume of metabolomics applications have grown in the past decade, as the technology continues to mature and expand. Many aspects of the technologies, from instrument upgrades, hyphenated platforms, chromatographic methods, statistical approaches to data analysis protocols are still in active development. (Holmes and Antti 2002, Zhang *et al.* 2012)

1.5 Overview of the thesis

Cancer and metabolism are intertwined at both the molecular signalling and the system levels, and the relationships between the two are complex. Decades of research mean that we now associate many phenotypic changes of metabolism with tumour cells, such as glycolysis and glutaminolysis. However, there remain deficits in our understanding especially regarding the context in which they are best applied. Metabolomics provides dynamic metabolite coverage, and has been demonstrated to be a valuable platform for studying tumour metabolism. It has vast potential to bridge the gap between basic research and clinical applications, particularly through the use of positron emission tomography (PET) and magnetic resonance spectroscopy (MRS). One of the promising metabolic modules under investigation is the choline phospholipid metabolite phenotype (i.e. the relative abundance of choline, phosphocholine, and glycerophosphocholine). These aqueous metabolites are relatively abundant and could be detectable using MRS. Furthermore, choline-PET has found numerous applications, particularly in the context of prostate cancer management (Husarik *et al.* 2008). In this thesis, I have utilised a range of metabolomics platforms to explore different aspects of choline metabolism in tumour development:

PIK3CA is one of the most frequently found mutated genes in breast cancers (Koboldt *et al.* 2012), and it is an important activator of PI3K/Akt signalling. Previous reports have linked PI3K/Akt signalling in tumour cells to deregulated choline phospholipid metabolism (de Molina *et al.* 2002, Yalcin *et al.* 2010, Glunde *et al.* 2011). In Chapter 3 of the thesis, I report my findings on the metabolic changes associated with 'knock-in' *PIK3CA* mutation, using the non-tumorigenic MCF10A breast line as a model. An interesting feature I have observed in the *PIK3CA*-mutant cells was the possible reduction in glycerophosphocholine (GPC), which function in cancer remains unclear. In Chapter 4, I examine the metabolome-wide effect of interfering with the activity of a previously uncharacterised GPC-selective glycerophosphodiester phosphodiesterase. Finally in Chapter 5, I explore the potential values in using relative choline metabolite abundances as biomarkers for monitoring therapies targeting macrophage infiltration, using a murine pancreatic tumour model.

Chapter 2 Analytical methods and protocols

2.1 NMR Spectroscopy

2.1.1 Physical basis and concepts

Spin is an intrinsic property of angular momentum associated with fundamental particles, and nuclear magnetic resonance (NMR) is a natural phenomenon whereby nuclei possessing spin absorb and emit energy in a magnetic field. Protons and neutrons have spin quantum number ½, and spin quantum number of nuclei are defined according to their proton and neutron compositions. Degeneracy is used in quantum mechanics to describe the degree of which a quantum state can correspond to multiple measureable energy levels, and a nuclear spin with spin quantum number I is considered $(2I + 1)$ fold degenerate. Nuclear spin populations of spin quantum number I previously occupying the same well-defined energy state would fill a multiple number of energy states $(2I + 1)$ under the influence of an external magnetic field (Figure 2.1). This is known as the nuclear Zeeman splitting, and NMR spectroscopy is used to probe and record the nuclear Zeeman subpopulation dynamics (Levitt 2008).

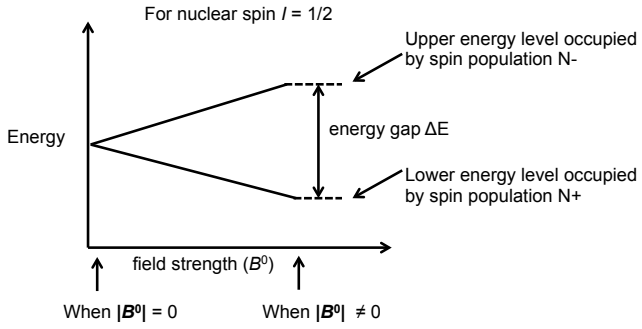

Figure 2.1 The nuclear spin population of spin quantum number I = ½, such as ^{1}H, can occupy two distinct energy levels when they interact with an external magnetic field.

The energy gap (ΔE) shown in the diagram is proportional to the magnet field strength (B_0) of the spectrometer, while the relative spin populations occupying the upper and lower energy levels are determined by the energy gap (ΔE) through the equation $\frac{N-}{N+} = e^{-\frac{\Delta E}{kT}}$, where k is the Boltzmann constant and T is the temperature measured in Kelvin. ΔE is typically small compared to kT at room temperature in conventional NMR spectrometers, resulting in the spin population predominantly occupying the lower energy level at thermal equilibrium. This diagram above is adapted and redrawn using figures and concepts shown in (Levitt 2008).

A nuclear spin with spin angular momentum possesses also an intrinsic magnetic moment, and Zeeman splitting is the direct result of the interaction between the magnetic moment of the nuclear spins and that from an external field. Thus, the energy gaps between the Zeeman subpopulations are directly proportional to the magnetic field strength and are associated with a well-defined electromagnetic wave frequency. This is referred to as the Larmor frequency, which is nuclei-specific as the magnitude of nuclear spin magnetic moment is likewise also distinctive between nuclei (Figure 2.1). Under the influence of a external magnetic field, the nuclear spin vector moves around the field axis at a fixed angle in a precessional motion with Larmor frequency, and the concepts of precession and macroscopic nuclei spin polarisation enable many aspects of the instrumentation, design and interpretation of NMR experiments to be understood using classical vector models.

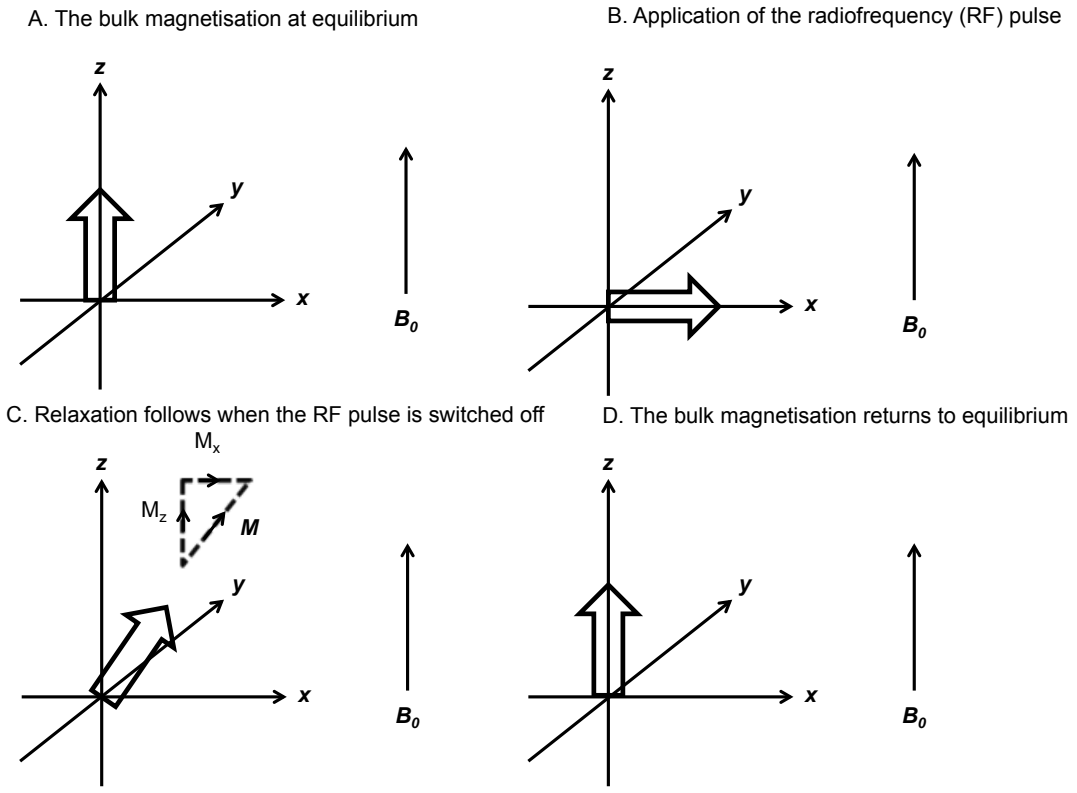

Figure 2.2 Evolution of the bulk magnetisation vector through a 90-degree pulse in the rotating frame

B_0 is the external static magnetic field vector generated by the spectrometer magnet. A) The bulk magnetisation vector is aligned longitudinally along the magnetic field of the NMR spectrometer at thermal equilibrium. B) Application of the 90-degrees radiofrequency pulse directs the bulk magnetisation vector onto the transverse plane, resulting in no net magnetisation longitudinally along the magnetic field of the NMR spectrometer. C) As the applied pulse is switched off, the bulk magnetisation vector begins to return to its original equilibrium position through longitudinal and transverse relaxations. The bulk magnetisation vector contains both longitudinal and transverse vector components. D) When fully relaxed, the bulk magnetisation vector returns to its equilibrium position. The above diagram is adapted and redrawn using figures and concepts from (Levitt 2008).

When a sample is placed inside a spectrometer, nuclear spins precess around the axis of the spectrometer magnetic field (**B_0**) and this results in a net longitudinal magnetisation along **B_0** (Figure 2.2A). In NMR experiments, electromagnetic waves at the Larmor frequency are pulsed to excite the ground state population to redirect the spin magnetisation onto the transverse plane, thereby generating a net transverse vector component for the nuclear spins (Figure 2.2B). Once the applied pulse is switched off, the nuclear spins gradually return to the original thermal equilibrium configuration through relaxation processes (Figure 2.2C and Figure 2.2D). During

relaxation, whilst the transverse magnetisation diminishes individual spins would continue to precess at their well-defined resonance frequencies, producing an oscillating transverse magnetic field and a current signal in the detector coil (Figure 2.3). This signal is recorded as the free induction decay (FID), and the FID signal in the time domain is then converted to the frequency domain through Fourier Transform, forming a conventional NMR spectrum (Figure 2.4). (Levitt 2008)

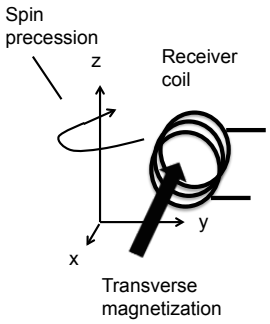

Figure 2.3 Signal induction through the receiver coil.

The diagram above illustrates the process of signal induction. As a result of relaxation processes and continuous nuclear spin precession, an oscillating magnetic field is generated in the transverse plane and thus signal is induced in the receiver coil. The above diagram is adapted and redrawn from a figure in (Levitt 2008).

Electrons are diamagnetic, producing opposing magnetic moments to $\mathbf{B_0}$ and thus reducing the effective field strength sensed by the nuclei. On the NMR spectrum the frequency axis is referred to as the chemical shift as it indicates the degree of which the molecular-specific, functional group-specific nuclear resonances are shielded by molecular electrons. ^{1}H, ^{13}C and ^{31}P NMR spectroscopy are all widely used for metabolic profiling.

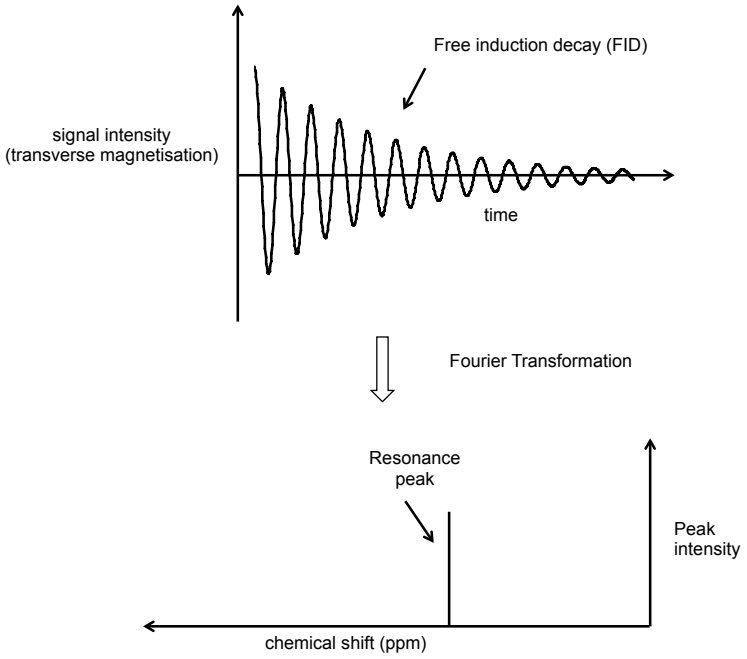

Figure 2.4 The detector coil in the NMR probe records signals in the time domain, which are then converted into resonance peaks in the frequency/chemical shift domain through Fourier Transform.

The diagram above is adapted and redrawn using figures and concepts from (Levitt 2008).

2.1.2 Carr-Purcell-Meiboom-Gill (CPMG) pulse experiment

The one dimensional Carr-Purcell-Meiboom-Gill (CPMG) spin-echo pulse sequence is widely used in metabolomics studies (Figure 2.5). The main reason is because the CPMG pulse sequence can selectively suppress resonance signals from protein and lipid molecules, allowing resonances from small molecules to be better resolved. Resonance signals arising from heavy, slow tumbling molecules such as proteins typically have shorter transverse relaxation times (T_2) compared to rapidly tumbling small molecules, and are selectively attenuated during the spin echo sequence (Figure 2.6). Also, the CMPG pulse sequence has the added benefit of eliminating the effect of line broadening due to molecular diffusion and longitudinal magnetic field inhomogeneity (Figure 2.7), as de-phasing resulting from longitudinal relaxation can be refocused through the application of a series of 180-degree pulses as part of the spin echo sequence (Carr and Purcell 1954, Meiboom 1958).

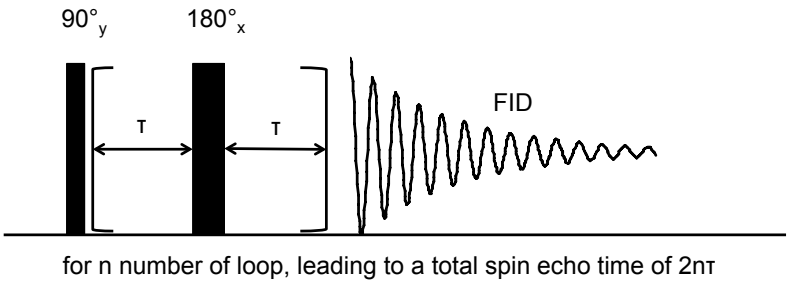

Figure 2.5 Schematic of the CPMG spin echo pulse sequence

The CPMG pulse experiment consist of an initial 90° pulse, followed by successive 180° pulses separated by a time period of 2τ. The total spin echo time is given by 2nτ, where n represents the number of 180° pulse in the sequence. Free induction decay (FID) is recorded at the end of the series of 180° pulses.

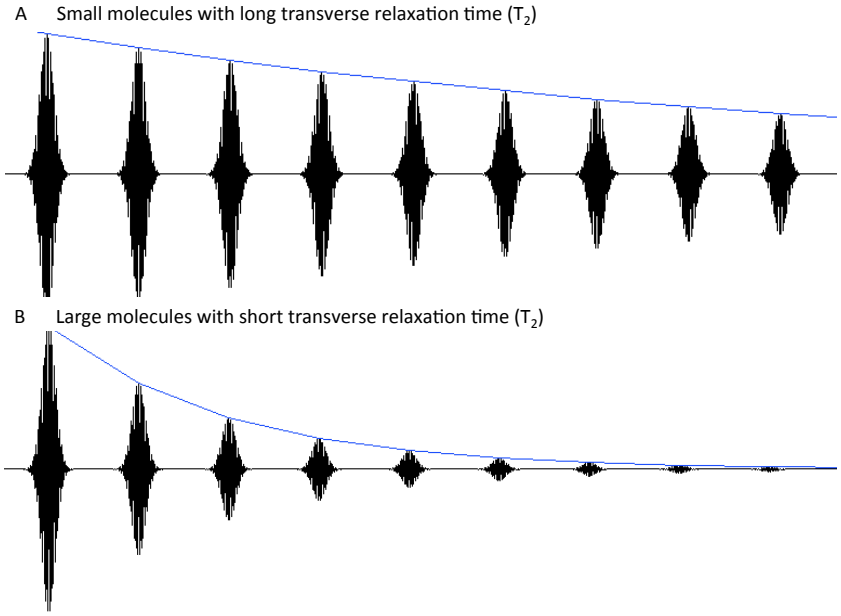

Figure 2.6 A train of spin echoes attenuates signals from larger molecules such as proteins with short transverse relaxation times

The diagram above shows the evolution of signal intensity (vertical axis) as a function of the total spin echo time, 2nτ (horizontal axis).

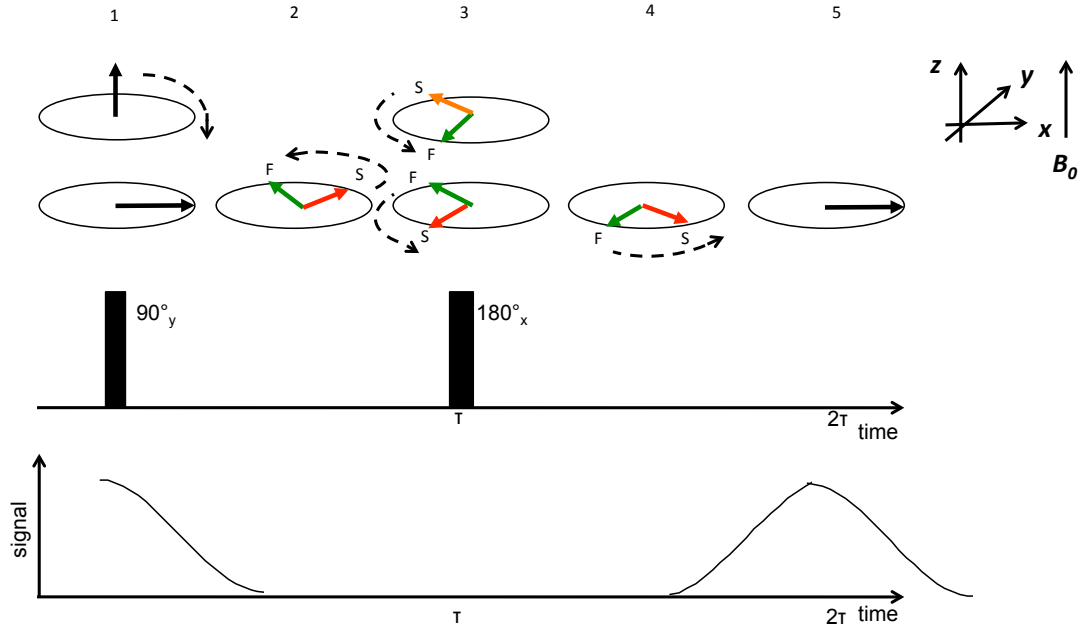

Figure 2.7 A schematic diagram illustrating how spin vectors are refocused through a single spin echo.

1) The initial 90° pulse directs the bulk magnetisation vector onto the transverse (*x*-*y*) plane. 2) The magnetisation vector de-phases and 'fans out' due to inhomogeneous external field and molecular diffusion motion, leading to a reduction in the magnitude of the induced signal. Magnetic moment vectors with higher precessional frequencies (F, in green) 'lead' and magnetic moment vectors with lower precessional frequencies 'trail' (S, in red). 3) Application of the 180° pulse at time τ flips the magnetic moment vectors along the transverse plane. 4) Magnetic moment vectors with higher precessional frequencies (F, in green) now 'trail' and magnetic moment vectors with lower precessional frequencies now 'lead' (S, in red). 5) At time 2τ, the magnetic moment vectors are realigned, and the bulk magnetisation is back in-phase and refocused and maximal signal induction is achieved. The diagram above is adapted and redrawn from concepts and figures shown in Carr and Purcell's seminal paper (Carr and Purcell 1954).

2.1.3 High-resolution magic angle spinning (HR-MAS)

High-resolution magic angle spinning (HR-MAS) NMR is a technique that enables the metabolic phenotyping of intact cells and tissues. In HR-MAS samples are cylindrically rotated about an axis at 54.7° to the main magnetic field of the NMR spectrometer. Tissues samples are in semi-solid state, and display many quantum characteristics of solid materials that include reduced molecular mobility. Mathematically, interactions such as dipolar couplings and chemical shift anisotropy (CSA) have angular dependences of $(3\cos^2\theta - 1)/2$. While these normally do not apply to samples in solution as nuclear spins distribute themselves isotropically

under free rotational motion, these are relevant in the case of solid/semi-solid samples. The additional local spin interactions in solids have the effect of leading to complicated and poorly resolved spectra with very broad linewidths. HR-MAS provides a practical solution to eliminating the dipolar coupling and CSA interactions. It adjusts the axis of the sample rotor in relation to the axis of the spectrometer field, so that the angular-dependent elements of the interactions in liquid crystals like tissue samples can be conveniently nullified during rotation (Lowe 1959). This occurs at 54.7°, the 'magic angle', since $3\cos^2(54.7°) - 1 = 0$. The sample rotor is inserted into a hinged, flexible stator block section of the MAS probe, allowing the sample rotor to be positioned and spun by a stream of nitrogen gas at the required magic angle to the spectrometer. The magic angle technique reduces the number of relaxation mechanisms involved, and the lengthier transverse relaxation timeframe in turn leads to sharper lineshapes on NMR spectra of solid/semi-solid samples (Beckonert *et al.* 2010).

2.2 GC-Mass Spectrometry

GC-MS is a robust metabolomics platform with high sensitivity. Through derivatisation, analytes of interest are first chemically modified to render them volatile, and are then separated inside a capillary column in the gas phase at temperatures of around 300°C. Once the chemical species are eluted from the column, they enter the mass spectrometer. They are ionised typically through electron ionisation before traveling down to the detector e.g. quadrupole/time-of-flight (TOF) and are detected according to their mass to charge ratios (m/z). (Dettmer *et al.* 2007)

The m/z spectrum can be analysed under full scan mode or selected ion monitoring mode (SIM), and SIM methods are sometimes preferred to improve the threshold of detection and to increase signal to noise ratios. For metabolomics analysis typically only 1 µl of the sample is required for injection and an analysis of a single sample takes around 45 minutes to complete.

2.2.1 Derivatisation

Derivatisation enables the functional groups of the metabolites to be chemically modified. The main aims of derivatisation is to reduce polarity and to increase volatility and thermal stability of the compounds, and it is an important step in making the analysis as robust as possible. For example, alkylation, acylation and silylation target active hydrogen such as –COOH, -OH, -NH, and –SH groups and in silylation, active hydrogen groups are replaced by alkylsilyl groups such as trimethylsilyl. MSTFA (N-methyl-N-trimethylsilyl-trifluoroacetamide) and MTBSTFA (N-methyl-N-tert-butyl-dimethylsilyl-trifluoroacetamide) are both widely used silylation reagents (Figure 2.8), and tert-butyl-dimethylsilyl derivatives often produce characteristic $[M-57]^+$ fragment ions, which can be useful for identifying unknown metabolites. In addition, carbonyl groups can be transformed into oximes using methoxyamine which help stabilises compounds such as ketoacids and sugars. Methoximation followed by silylation is typically used for the profiling of aqueous metabolites (Dettmer *et al.* 2007), and sodium methoxide and methanol

are used to catalyse and initiate transesterification reactions for the analysis of bound fatty acids (Figure 2.9) (Metcalfe and Wang 1981).

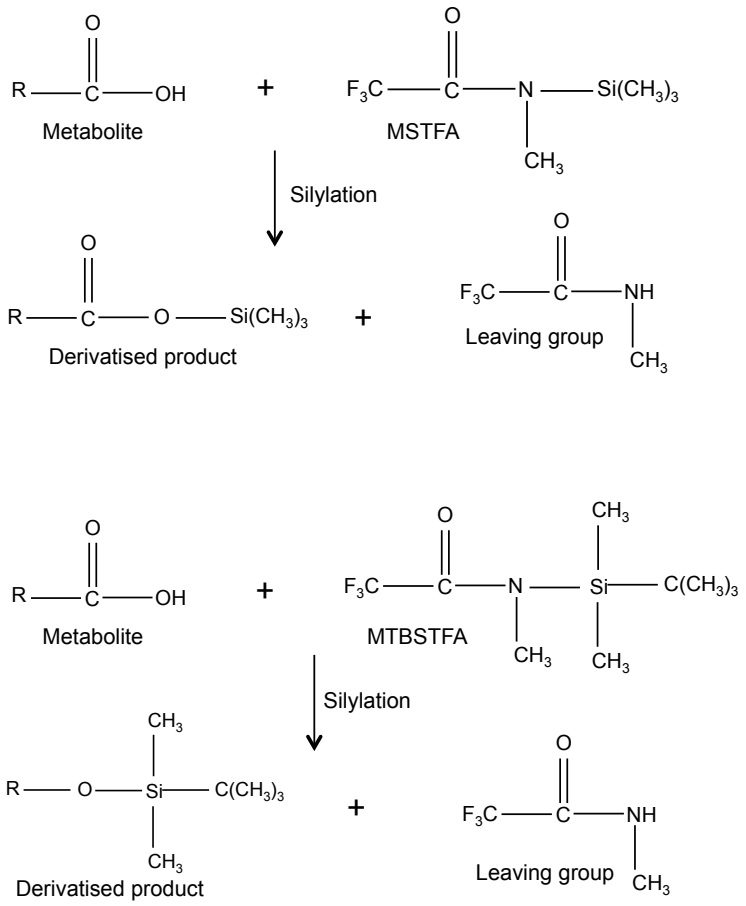

Figure 2.8 Schematic of silylation reaction

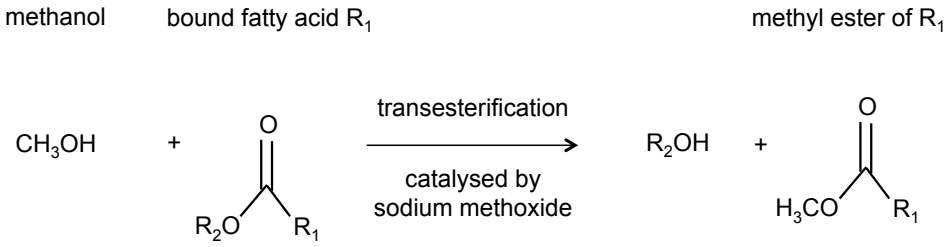

Figure 2.9 Schematic of bound fatty acid transesterification

2.2.2 Data Processing

The resulting mass spectra contain information about the distribution of mass fragment ions detected for the duration of the chromatographic separation, and thus the full dataset are often large and can be difficult to inspect visually. To speed up the analysis many aspects of the data processing, from peak deconvolution, library matching, to signal integration are semi-automated. We have employed AMDIS (Automated Mass Spectral Deconvolution and Identification System) (Stein 1999) in conjunction with the NIST (National Institute of Standards and Technology) library and the published Fiehn library (Kind *et al.* 2009) for peak deconvolution and metabolite identification. We also use GAVIN (Behrends *et al.* 2011), a MATLAB graphic user interface, for selecting signal boundaries in the retention time domain for systematic integration across the full study dataset.

2.2.3 ^{13}C Stable isotopes tracer of glucose and glutamine

Stable isotope labelling of precursor metabolites has found numerous applications in the studies of cell culture tumour models. The distribution of the mass isotopomers can be readily inferred from the mass fragmentation pattern, and metabolites enriched with ^{13}C tracer e.g. $^{13}C_6$-glucose (Figure 2.10) and $^{13}C_5$-glutamine (Figure 2.11) can be detected using GC-MS. Following data acquisition, the raw data from the mass fragmentation pattern are corrected for elemental natural isotopic abundance using computational methods (Millard *et al.* 2012). The experimental data provide information about the carbon flow around key cellular metabolic pathways, including glycolysis, TCA cycle and glutaminolysis.

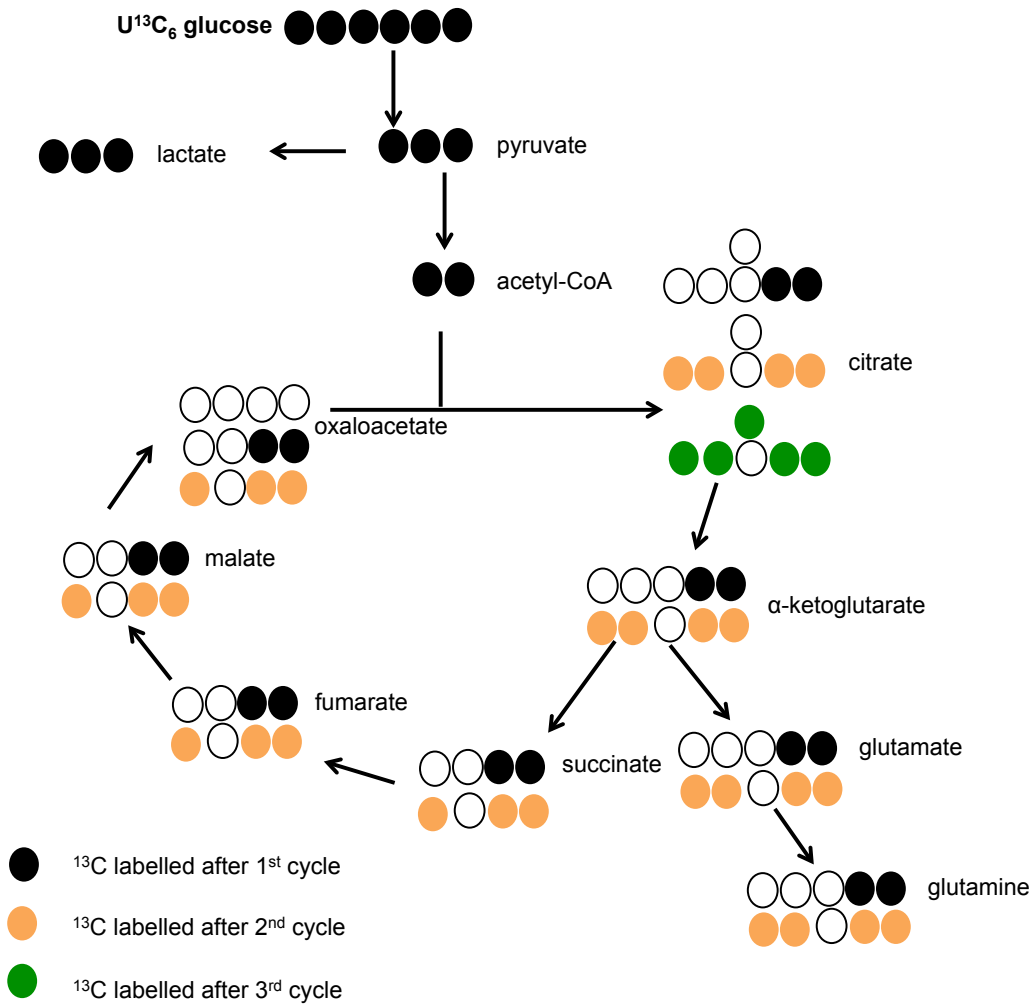

Figure 2.10 Schematic of $^{13}C_6$ glucose labelling into TCA cycle intermediates

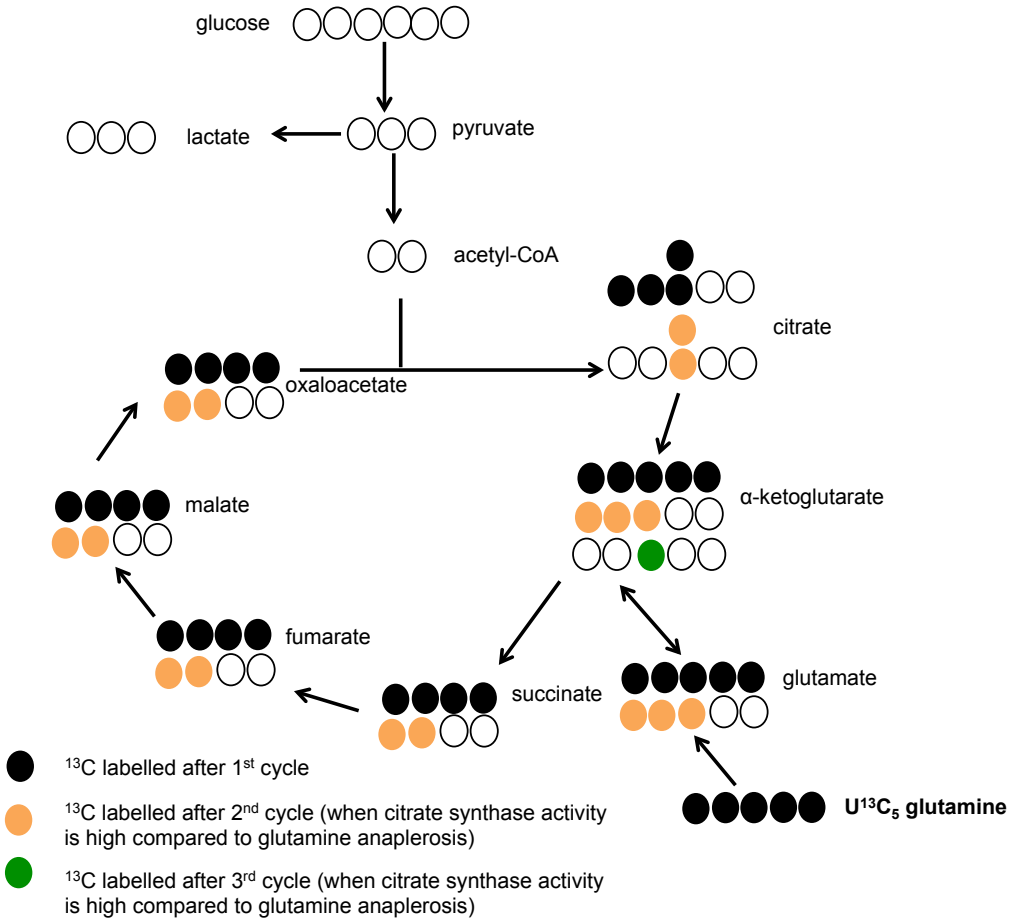

Figure 2.11 Schematic of $^{13}C_5$ glutamine labels into TCA cycle intermediates via oxidative pathway

2.2.4 Isotopomer Spectral Analysis

Isotopomer Spectral Analysis (ISA) is a deconvolution method of the ^{13}C tracer fatty acid mass isotopomer distribution data. The fraction of labelled acetyl-CoA (D), *de novo* biosynthesis rate of the fatty acid (G (t)), and elongation (E) are taken into account to simulate the mass isotopomer abundance (Kelleher and Masterson 1992), (Figure 2.12). Solutions are compared with the experimental spectra, and are optimised iteratively until the simulated spectra and the experimental data are well matched. The model is based on the assumption that fatty acid species synthesised *de novo* are derived from the sequential linkages of two-carbon acetyl CoA units, which can either come from ^{13}C enriched tracers or alternative sources. The Isotopomer Spectral Analysis is able to describe this process computationally and reconstructs the fatty acid mass isotopomer distributions.

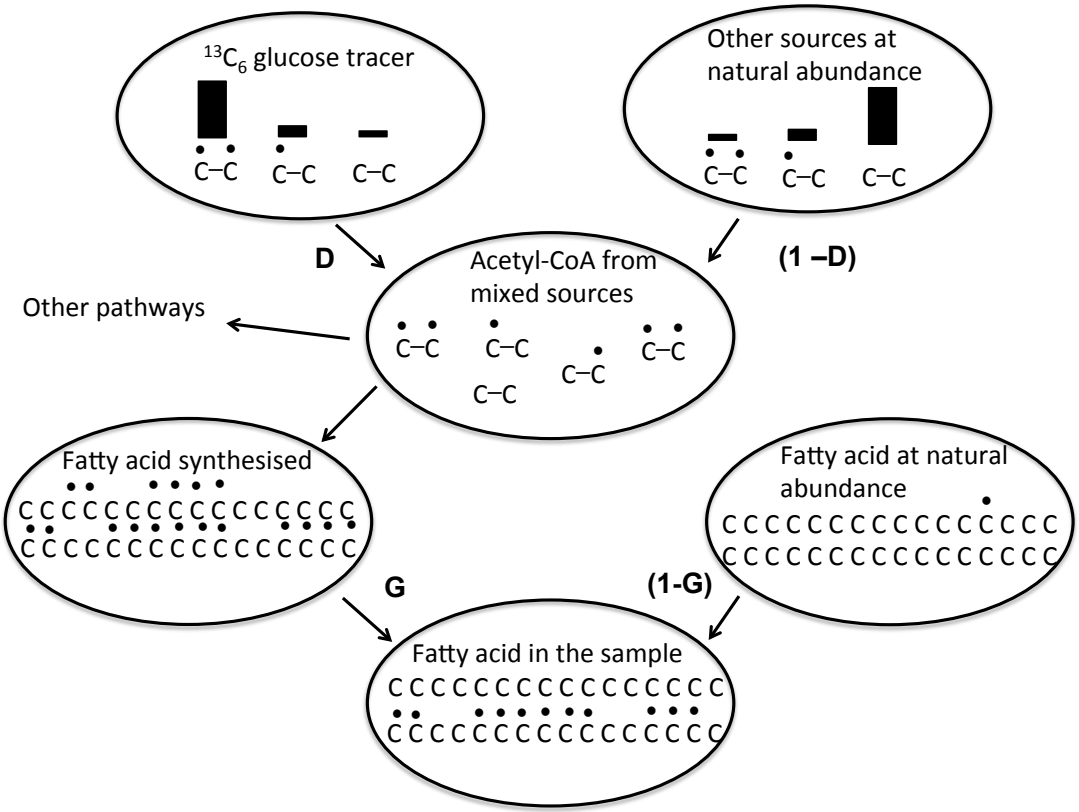

Figure 2.12 Modelling of fatty acid metabolism using Isotopomer Spectral Analysis

The diagram above illustrates the conceptual basis as well as the input and output parameters of the Isotopomer Spectral Analysis (ISA) model, using fatty acids cultured in the $^{13}C_6$-glucose medium as an example. The 'dots' represent carbon atoms that are ^{13}C labelled, and the relative bar heights at the top of the diagram represent the distribution of ^{13}C isotopomer population of acetyl-CoA as would be expected from the natural isotope abundance of carbon. ISA uses a deconvolution technique to deduce parameters D and G, and by matching simulated distributions of ^{13}C labelled isotopomers to the experimental data. This diagram above is adapted from a figure in a publication by Kelleher *et al.* (Kelleher and Masterson 1992).

2.3 Principal component analysis (PCA) in metabolomics

PCA has found numerous applications in system biology and in many other scientific disciplines (Price *et al.* 2006). PCA is one of the simplest forms of multivariate analysis. It requires no *a priori* knowledge of the biological samples and is a valuable method for visualising complex datasets in metabolomics. PCA reduces the dimensionality of the dataset while retaining important information about the variations and differences between biological samples. In metabolomics, it is often used to identify metabolite signal peaks that discriminate between samples in the dataset, and for clustering biological samples that are alike. (Wold *et al.* 1987)

Within the context of metabolomics data analysis, data variables could be metabolite signal peaks from NMR or mass-spectrometry spectra, or it could be other information related to the biological samples such as age, BMI or timepoints. Each variable can be thought of as an independent data 'axis', and PCA constructs new orthogonal 'axes' using linear combinations of the original variables and matrix algebra (Figure 2.13). PCA exploits the covariance structure of the underlying data, and the orthogonal linear transformation is designed to emphasise the variance in the dataset. The resultant matrix consists of eigenvectors, which represent the transformed axes and the corresponding eigenvalues confer information about the amount of data variance explained. The first principal component is the most important, as it describes the greatest amount of variance and thus information in the dataset, and lesser information is contained in each of the subsequent principal components (Wold *et al.* 1987). Variables are represented on the loading plot, which specifies the degree to which they contribute towards a particular principal component; whereas biological samples are represented on the score plot, which specifies the degree by which the data profile of each sample can be explained through the corresponding transformed data axis. Various computational methods can be applied to perform the matrix transformation, and PCA can be carried out using functions already implemented in MATLAB or other specialised software.

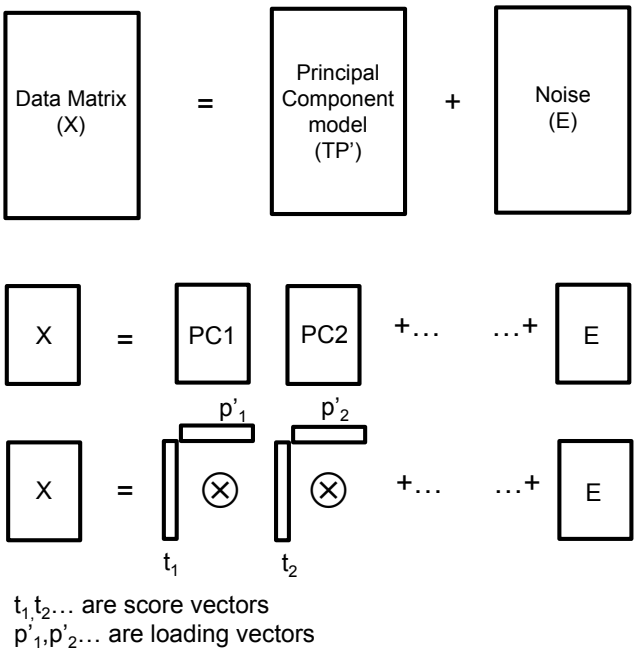

Figure 2.13 Principal Component Analysis requires orthogonal transformation of the original data matrix into principal component score and loading vectors.

The diagram is redrawn using concepts and figures from Wold's publication (Wold *et al.* 1987). ⊗ represents matrix multiplication.

2.4 Protocols

2.4.1 Metabolite extraction

In order to perform metabolomics analysis on metabolites from adherent cell cultures, cells were collected from the culture vessels (i.e. flasks/plates/dishes) by methanol quenching and cell scraping. Metabolomics experiments were conducted in 6-well plates and after the cell media were collected initially, cells were washed either using phosphate saline buffer (for NMR analysis) or Ringer's buffer (for GC-MS analysis) before methanol was promptly added onto the sample wells. Approximately, 400,000 to 1,000,000 cells were harvested in methanol using cell scraper to make up a cell extract sample for analysis.

For metabolite extraction, a dual-phase methanol/chloroform method was then used to separate out the aqueous metabolites, and the non-polar metabolites from the cell proteins. Metabolites were extracted from the dried down methanol-quenched cell pellet samples and the samples were kept on ice during the extraction. 300 μl of chloroform/methanol in a 2:1 ratio was added to the cell pellet and was mixed using vortex. Then 300 μl of HPLC/UPLC graded H_2O was added to the samples, which was again mixed using vortex and centrifuged at 16000g for 5 min. The upper aqueous fraction and lower chloroform fraction were carefully separated, and were then transferred either into new eppendorfs for NMR samples, or silanized glass vials for GC-MS analysis. This extraction process (adding chloroform/methanol/water, mix and centrifuge, followed by separation of aqueous and chloroform fractions) was repeated for a second time, and the corresponding aqueous and organic fractions were pooled.

2.4.2 Sample preparation of culture medium for ^{1}H NMR analysis

Culture medium samples were kept frozen in eppendorfs in -80°C freezers after sample harvesting, and samples were prepared into NMR tubes on the day of the spectroscopic analysis. After the samples were thawed, they were kept on ice. 550 μl of the medium sample was transferred into a new eppendorf, and 50 μl of internal standard DSA (4,4-Dimethyl-4-silapentane-1-ammonium trifluoroacetate) in D_2O

(11.6mM) was added into the sample as a quantitation reference. The mixture was then pipetted into a standard 5mm NMR tube.

DSA (4,4-Dimethyl-4-silapentane-1-ammonium trifluoroacetate) has been proposed as a universal internal standard for biofluids. (Alum *et al.* 2008). In biofluid of high protein content such like serum, DSA peak signals have been demonstrated to show consistent linewidth and chemical shift, unaffected by changing pH. It was shown to be a valid alternative to TSP (trimethylsilyl propionate).

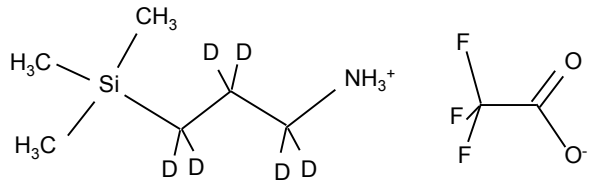

Figure 2.14 Chemical structure of DSA

The structure is redrawn from a figure in (Alum et al. 2008)

2.4.3 Sample preparation of intracellular metabolites for ^{1}H NMR analysis

After methanol/chloroform/water dual phase extraction (see 2.4.1), aqueous fractions were dried down in eppendorfs using a freeze-dryer. The dried down samples were then reconstituted in 600 µl of phosphate buffer (composition of the phosphate buffer: 0.2M Na_2HPO_4, 0.043M NaH_2PO_4, 100µM TSP, 3mM NaN_3 in 100% D_20). Samples were then centrifuged at 16,000 g for 5 mins to spin down any insoluble material, and 550 µl of the reconstituted samples were transferred to clean standard 5 mm NMR tubes. The purity of the phosphate buffer was checked and confirmed using ^{1}H NMR before use.

2.4.4 ^{1}H NMR experiment acquisition and data processing

High-resolution ^{1}H NMR spectra were acquired using either a 5mm broadband-inverse tube probehead or a 5-mm cryoprobe using a 14.1T Bruker AVANCE 600 spectrometer (Bruker Biospin). Carr- Purcell-Meilboom-Gill (CPMG) spectra were acquired using a standard presat pulse sequence, with the fixed echo time (τ) set at

400 μs and the total spin echo time of 64 ms. Spectra were recorded with 64 transient scans, following 16 dummy scans. A 3s relaxation delay was incorporated, and gradient shimming was used before all spectral acquisitions to improve magnetic field homogeneity across the detected sample volume. In some experiments, a BACS60 sample changer (Bruker BioSpin) was used to automate the analytical run. Data were imported and processed in MATLAB® (MathWorks) using scripts written in house by J.T. Pearce, H.C. Keun, T.M.D. Ebbels, and R. Cavill (Imperial College London, UK). ^{1}H NMR spectra were automatically phased, baseline-corrected, and referenced to the internal standard resonance at 0 ppm. Spectral integration was performed in MATLAB® (MathWorks) after metabolite identification. Identifying metabolites from the signal peaks are made often through the use of databases at the Human Metabolome Database and at the Biological Magnetic Resonance Bank, or through published literature.

2.4.5 Metabolite quantification from ^{1}H NMR analysis of cell media

Concentration estimates were based on metabolite resonance integrals referenced to internal standard DSA signal intensities. Peak signal integrals of internal standard DSA (located at 0 ppm) and other metabolite peaks of interest were obtained by estimating the area under the curve. Concentrations were estimated from integral ratios between DSA and the metabolite of interest, and by accounting for the molecular proton number of the individual resonances. A blank unused media sample was analysed alongside with the biological samples, to enable the uptake and release of metabolites to be calculated. Differences in transverse and longitudinal relaxation times between metabolites and the DSA could lead to bias in absolute qualification, thus we analysed calibrated samples containing selected metabolites (including glucose, lactate, glutamine) of known concentrations, and estimated measurement bias in absolute quantification in our experiments to be around ± 15%.

2.4.6 Sample preparation of intracellular aqueous metabolites for GC-MS analysis

The aqueous fractions of the intracellular cell extracts (~ 10^{6} cells, approximately 1 mg of dried weight) from methanol/ chloroform/ water dual phase extraction (see

2.4.1) were derivatised and analysed by GC-MS. Before the start of derivatisation, 10 μl of 1.5mg/ml myristic acid-d27 was added to the dried aqueous fractions as an internal standard, and the samples were dried down using a vacuum concentrator (SpeedVac^{TM}). Samples were first derivatised through methoxyamination, where 20 μl of methoxyamine (20 mg/ml in anhydrous pyridine) was added to samples using a multipipette, and samples were mixed using vortex and spun in centrifuge. The samples were placed in a heater block for 90 min at 37°C. At the end of the period, samples were cooled and spun in a centrifuge again. Samples were then silylated by adding 80 μl of MTBSTFA (with 1% TBDMS) (Thermo). After mixing by vortex, and centrifugation, samples were placed in a heater block, and were incubated for a further 60 min at 70°C. At the end of the period, samples were cooled and spun in a centrifuge again. Finally 10 μl of 1mM 2-fluorobiphenyl (in anhydrous pyridine) was added to the samples as an injection standard, and the samples were then transferred to deactivated glass vial inserts.

2.4.7 Sample preparation of non-polar metabolites for GC-MS analysis

The free fatty acids were silylated with MSTFA, whereas the fatty acid esters present in the organic fraction were transesterified. First, 10 μl of 1.5mg/ml myristic acid-d27 was added to the samples as an internal standard. Then, the samples were dried down using a vacuum concentrator before they were reconstituted in 333 μl of methanol/toluene solution (1:1 v/v ratio), and were treated with 167 μl of 0.5M sodium methoxide and incubated at room temperature for 1 hour. Reaction was halted by the addition of 500 μl of 1 M NaCl and 25 μl of concentrated HCl. The fatty acids were then extracted using two volumes of hexane (500 μl), and the combined organic layers were dried under N_2. Samples were then reconstituted with 40 μl acetonitrile, silylated by adding 40 μl of MSTFA (with 1% TMCS) (Thermo), and were incubated for 30 min at 37°C. At the end, 10 μl of 1mM injection standard 2-fluorobiphenyl (in anhydrous pyridine) was added to the samples. Samples were then transferred to deactivated glass vial inserts ready for GC-MS analysis.

2.4.8 GC-MS instrument set up and data processing

GC-MS analysis was performed on an Agilent 7890 GC system with a 30m DB-5MS capillary column. A 10m Duraguard column was connected to an Agilent 5975 MSD triple-axis detector operating under electron impact ionization (Agilent Technologies). Samples were injected with an Agilent 7693 autosampler injector into deactivated splitless using helium as the carrier gas. The analysis was performed based on the Fiehn method (Kind *et al.* 2009) and the data were acquired under selected ion monitoring (SIM) mode, with representative samples from each biological group also run under full scan mode. The identities of the GC-MS features were confirmed either through running standards or matching to the NIST library, aided by an in-house generated library using the AMDIS program for deconvolution (Stein 1999). Individual isotopomer peaks were integrated using in-house MATLAB® (MathWorks) scripts by Dr G.T. Tredwell (Imperial College London) based on the program GAVIN (Behrends *et al.* 2011). The mass isotopomer distribution vectors (MID) for each metabolite were normalised i.e. the sum of the metabolite isotopomer abundances equal to one. MATLAB® (MathWorks) scripts were written in-house by Dr G.T. Tredwell (Imperial College London) to automatically correct for naturally occurring elemental isotopes based on the method described by Millard *et al.* (Millard *et al.* 2012).

2.4.9 Isotopomer Spectral Analysis (ISA)

ISA was performed with MATLAB® scripts developed in-house by Dr G.T. Tredwell (Imperial College London). The computation provided estimates for two (D, G) or three (D, G, E) parameter ISA models based on minimising the differences between the acquired spectral mass isotopomer distribution data and the data simulated using method described in the method section (see 2.2.4).

2.4.10 Statistical analysis

Principal component analysis and one-way Anova were performed in MATLAB®. Student's t-tests were computed either in MATLAB® or Microsoft Excel.

Chapter 3 Metabolomics response resulting from *PIK3CA* mutant knock-in transformation in MCF10A breast cells

3.1 Abstract

Somatic mutations in *PIK3CA* are frequently found in human breast tumours, making the gene an attractive molecular target for early detection and personalised therapy (Wu *et al.* 2005). *PIK3CA* mutations contribute towards disease progression, and also impact upon the cellular physiology and drug resistance of the tumours. The MCF10A line is an important and relevant cell model for studying oncogenic transformation in breast tissues, as it is non-tumourigenic and retains many normal breast epithelial characteristics (Dawson *et al.* 1996). While the activation of cell signalling induced by mutant *PIK3CA* are well characterised at the molecular level, less is known about how mutant *PIK3CA* reprograms metabolism to facilitate physiological adaptation in MCF10A cells. Using metabolomics and ^{13}C stable isotope-labelled glucose and glutamine as tracers, we probed the phenotypic alterations of metabolism following a single copy knock-in of mutant *PIK3CA* (H1047R) in the non-transformed MCF10A cell line. We identified increased glutaminolysis, *de novo* fatty acid synthesis, pyruvate entry into the TCA cycle, and decreased glycerophosphocholine as the most prominent phenotypes following *PIK3CA* mutation.

3.2 Introduction

PIK3CA encodes for the 110kDa p110α subunit of the class 1 phosphatidylinositol 3-kinase (PI3K), a family of lipid kinases that are involved in regulating molecular growth and survival signalling. Along with *TP53*, *PIK3CA* is one of the two most frequently mutated genes in breast tumours, and a comprehensive study recently found that as much as 36% of all breast tumours harboured *PIK3CA* mutations (Koboldt *et al.* 2012). Some literature suggest *PIK3CA* mutation may have prognostic value in predicting survival outcome in breast cancer patients (Loi *et al.* 2010) – partly because *PIK3CA* mutations tend to be associated with hormone receptor-positive tumours that are responsive to hormone therapies (Pang *et al.* 2014). Somatic *PIK3CA* mutations are oncogenic and result in increased catalytic PI3K kinase activity. PI3K phosphorylates phosphatidylinositol 4,5-diphosphate (PIP_2) and produces phosphatidylinositol 3,4,5-triphosphate (PIP_3), a lipid second messenger that activates the PI3K-AKT signalling cascade (Vivanco and Sawyers 2002). The PI3K-AKT signalling pathway is important in cancer cells, as it is associated with many hallmarks of cancer, such as the cell cycle, genomic instability, angiogenesis and inflammatory response (Engelman *et al.* 2006, Liu *et al.* 2009). Consequently, as part of the drive towards targeted therapies, a number of small chemical inhibitors were developed to target the signalling pathway activity at various nodes, and many are currently in clinical trials. However, early results from these clinical trials generally showed limited single agent activity in advanced tumours. This is partly because PI3K pathway inhibition can lead to the selection for compensatory pathways which restore survival and tumour growth (Fruman and Rommel 2014). More effective treatments are currently required to help target the *PIK3CA*-mutant patient populations - one strategy that has been suggested is to exploit tumour metabolic dependency (DeBerardinis *et al.* 2008, Dang 2012) by discriminating the metabolic regulation of the various oncogenic mutations. Akt signalling has been reported to stimulate glucose metabolism (Elstrom *et al.* 2004), and mutant *PIK3CA* has also been shown to increase growth dependence on glucose (Foster *et al.* 2012).

MCF10A is a spontaneously immortalized non-tumorigenic mammary epithelial cell line derived from a 36-year old patient, and it displays many characteristics of

normal breast epithelium (Debnath *et al.* 2003). It is a valuable model for studying disease progression, epithelial-mesenchymal transition (Sarrio *et al.* 2008) and metabolism (Schafer *et al.* 2009) (Dawson *et al.* 1996, Ma *et al.* 2004, Fillmore and Kuperwasser 2008, Sarrio *et al.* 2008). By performing a series of metabolomics experiments in the non-transformed MCF10A mammary epithelial line, here we report the metabolic alterations resulting from a single copy knock-in of mutant *PIK3CA* (H1047R). We identified increased glutaminolysis, *de novo* fatty acid synthesis, pyruvate entry into the TCA cycle, and decreased glycerophosphocholine as the most prominent phenotypes following *PIK3CA* mutation.

3.3 Materials and Methods

MCF10A and PIK3CA H1047R (+/-) mutant MCF10A cells were purchased from Horizon Discovery. I was solely responsible for cell culture, performing proliferation assays, generating the ^{13}C-glucose and ^{13}C-glutamine labelled cell samples for metabolomics analysis, and for performing the ^{1}H NMR and GC-MS metabolomics analysis.

3.3.1 Cell Culture

MCF10A cells were cultured in DMEM/F12, supplemented with 5% horse serum, 0.1ug/ml cholera toxin, 20ng/ml hEGF, 10ug/ml insulin, 0.5 ug/ml hydrocortisone, and 2mM L-glutamine. Cells were cultured as a monolayer at 37° C in a humidified atmosphere with 5% CO2 under normal oxygen conditions. The cells were passaged every 3-4 days, and were split 1:8 -1:12 at ~ 80% confluency. Only low passage cells were used for experiments.

3.3.2 Proliferation assay

The number of viable cells in individual wells of 96-well plates was determined using the colorimetric cell counting kit-8 (CCK8) following the manufacturer's instructions (Sigma-Aldrich). The assay is based on the reduction of the WST-8 dye by cellular dehydrogenases to an orange formazan product that is soluble in tissue culture medium. The amount of the generated formazan is assumed to be directly proportional to the number of living cells. To assess the number of viable cells, 10 µl of the CCK8 reagent were added to wells in 96 well plates and incubated for 3 hours; the absorbance at 450 nM was then measured for each well and was subtracted from background.

3.3.3 Assessing impact of growth factors in the culture media

While MCF10A is spontaneously immortalized, growth factors such as EGF and insulin are normally used in routine cell culture to stimulate growth. However, both are critical modulators of multiple signalling pathways and hence it would be

desirable to observe their metabolic phenotypes with the additives removed. Thus, prior to the metabolic profiling, experiments on the impact of media change, from fully supplemented to without supplements, on growth phenotype in the wild type and mutant *PIK3CA* cells were assessed using a proliferation assay. Reduced growth factor availability did not affect the mutant *PIK3CA* cells. However, significant differences in growth were observed in the wild type cells by 48 hours (Figure 3.1). Hence, 24 hours was selected as the time period over which subsequent metabolomics experiments were conducted.

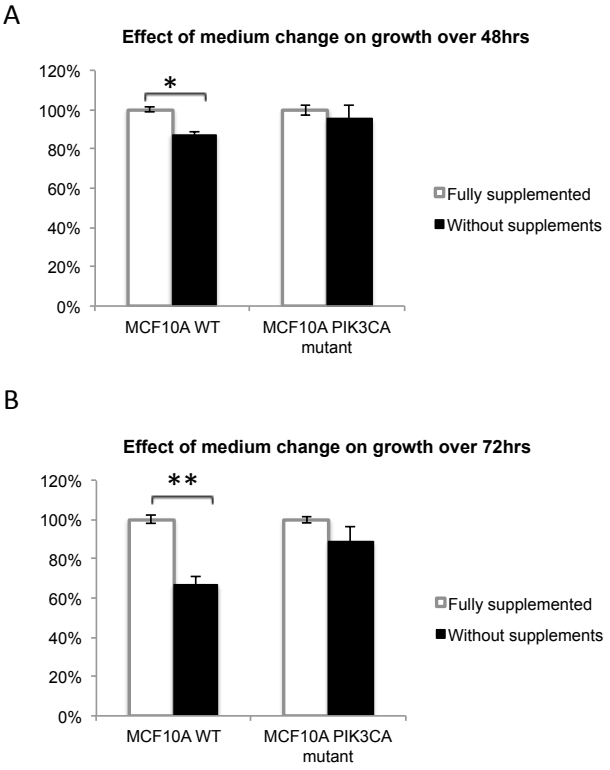

Figure 3.1 Effect of withdrawing supplements of cell growth in MCF10A

Effect of withdrawing supplements on MCF10A wild type and mutant *PIK3CA* cells over 48 hours (A) or 72 hours (B). Fully supplemented cells were provided with EGF, insulin, hydrocortisone and cholera toxin; growth was assessed using the CCK8 proliferation assay. The bar graphs represent the mean ± SEM from four technical replicates. Two-tailed Student's t tests were performed to evaluate the statistical significance of growth under the two conditions.

3.3.4 ^{13}C-glucose and ^{13}C-glutamine labelling experiment

On the day of seeding: after trypsinisation, MCF10A cells were resuspended in full media (DMEM/F12, supplemented with 5% horse serum, 0.1ug/ml cholera toxin, 20 ng/ml hEGF, 10 ug/ml insulin, 0.5 ug/ml hydrocortisone, 2 mM L-glutamine) and 120k cells were seeded per well on a six well plate and were allowed to adhere overnight. The medium was aspirated the next day (24 hours after seeding) and was replaced with experimental culture media, and incubated for 24 hours. The media used for the glucose-labelled experiment were as follow: glucose free, glutamine free, pyruvate free DMEM, supplemented with 10% dialysed-FBS (BioSera), and 11.2 mM U-$^{13}C_6$-glucose and 2mM L-glutamine. The media used for the glutamine-labelled experiment were as follow: glucose-free, glutamine-free, pyruvate-free DMEM, supplemented with 10% dialysed-FBS (BioSera), 11.2 mM glucose and 2 mM $^{13}C_5$-glutamine. Dialysed serum was used to filter out the serum small molecule metabolite background to ensure content consistency in the experiment. Three independent biological replicate experiments were performed with U-$^{13}C_6$ glucose, and four independent biological replicate experiments were performed with U-$^{13}C_5$ glutamine.

The samples were harvested after 24 hours. The media were collected and immediately placed on ice. The cell monolayer was washed with 500 μL of cold (4°C) Ringer's buffer, which was aspirated before the addition of 750 μL of cold methanol (straight from a -20°C freezer and kept cold in ethanol bath). The methanol-quenched cells were then scraped from the surface of the well and the entire sample was transferred to a clean 2 ml eppendorf tube. To increase metabolite recovery, each well was washed with a further 750 μL of cold methanol and pooled with the first sample. The methanol-quenched samples were dried down in a rotary evaporator under reduced pressure. Representative wells from each cell line/ condition were used for cell counting at the beginning and at the end of the experiments; cell counting was done using a Sceptor™ 2.0 Cell Counter (Millipore). For the extracellular media samples 1 ml of the culture media were transferred to fresh Eppendorf™ tubes, and were centrifuged (10 000 rpm, 5 min) to remove

potential cell debris. They were then stored at -80°C for subsequent analysis. Both dried down cell samples and media were stored in an -80°C freezer.

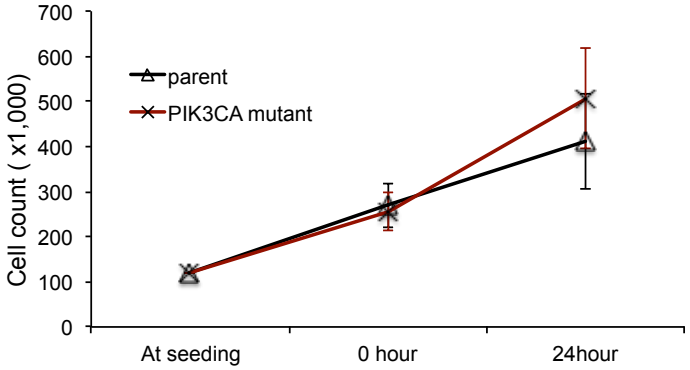

Figure 3.2 Growth in wild type MCF10A and *PIK3CA* mutant MCF10A cells

Cell counting data of the MCF10A wild type and mutant *PIK3CA* cells over the course of the ^{13}C-glucose and ^{13}C-glutamine labelling experiments. Cells were seeded 24 hours before they were replenished with ^{13}C labelled tracer-containing media. The graphs represent the mean ± SEM from a total of 7 replicates. The difference in cell number at 24 hours was not found to be statistically significant using two-tailed Student's t test.

3.4 Results

To investigate the metabolic alterations resulting from the single copy of knock-in mutant *PIK3CA* (H1047R) in MCF10A cells, stable isotope tracer and metabolomics experiments were performed on MCF10A *PIK3CA* H1047R (+/-) mutant cells, and results were compared to the isogenic parental line expressing wild type *PIK3CA*. Unlabelled glucose or glutamine was substituted with either uniformly ^{13}C-labelled glucose or uniformly ^{13}C-labelled glutamine, to enable discrimination of the fate of these two major nutrients. Also, careful consideration was given to the culture media composition used so the metabolite background at the start of the experiment could be controlled, while the effect of mutational status in the isogenic lines would not be masked by the addition of routine culture supplements (see 3.3.3). In addition, cell number at the beginning and at the end of the metabolomics experiment were measured, and no significant differences in growth between the wild type and PIK3CA mutant MCF10A cells were observed over the time-course of the experiment (Figure 3.2).

3.4.1 Culture medium analysis: mutant *PIK3CA* modulated extracellular pyruvate and glutamate release in the MCF10A cells

In culture, metabolite concentrations in the extracellular environment could trigger metabolic feedback (Argaud *et al.* 1997, Iyer *et al.* 2010) and regulate important functional phenotypes (Gao *et al.* 1999, Wu *et al.* 2012), and are thus valuable physiological indicators. We employed ^{1}H NMR to analyse the spent culture media sample, which enabled us to examine the consumption and release profiles of key metabolites, including the uptake of glucose, glutamine and choline, and the production of pyruvate, lactate, and non-glucose carbon derived glutamate (Figure 3.3). We noticed that extracellular pyruvate release was significantly decreased by ~40% ($p = 0.01$) in the *PIK3CA* mutant cells compared to the parental wild type cells. Pyruvate was predominantly an intermediate metabolite of glucose metabolism, with over 90% of the methyl carbon of pyruvate found to be glucose-derived in this cell model (Figure 3.3). However, despite a decrease in pyruvate release in the *PIK3CA* mutant cells, both glucose consumption and glucose-derived lactate release remained unaffected, suggesting that any alteration of the fate of

pyruvate was limited to either the fraction entering mitochondria or pyruvate converted to alanine. Furthermore, glutamate release and glutamine uptake were also affected in the *PIK3CA* mutant cells. Non-glucose-derived glutamate release, as assessed by the C4 glutamate proton resonance, doubled ($p = 0.02$) while glutamine uptake recorded an approximately 50% increase (pairwise t test p value < 0.05) in the *PIK3CA* mutant cells compared to the wild type parental line, signifying up-regulation of glutamine utilisation and metabolism. Glutamine, once imported into the cells was converted to αKG via glutamate to replenish substrates in the TCA cycle, and glutaminolysis has been reported to support growth and survival in rapidly proliferating tumour cells (DeBerardinis *et al.* 2007). Overall, our data on extracellular pyruvate, glutamine and glutamate suggest that metabolic substrate entry into the TCA cycle might have been altered in the transformed *PIK3CA* mutant cells. In addition, we were also able to measure uptake of extracellular choline in the culture media, and we found no significant differences between the *PIK3CA* mutant and the wild type MCF10A parental cells.

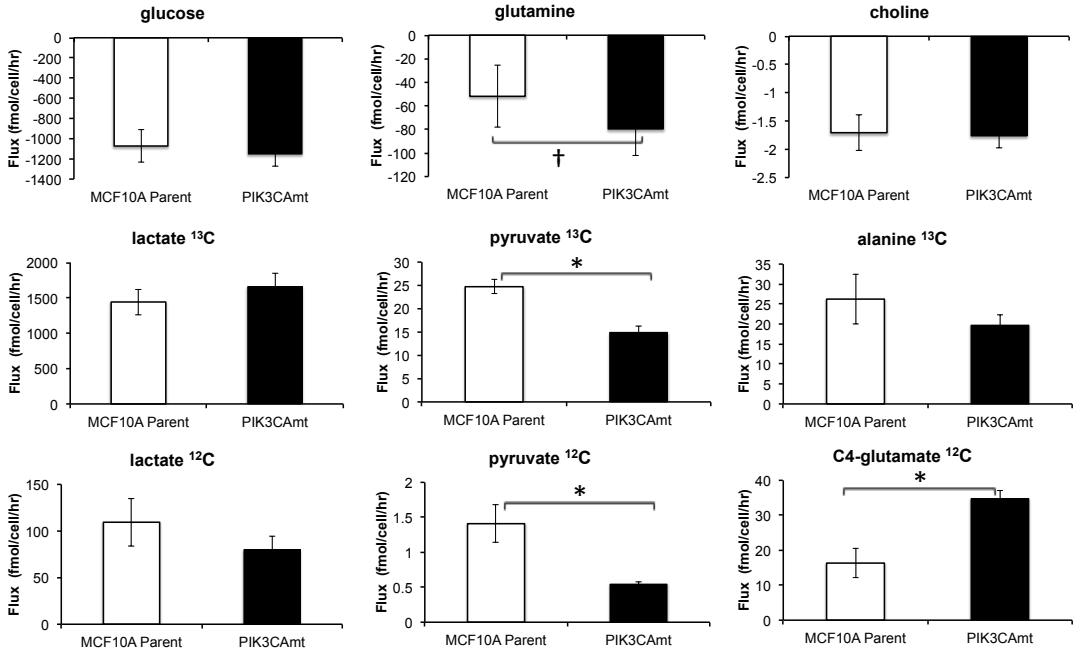

Figure 3.3 MCF10A metabolite consumption and release from culture medium

Samples from U-$^{13}C_6$ glucose tracer experiment harvested after 24 hours were analysed by ^{1}H NMR. Negative values indicate consumption and positive values indicate net efflux; detailed resonance assignments can be found in the supplementary section. Bar graphs represent mean ± SEM from three independent biological replicates. * denotes two-tailed t-test p values < 0.05; † denotes pairwise t-test p values < 0.05

3.4.2 Intracellular aqueous metabolites analysis: pyruvate entry into TCA cycle is altered in the *PIK3CA* transformed cells

GC-MS profiling of the intracellular metabolites from the U-$^{13}C_6$ glucose and U-$^{13}C_5$ glutamine labelled cultures enabled us to systematically compare the relative abundance of metabolites between the *PIK3CA* mutant and the non-transformed cells, to determine the ^{13}C mass isotopomer distribution, and to apportion the overall molecular carbons derived from glucose and glutamine for each metabolite. When examining the relative abundance data, we found the relative quantities of glycolytic intermediates (dihydroxyacetone phosphate, PEP, 3PG) and TCA cycle intermediates (αKG, fumarate, malate, glutamate) to be consistently higher (pairwise t test $p < 0.05$) in the mutant cell samples (Figure 3.4, Figure 3.5), possibly indicating that the metabolic demand for energy generation was higher in the *PIK3CA*-transformed cells. At the same time we found glutamine to be an important metabolic precursor to TCA cycle intermediates. While glucose and glutamine each contributed approximately equally to the citrate carbon skeleton (around 30% each), glutamine accounted for over 40% of the malate and fumarate carbons versus <30% from glucose (Figure 3.6, Figure 3.7). This demonstrates that glutamine was a more substantial carbon donor than glucose in maintaining TCA cycle activity in the MCF10A cells and that the carbon flow was predominantly in the oxidative direction of the TCA cycle. It is conceivable that the increased glutamine uptake and glutamate production, as revealed through the extracellular media data, were used to fuel higher TCA activities in the mutant *PIK3CA* MCF10A cells. Furthermore, by closely inspecting the mass isotopomer distributions of individual metabolites we detected sizeable and significant shifts in the means by which ^{13}C glucose carbons were incorporated into citrate (Figure 3.8). In particular, the citrate M2 labelled from the U-$^{13}C_6$ glucose tracer increased by one third ($p < 0.005$), whereas citrate M3 labeling decreased by one half ($p < 0.05$) in the *PIK3CA* mutant cells. The synthesis of citrate is normally catalysed by citrate synthase, which utilises four-carbon oxaloacetate and two-carbon acetyl-CoA as substrates. Mitochondrial acetyl-CoA is predominately derived from pyruvate via pyruvate dehydrogenase activity whereas oxaloacetate can be formed by carboxylation of pyruvate or oxidation of malate. Importantly, pyruvate dehydrogenase contributes to citrate M2 labels ($^{13}C_6$ glucose

→ $^{13}C_3$ pyruvate → $^{13}C_2$ acetyl-CoA → $^{13}C_2$ citrate) and pyruvate carboxylase contributes to citrate M3 labels ($^{13}C_6$ glucose → $^{13}C_3$ pyruvate → $^{13}C_3$ oxaloacetate→$^{13}C_3$ citrate). The increase in M2 citrate labels accompanied by the decrease in M3 citrate labels indicated that pyruvate entry into citrate via pyruvate dehydrogenase occurred more rapidly in the *PIK3CA* mutant MCF10A cells.

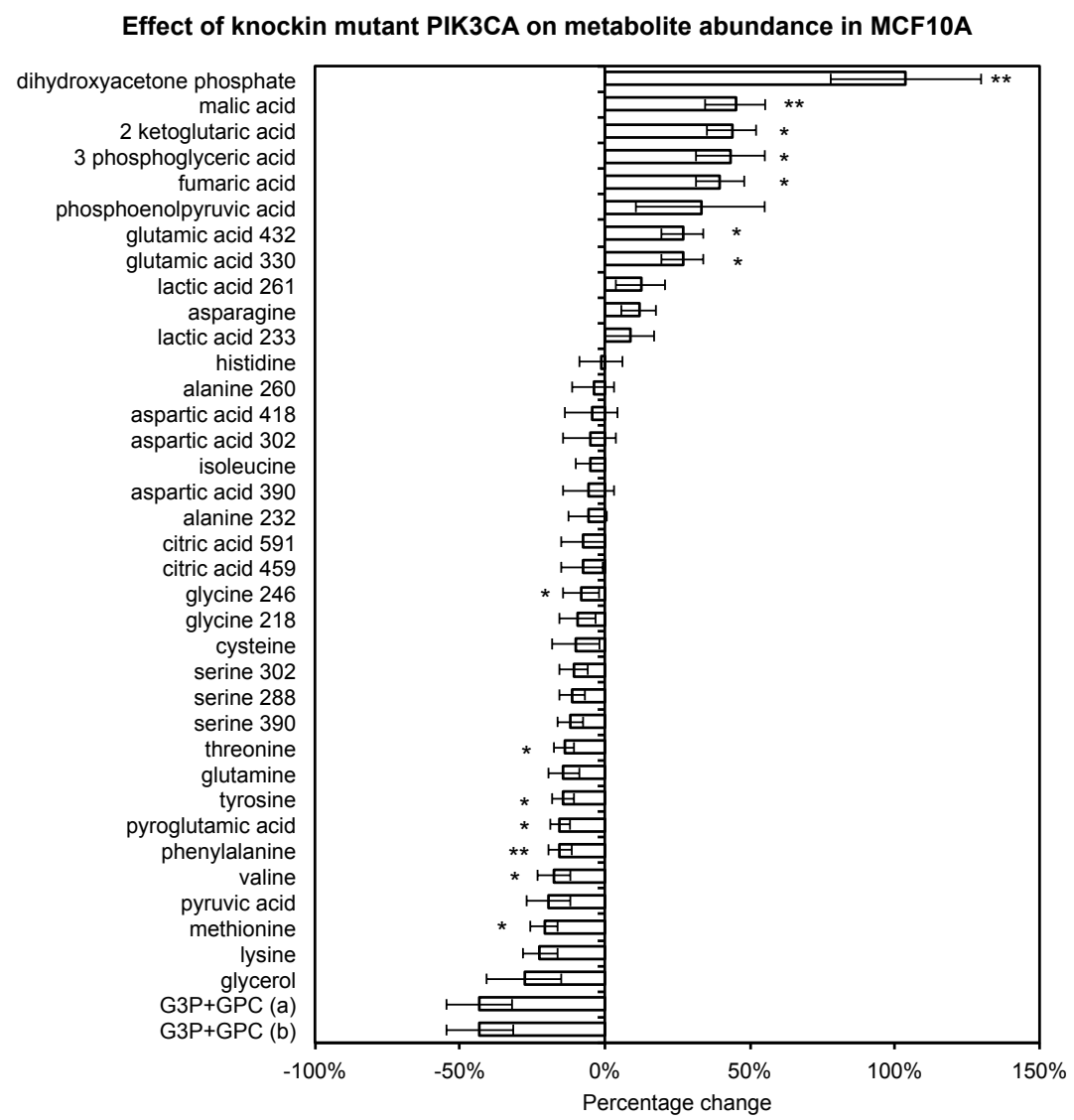

Figure 3.4 *PIK3CA* mutation altered intracellular aqueous metabolite abundance in MCF10A cells

Analysis was performed by GC-MS and data from both U-$^{13}C_6$ glucose and U-$^{13}C_5$ glutamine tracer experiments are included. The raw integrals were normalised through median fold change normalisation (Dieterle et al. 2006). The bar graphs represent the mean ± SEM. Seven separate biological experiments are represented and the metabolite features are ranked according to the magnitude of difference between the mutant PIK3CA and the wild type parental line, with positive change representing an increase in the mutant compared to wild type cells. Multiple mass ion fragments may be detected for some metabolites; in those cases the m/z values of the distinct fragments are given e.g. lactate 261 (see Figure 3.5). Glycerophosphocholine+glycerol-3 phosphate (GPC+G3P) was eluted at two separate retention times; * pairwise t test p values < 0.05; ** pairwise t test p values < 0.005.

GC/MS profile: Effect of PIK3CA knockin mutation on aqeuous metabolite abundance in MCF10A						
MS features	m/z	RI	% change	± error	T-test p value	FDR
dihydroxyacetone phosphate	484	2006	104%	26%	0.002	0.04
malic acid	419	1753	45%	10%	0.001	0.04
2 ketoglutaric acid	346	1652	44%	9%	0.007	0.06
3 phosphoglyceric acid	585	2254	43%	12%	0.022	0.07
fumaric acid	287	1449	40%	8%	0.013	0.06
phosphoenolpyruvic acid	453	1867	33%	22%	0.179	0.26
glutamic acid 432	432	1912	27%	7%	0.019	0.07
glutamic acid 330	330	1912	27%	7%	0.008	0.06
lactic acid 261	261	1154	12%	8%	0.151	0.24
asparagine	417	1945	12%	6%	0.154	0.24
lactic acid 233	233	1154	9%	9%	0.545	0.56
histidine	440	2220	-1%	8%	0.265	0.33
alanine 260	260	1195	-4%	7%	0.613	0.61
aspartic acid 418	418	1793	-5%	9%	0.458	0.48
aspartic acid 302	302	1793	-5%	9%	0.452	0.48
isoleucine	302	1379	-5%	5%	0.194	0.28
aspartic acid 390	390	1793	-5%	9%	0.415	0.46
alanine 232	232	1195	-6%	7%	0.304	0.35
citric acid 591	591	2223	-8%	8%	0.289	0.34
citric acid 459	459	2223	-8%	7%	0.289	0.34
glycine 246	246	1223	-8%	6%	0.049	0.13
glycine 218	218	1223	-9%	6%	0.052	0.13
cysteine	406	1845	-10%	8%	0.137	0.23
serine 302	302	1628	-11%	5%	0.091	0.17
serine 288	288	1628	-11%	5%	0.081	0.15
serine 390	390	1628	-12%	5%	0.122	0.21
threonine	404	1659	-14%	4%	0.007	0.06
glutamine	431	2061	-14%	5%	0.067	0.15
tyrosine	466	2269	-14%	4%	0.025	0.08
pyroglutamic acid	300	1596	-15%	3%	0.003	0.04
phenylalanine	336	1732	-15%	4%	0.019	0.07
valine	288	1310	-17%	6%	0.015	0.06
pyruvic acid	174	941	-19%	8%	0.061	0.14
methionine	320	1610	-21%	5%	0.014	0.06
lysine	431	2019	-22%	6%	0.051	0.13
glycerol	377	1522	-28%	13%	0.080	0.15
G3P+GPC (a)	571	2160	-43%	11%	0.235	0.30
G3P+GPC (b)	571	2205	-43%	12%	0.223	0.30

Figure 3.5 Assignment and quantification of GC-MS detected metabolite features

The identities of the GC/MS features were confirmed either through running standards or matching to the NIST library. RI represents retention time indices. The data represent averages and SEM from seven biological replicate experiments and metabolites are ranked by the magnitudes of percentage changes. Pairwise Student's t-tests and false discovery rate (Benjamini and Hochberg procedure) analysis were used to evaluate statistical significance. FDR values and t test p values of < 0.05 are highlighted in red.

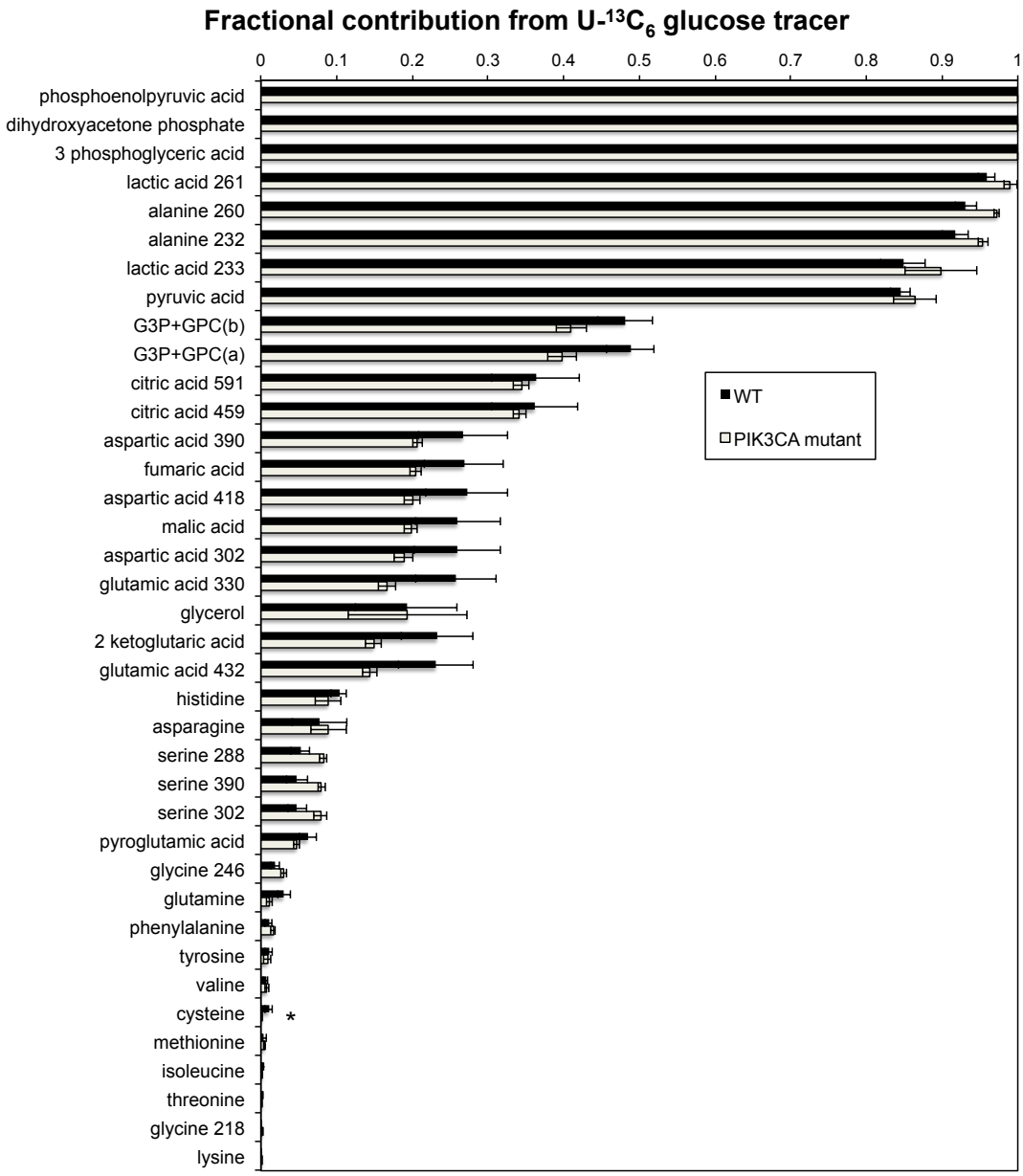

Figure 3.6 ^{13}C glucose carbon incorporation into aqueous metabolites

Incorporation is calculated using the natural abundance-corrected mass isotopomer distribution (MID) data from the U-$^{13}C_6$ glucose tracer cultured samples. The bar graphs represent the mean ± SEM from three separate biological replicate experiments. * two-tailed Student's tttest $p < 0.05$. Multiple mass ion fragments may be detected for some metabolites; in those cases the m/z values of the distinct fragments are given e.g. lactate 261 (see Figure 3.5). GPC+G3P was eluted at two separate retention times.

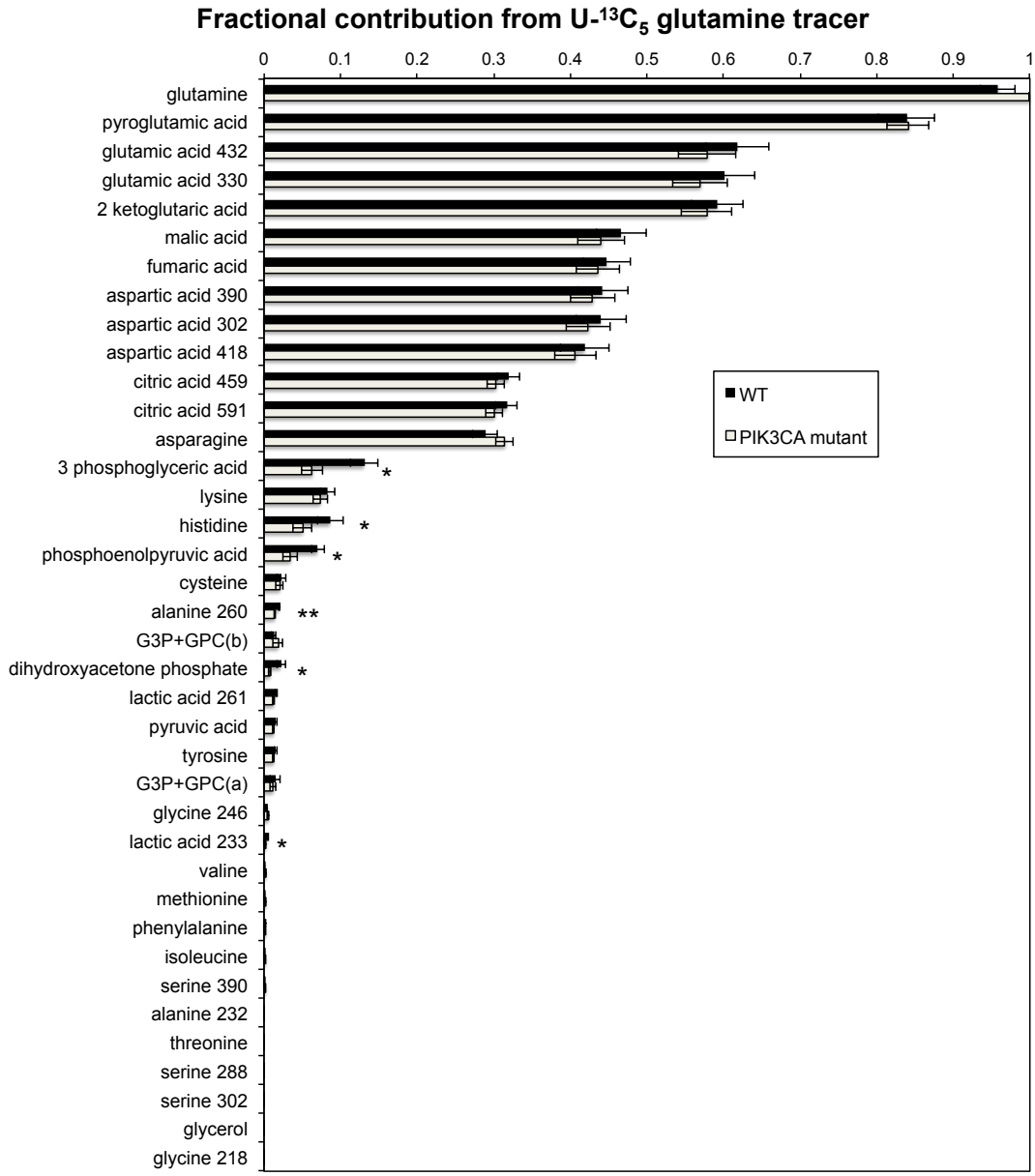

Figure 3.7 ^{13}C glutamine carbon incorporation into aqueous metabolites

Incorporation is calculated using the natural abundance-corrected mass isotopomer distribution (MID) data from the U-$^{13}C_5$ glutamine tracer experiments. The bar graphs represent the mean ± SEM from four separate biological replicate experiments. * two-tailed Student's t-test $p < 0.05$; ** two-tailed Student's t-test $p < 0.005$. Multiple mass ion fragments may be detected for some metabolites; in those cases the m/z values of the distinct fragments are given e.g. lactate 261 (see Figure 3.5). Glycerol-3 phosphate+ glycerophosphocholine (G3P+GPC) was eluted at two separate retention times.

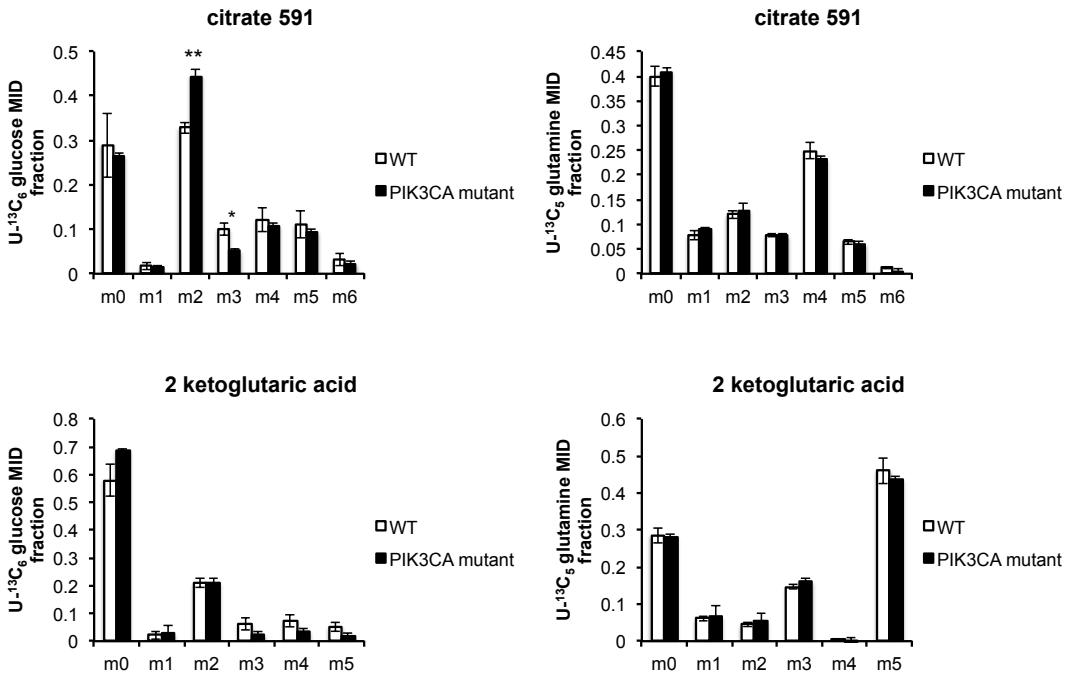

Figure 3.8 Comparison of mass isotopomer distribution (MID) of citrate and 2-ketoglutaric acid (αKG) from ^{13}C glucose and glutamine tracers

In the glutamine tracer data, the bar graphs represent the mean ± SEM from four separate biological replicate experiments. In the glucose tracer data, the bar graphs represent the mean ± SEM from three separate biological replicate experiments in the glucose tracer data. ** two-tailed Student's t-test $p < 0.005$; * two-tailed Student's t-test $p < 0.05$.

3.4.3 Analysis of lipid species: increased *de novo* lipid synthesis in the *PIK3CA* mutant MCF10A

Intracellular lipid species were analysed by GC-MS using an extraction and derivatisation method that enabled both fatty acid esters and free fatty acids in the samples to be detected. The origins of the fatty acid methyl esters detected were not restricted to a specific class of lipid molecule, but they were instead fatty acid chain components from a broad range of lipid molecules that were transesterified in the extraction process. These transesterified fatty acids could come from membrane phospholipids such as phosphatidylcholine or signalling and functional lipids such as phosphatidic acid or diacylglycerol. Our analysis was more successful in quantifying fatty acid methyl esters, and we were able to examine the relative abundance of a number of lipid species (Figure 3.9). For example we found that both ratios of esterified linolenate to palmitate and esterified linolenate to oleate were significantly lower (pairwise t-test $p < 0.05$) in the *PIK3CA* mutant extracts. Whereas oleate and palmitate can be synthesised *de novo*, linolenate (C18:3) is an essential polyunsaturated fatty acid in mammalian cells and must be imported from the culture medium directly; our data indicated there was a possible shift in the *PIK3CA* mutant cells, away from relying on fatty acid uptake and towards *de novo* biosynthesis. Furthermore, the mass isotopomer data from U-$^{13}C_6$ glucose and U-$^{13}C_5$ glutamine both provided strong independent evidence that the rate of *de novo* biosynthesis of fatty acids was elevated in the *PIK3CA* mutant cells. In particular, we found increased incorporation of both glucose and glutamine derived two-carbon acetyl-CoA units into methyl palmitate (Figure 3.10, Figure 3.11), the most abundant fatty acid chain in mammalian cells. By modelling the mass isotopomer distribution of methyl palmitate using Isotopomer Spectral Analysis (ISA), a technique that untangles the effect of changes in the acetyl CoA pool contribution from the biosynthetic rate (see section 2.2.4), it was established that the increases in ^{13}C tracer label incorporation were results of higher rates of *de novo* biosynthesis in the *PIK3CA* mutant cells (Figure 3.12, Figure 3.20). According to the U-$^{13}C_5$ glutamine data methyl palmitate *de novo* biosynthesis was higher by around 50% ($p < 0.05$) in the *PIK3CA* mutant cells compared to the wild type MCF10A parental line. Additionally, the modelled data suggest that glucose-derived citrate was

preferentially used as substrate for forming lipogenic acetyl-CoA; roughly 60% of acetyl-CoA came from glucose as opposed to around 10% from glutamine (Figure 3.12).

Effect of mutant PIK3CA on lipid metabolite abundance in MCF10A				
lipid metabolite ratios		% change	error (SEM)	pairwise t test
methyl palmitate, ratio to	methyl oleate	9%	8%	0.98
	methyl stearate	21%	7%	0.10
	oleic acid	17%	3%	0.01
	methyl linolenate	22%	7%	0.03
methyl oleate, ratio to	methyl palmitate	-5%	7%	0.22
	methyl stearate	-4%	12%	0.65
	oleic acid	11%	7%	0.10
	methyl linolenate	14%	5%	0.03
methyl stearate, ratio to	methyl palmitate	-17%	5%	0.09
	methyl oleate	8%	15%	0.73
	oleic acid	2%	10%	0.95
	methyl linolenate	14%	5%	0.07
methyl linolenate, ratio to	methyl palmitate	-16%	5%	0.03
	methyl oleate	-11%	4%	0.04
	methyl stearate	-12%	4%	0.12
	oleic acid	-2%	6%	0.72
oleic acid, ratio to	methyl palmitate	-14%	2%	0.03
	methyl oleate	-7%	6%	0.47
	methyl stearate	1%	9%	0.97
	methyl linolenate	5%	6%	0.42

Figure 3.9 Lipid metabolite ratios are altered in the *PIK3CA* mutant cells

Analysis was performed by GC-MS and data from both U-$^{13}C_6$ glucose U-$^{13}C_5$ glutamine tracer experiments were included. Both free fatty acids and fatty acid methyl esters were detected. Averages and S.E.M. from seven separate biological experiments are represented (apart from methyl stearate where S/N was low and data from only three independent biological replicates were included).

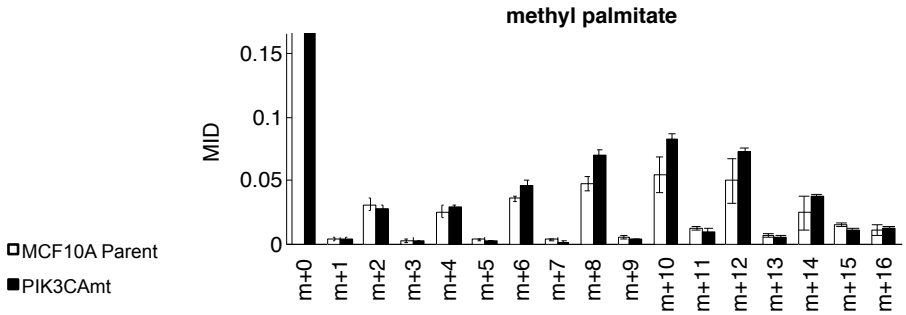

Figure 3.10 U-$^{13}C_6$ glucose carbon incorporation into transesterified palmitate.

The bar graphs represent the mean ± SEM from three separate biological experiments.

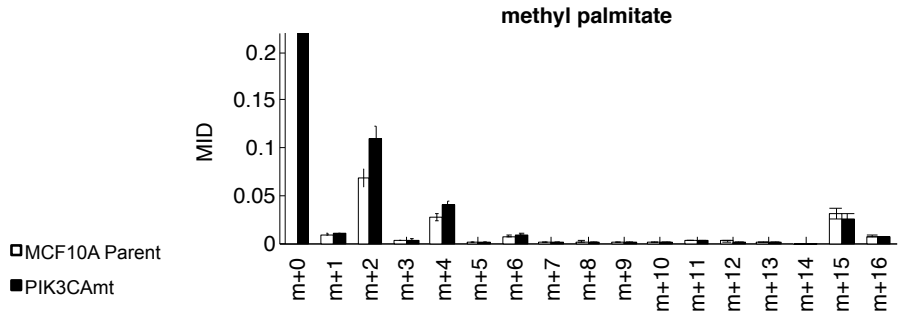

Figure 3.11 U-$^{13}C_5$ glutamine carbon incorporation into transesterified palmitate

The bar graphs represent the mean ± SEM from four independent biological experiments.

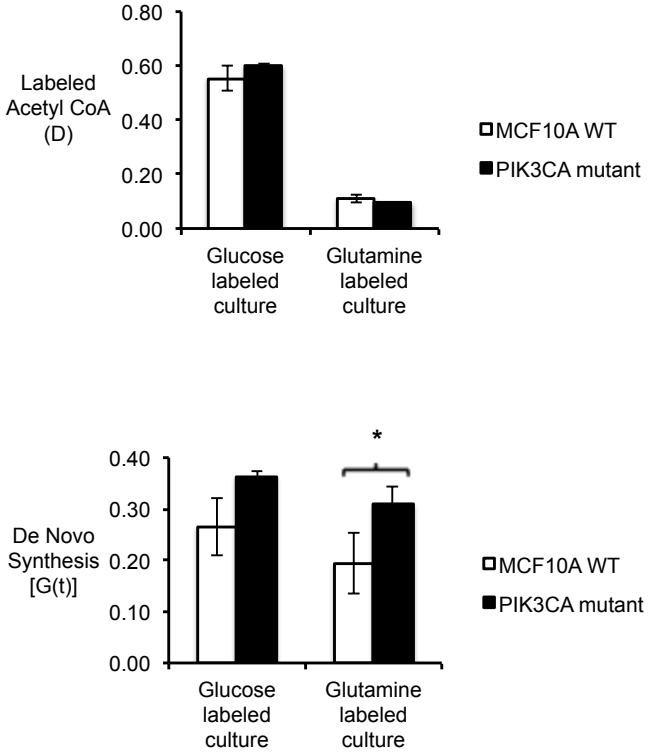

Figure 3.12 Modelled metabolic parameters from fatty acid Isotopomer Spectral Analysis (ISA)

In the glutamine tracer data, the graphs represent the mean ± SEM from four independent biological replicate experiments and in the glucose tracer data the graphs represent the mean ± SEM data from three independent biological replicate experiments. Two-tailed Student's t-test was used to determine statistical significance, and * denotes $p < 0.05$.

3.4.4 Analysis of glycerophosphocholine

During the analysis of the intracellular aqueous metabolites, we noted a substantial drop of around 40% (not reaching significance) in the relative abundance of [glycerol-3 phosphate (G3P) + glycerophosphocholine (GPC)] in the *PIK3CA* mutant cells, ranking it the most down-regulated metabolite feature in this study (Figure 3.4). The mass fragment (m/z: 591) represents the primary ion fragment from the derivatisation of G3P and the ambiguity of the assignment is down to the fact that the choline moiety in GPC can spontaneously detach under high temperature leaving the remaining molecule to be derivatised as G3P. Hence, subsequent to the initial analysis, additional analysis of G3P and GPC standards was performed on the GC-MS instrument under the same protocol to find additional mass fragments that discriminated between the two metabolites. We were able to identify a distinct GPC fragment peak (m/z: 325) and a putative structure for the fragment (Figure 3.13). Furthermore by referring back to the original sample data acquired under full scan mode, we found remarkable similarity in the patterns of U-$^{13}C_6$ glucose mass isotopomer distributions between GPC and the ambiguously assigned [G3P+GPC] ion fragments (Figure 3.14), suggesting that GPC contributed substantially to the [G3P+GPC (m/z: 591)] fragment signals in the dataset. Moreover, the U-$^{13}C_6$ glucose mass isotopomer distribution data showed GPC M3 levels were lower in the *PIK3CA* mutant cells ($p = 0.08$, Figure 3.14), indicating that the turnover of GPC and its glucose-derived glycerol carbon backbone were possibly lower in the *PIK3CA* mutant MCF10A. In addition, the level of GPC was also quantified using ^{1}H NMR, where samples were analysed in the aqueous phase rather than in the gaseous phase, and approximately 50% drop in both GPC: choline ($p = 0.08$) and GPC: PCho ($p = 0.13$) ratios were observed (Figure 3.15, Figure 3.19).

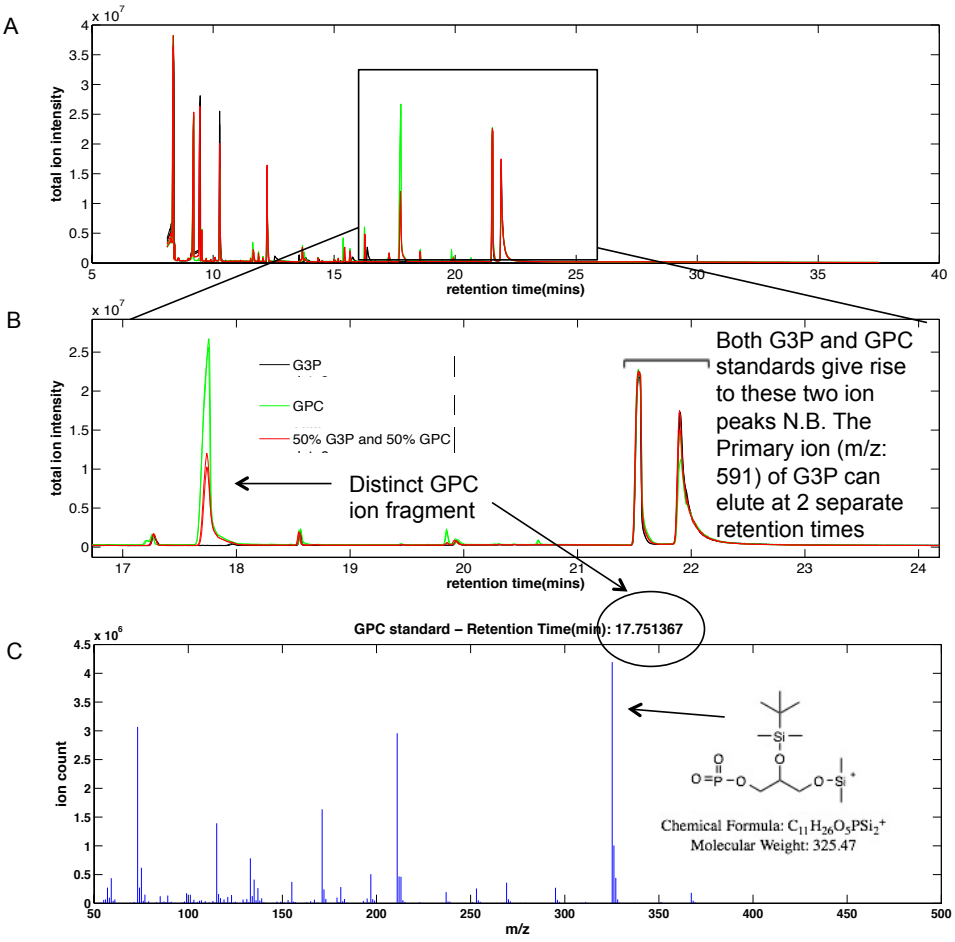

Figure 3.13 GC-MS Assignment of glycerophosphocholine (GPC) fragment through standard runs

Standards of GPC (green), G3P (black) were made up to 1mg/ml and, additionally a standard of 50:50 GPC:G3P mix (red) from the 1mg/ml stocks was also made up. Standards were run under identical protocols to the MCF10A cell samples. (A) The full GC-MS total ion chromatogram. (B) Enlarged version of the GC-MS total ion chromatogram. (C) Mass spectrum at RT 17.75mins from the GPC standard sample showing the dominant ion fragment (m/z 325) and its putative structure.

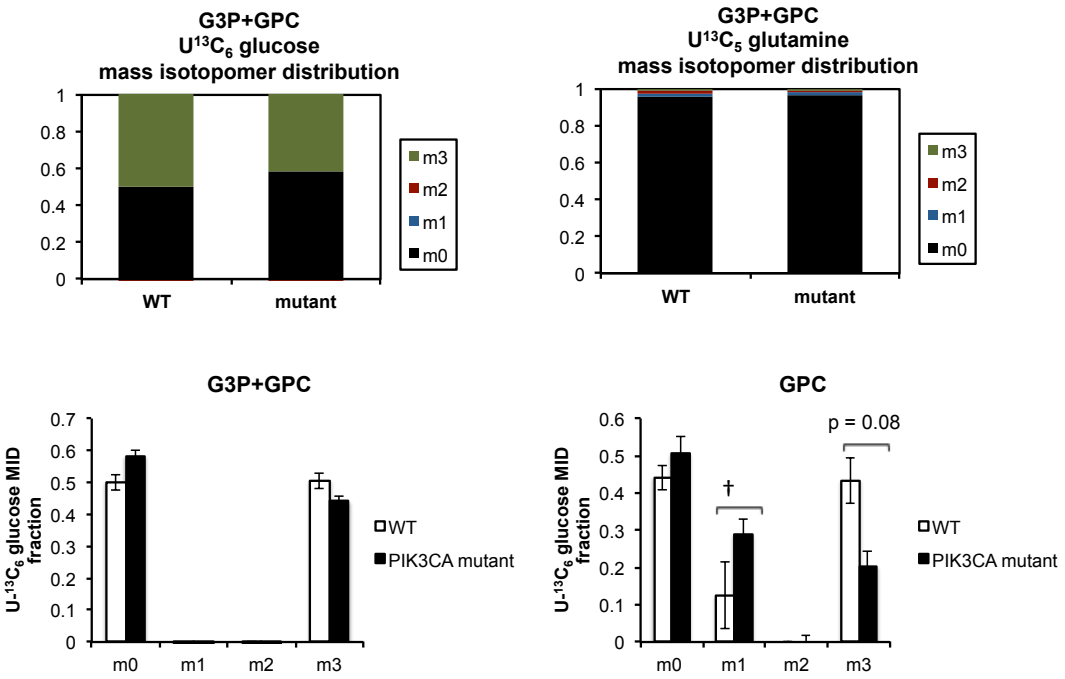

Figure 3.14 The glycerol carbon backbone of glycerophosphocholine is derived primarily from glucose, but not glutamine

Alteration in glycerophosphocholine (GPC) glucose carbon mass isotopomer distribution could be responsible for the changes observed in the overall G3P+GPC pool. The bar graphs represent the mean ± SEM from three separate biological replicate experiments. † glycerophosphocholine m1 label (m/z: 326) signals were interfered by other background ion fragments.

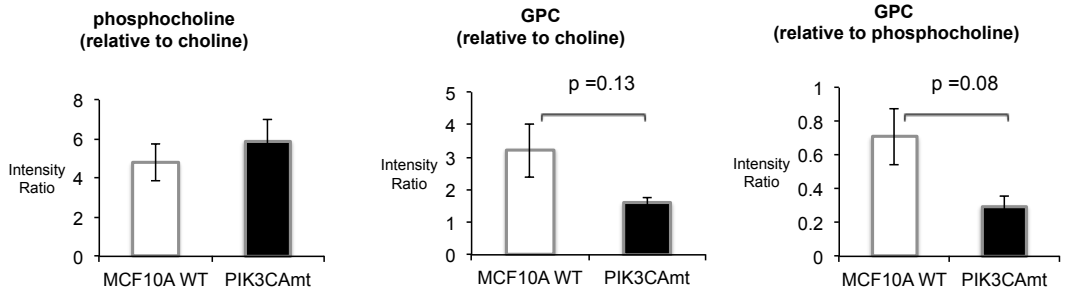

Figure 3.15 Analysis of intracellular choline, phosphocholine and glycerophosphocholine by ^{1}H NMR

The bar graphs represent the mean ± SEM from three separate biological replicate experiments. Details of resonance assignment can be found in section 3.6.

3.5 Discussion

3.5.1 *PIK3CA* transformation and metabolic reprogramming in MCF10A

In this study, the metabolic alterations induced by a single copy knock-in of mutant *PIK3CA* (H1047R) were evaluated in the MCF10A mammary epithelial cells. MCF10A is an immortalised, non-transformed cell line retaining many features of normal breast epithelium (Debnath *et al.* 2003), and is widely used to study the phenotypic changes of oncogenic transformations. The signalling pathway modulation resulting from the mutant knock-in *PIK3CA* (H1047R) in the MCF10A cells have previously been characterised, and it was reported that the three main recurrent somatic *PIK3CA* hotspot mutations (H1047R/E542K/E545K) all promote constitutive Akt and Erk activation in MCF10A, leading to growth factor independent growth (Isakoff *et al.* 2005, Gustin *et al.* 2009). We found that *PIK3CA* mutant transformation in MCF10A modulated cellular metabolism, including the metabolic fate of pyruvate. Cells with mutant *PIK3CA* exhibited reduced pyruvate efflux into the culture medium and increased pyruvate conversion into acetyl-CoA to fuel TCA biogenesis, suggesting that pyruvate dehydrogenase activity may be modulated as a result of the mutation. Insulin, a potent activator of PI3K/Akt pathway, is known to up-regulate pyruvate dehydrogenase activity (Coore *et al.* 1971), however this may be mediated through MAPK signalling (Johnson and Denton 2003). Elevated pyruvate dehydrogenase flux resulting from down-regulation of pyruvate dehydrogenase kinase isoform-4 has also been reported in ErbB2-overexpressing MCF10A cells (Grassian *et al.* 2011); ErbB2 expression also elevates PI3K and MAPK signalling. While *PIK3CA* transformation may up-regulate pyruvate dehydrogenase activity, this is down-regulated in the *HRAS* transfected MCF10A cells (Zheng *et al.* 2013), illustrating that different oncogenes can promote distinct pyruvate dehydrogenase modulations. It is likely that mutant *PIK3CA* modulates metabolic flux through enhanced kinase activity involving both PI3K/Akt and MAPK signalling.

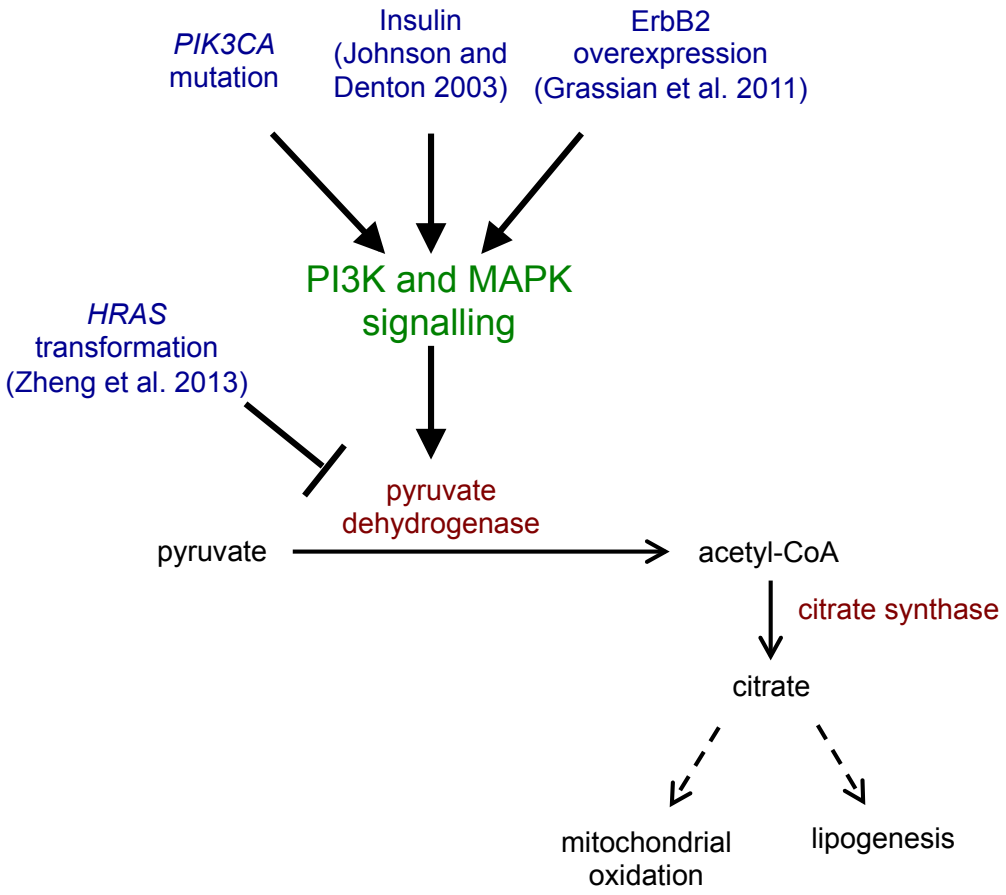

Figure 3.16 Pyruvate dehydrogenase regulation and oncogenic transformation in MCF10A

Moreover, we found evidence of increased glutamine uptake and glutamate production in the *PIK3CA* transformed cells. It has been reported that mutant *PIK3CA* enhances ATP generation in MCF10A cells (Schafer *et al.* 2009), and the additional energy supply could be met through increased mitochondrial oxidation and glutaminolysis, a process which is normally under the transcriptional control of c-myc (Wise *et al.* 2008). PTEN is a phosphatase which acts to reverse PI3K activity, and has been shown to repress c-myc and glutaminolysis in mice (Garcia-Cao *et al.* 2012). Furthermore, we also showed that mutant *PIK3CA* stimulated *de novo* fatty acid biosynthesis in MCF10A cells. Proliferating transformed cells are often required to meet their higher biomass demand either by lipid scavenging, as has been reported in *KRAS* transformed cells (Kamphorst *et al.* 2013), or through increased *de novo* synthesis. Many metabolic genes involved in the *de novo* synthesis pathway are transcriptionally regulated by SREBP, a downstream target of the Akt/mTORC1 signalling (Porstmann *et al.* 2008). Also ATP citrate lyase has been

reported to be a direct phosphorylation target of Akt (Berwick *et al.* 2002) and is responsible for delivering lipogenic acetyl-CoA. It is likely that ATP citrate lyase and SREBP may be up-regulated to support *de novo* fatty acid biosynthesis in the event of a knock-in *PIK3CA* mutation.

3.5.2 Regulation of glycerophosphocholine metabolism

A decrease in the glycerophosphocholine to phosphocholine ratio has previously been reported to be associated with disease progression and immortalization in mammary epithelial cells (Aboagye and Bhujwalla 1999). Here we observed evidence of decrease in glycerophosphocholine (not reaching statistical significance) specifically following *PIK3CA* transformation, while other PI3K inhibitor studies using ^{1}H NMR have also reported an alteration in the glycerophosphocholine and phosphocholine phenotype (Beloueche-Babari *et al.* 2006, Romanska *et al.* 2009, Al-Saffar *et al.* 2010). Previous studies have mainly attributed phosphocholine levels to changes in choline kinase expression (Al-Saffar *et al.* 2010, Yalcin *et al.* 2010), which converts choline to phosphocholine. However, less is known about the regulation of glycerophosphocholine. Interestingly, in this study the apparent changes in glycerophosphocholine appeared to be independent of choline uptake capacity, and are unlikely to be accounted for by the differences in cell growth alone (Figure 3.2). The origin of changes in the glycerophosphocholine phenotype remains unclear, but it has been suggested that reduced glycerophosphocholine turnover following oncogenic transformation could be indicative of lower phosphatidylcholine degradation upon enhanced survival signalling (Dawson 1955, Zablocki *et al.* 1991).

3.5.3 Limitations and Future work

In this study, we described a series of metabolic alterations following a single copy knock-in *PIK3CA* (H1047R) mutation in MCF10A breast cells, which included *de novo* fatty acid synthesis, pyruvate entry into mitochondria, and the GPC metabolite level. Our data suggest that the *PIK3CA* (H1047R) mutation led to increased fatty acid synthesis in the MCF10A cells; future experiments could focus on the characterisation of lipids in this cell model by taking other lipogenic parameters into

account, such as by measuring lipid droplets and probing for changes in mobile lipid resonances using NMR spectroscopy.

MCF10A is non-tumourigenic with different characteristics to breast tumour cell lines (Debnath *et al.* 2003). Different breast tumour cell lines have distinct mutation and signalling backgrounds that could interact with the effect of knock-in *PIK3CA* mutation (Cully *et al.* 2006). Thus, the effect of knock-in *PIK3CA* mutation on metabolite regulation is also likely to be context-dependent. Furthermore, knock-in *PIK3CA* mutation using additional cell lines might help elucidate the effect of genetic and signalling interactions on cellular metabolic behaviour. The use of *PTEN*-deleted cell models, and PI3K/AKT inhibitors and activators may also be beneficial to ascertain if *PIK3CA* mutation-induced metabolic alterations may be reversible at the signalling level.

Also, knock-in *PIK3CA* mutation introduced wholesale changes in MCF10A cells, and its effect on metabolism could in principle be mediated via regulatory changes at the transcriptional, as well as at the kinase signalling level. Given previous studies using alternative PI3K signalling stimuli have also found alterations in pyruvate, fatty acid, and glutamine metabolism (Coore *et al.* 1971), consequences of kinase signalling modulation were likely to have played a key role in determining the metabolic outcome observed in our cell model. Molecular characterisation of signalling events would be important in future studies.

One major challenge to the interpretation of the isotopomer distribution data presented is the small magnitude of changes observed. Future studies could incorporate metabolic modelling to explicitly confirm the changes in metabolic flux.

3.5.4 Conclusion

This study demonstrates that the key metabolic phenotypes associated with *PIK3CA* mutation in MCF10A cells include enhanced *de novo* fatty acid synthesis and increased pyruvate entry into mitochondrial citrate. Furthermore, evidence for *PIK3CA*-induced glycerophosphocholine down-regulation was also presented,

highlighting the potential of glycerophosphocholine as a physiological marker for tumourigenesis in this model.

3.6 Supplementary data

Flux (fmol/cell/hr)	Parental WT Mean	Parental WT SEM	PIK3CA mutant Mean	PIK3CA mutant SEM	% change	t-test p value two-tailed	t-test p value paired
alanine ^{13}C	26	6	20	3	-25%	0.39	0.44
choline	-1.7	0.3	-1.8	0.2	3%	0.89	0.76
glucose ^{13}C	-1072	159	-1152	120	7%	0.71	0.49
glutamate (C4) ^{12}C	16	4	35	2	113%	0.02	0.08
glutamine	-52	26	-80	22	54%	0.47	0.04
lactate ^{12}C	109	25	80	14	-27%	0.37	0.16
lactate ^{13}C	1443	184	1661	194	15%	0.46	0.27
pyruvate ^{12}C	1.4	0.3	0.5	0.04	-61%	0.03	0.06
pyruvate ^{13}C	25	1	15	1	-40%	0.01	0.08

Figure 3.17 Extracellular consumption and release profile

The table above represents data from three independent biological replicate experiments

Assignment	ppm	moiety	Signal range (ppm)
alanine ^{13}C	1.36	$^{13}C\mathbf{H_3}CH(NH_2)COOH$	1.336 - 1.374
choline	3.19	$(C\mathbf{H_3})_3N(CH_2)_2OH$	3.19 - 3.195
glucose ^{13}C	5.08	Carbon-1 α anomeric H	5.054 - 5.106
glutamate (C4) ^{12}C	2.34	$HOOCCH(NH_2)CH_2C\mathbf{H_2}COOH$	2.317 - 2.36
glutamine	2.42	$HOOCCH(NH_2)CH_2C\mathbf{H_2}COH_2N$	2.407 - 2.454
lactate ^{12}C	1.33	$C\mathbf{H_3}CH(OH)COOH$	1.319 - 1.332
lactate ^{13}C	1.42	$^{13}C\mathbf{H_3}CH(OH)\,^{13}COOH$	1.4 - 1.445
pyruvate ^{12}C	2.36	$C\mathbf{H_3}COCOOH$	2.361 - 2.365
pyruvate ^{13}C	2.47	$^{13}C\mathbf{H_3}COCOOH$	2.47 - 2.477

Figure 3.18 ^{1}H NMR spectral resonance assignments for culture media samples and signal regions used for quantification

Assignment	ppm	moiety	Signal range (ppm)
choline	3.21	$(C\mathbf{H_3})_3N^+(CH_2)_2OH$	3.204 – 3.213
phosphocholine	3.22	$(C\mathbf{H_3})_3N^+(CH_2)_2OPO(OH)_2$	3.213 – 3.23
glycerophosphorylcholine	3.24	$(C\mathbf{H_3})_3N^+(CH_2)_2OPOO^-OCH_2CH(OH)CH_2(OH)$	3.23 – 3.241

Figure 3.19 ^{1}H NMR spectral resonance assignments for choline metabolites of cell extract samples and signal regions used for quantification

methyl palmitate ISA parameters		MCF10A Parent mean	MCF10A Parent SEM	PIK3CAmt mean	PIK3CAmt SEM	Statistical significance unpaired p value	
Labeled Acetyl CoA	U13C6 Glucose labeled culture	0.55	0.049	0.60	0.008	0.435	
	U13C5 Glutamine labeled culture	0.11	0.015	0.10	0.002	0.107	
De Novo Synthesis	U13C6 Glucose labeled culture	0.26	0.055	0.36	0.009	0.152	
	U13C5 Glutamine labeled culture	0.20	0.060	0.31	0.034	0.046	*

Figure 3.20 Fatty acid ISA modelled parameters

The table above represents data from three biological U-$^{13}C_6$ glucose culture replicates and four biological U-$^{13}C_5$ glutamine culture replicate experiments

Chapter 4 Silencing choline-releasing EDI3 suppresses central carbon metabolism in tumour cells

4.1 Abstract

Endometrial carcinoma differential 3 (EDI3) is a glycerophosphodiester phosphodiesterase with high specificity for glycerophosphocholine (GPC); EDI3 hydrolyses GPC and releases choline and glycerol-3 phosphate (G3P). Recently, EDI3 expression has been shown to be associated with metastasis in endometrial cancers, and to promote migration via Protein Kinase C-alpha (PKCα) signalling (Stewart *et al.* 2012). It has been suggested that the role of EDI3 in cancer could be mediated by metabolite regulation. Through the use of cell models transfected with EDI3 siRNA, we examined the impact of EDI3 knockdown on cellular metabolic profiles with ^{1}H NMR spectroscopy and GC-MS. Elevated GPC and GPC:PCho ratios were observed in multiple tumour cell lines. In addition, we found decreased glycolysis and lipogenesis in MCF7 cells transfected with EDI3 siRNA.

4.2 Introduction

Endometrial carcinoma differential 3 (EDI3), also named GDE5/GPCPD1, is a recently characterised member of the glycerophosphodiester phosphodiesterase (GDE) family of enzymes (Stewart *et al.* 2012). Seven mammalian GDEs have now been described in the literature, and many have been reported to be important for physiological development (Yanaka 2007). However, their functional roles and therapeutic values in cancer remain unclear. While most other GDEs are transmembrane proteins, EDI3 is localized in the cytoplasm (Zheng *et al.* 2000, Rao and Sockanathan 2005). Glycerophosphoinositol, glycerophosphoserine, glycerophosphoethanolamine, and glycerophosphocholine (GPC) are all potential substrates of GDEs (Corda *et al.* 2014). Mammalian glycerophosphodiesterases have high substrate specificities, and EDI3 preferably utilises GPC (Stewart *et al.* 2012). Using whole cell lysates from models overexpressing EDI3 or recombinant EDI3, Stewart *et al.* conclusively demonstrated that EDI3 catalyses the enzymatic cleavage of GPC into choline and glycerol-3 phosphate (G3P) (Stewart *et al.* 2012).

In the same study, high EDI3 expression was shown to be positively associated with metastasis in endometrial tumours, and negatively associated with relapse-free survival in both endometrial and ovarian cancer patient populations (Stewart *et al.* 2012). Consistent with this observation, EDI3 silencing was also demonstrated to downregulate cell migration via Protein Kinase C-alpha (PKCα) signal transduction. Additionally, Lesjak *et al.* has recently shown that EDI3 regulates other important processes for metastasis including integrin expression, adhesion and cell spreading in breast and ovarian cell lines (Lesjak *et al.* 2014).

Whilst the link between the metabolic function of EDI3 and metastasis is still unclear, Stewart *et al.* has shown that silencing EDI3 suppressed levels of lysophosphatidic acids and phosphatidic acids (Stewart *et al.* 2012). Both lysophosphatidic acids and phosphatidic acids can be synthesised directly from G3P, and they are precursor molecules to signalling lipid diacylglycerol - a known activator of PKC signalling (Nishizuka 1992). Enzymatic products of EDI3, choline (Fernandez-Murray and McMaster 2005) and glycerol-3 phosphate (Topanurak *et al.* 2013) are central to tumour metabolism; hence we hypothesised that EDI3 activity

could exert a wider influence on cellular metabolism. This prompted us to investigate the impact of EDI3 silencing on the global metabolome using NMR and GC-MS profiling.

First, using two breast cell lines and one endometrial cell line as models, we showed that increases in GPC level and GPC: PCho ratio were prominent ^{1}H NMR detectable phenotypes associated with EDI3 silencing. Interestingly, this was accompanied by consistent changes in the abundance of lactate, alanine and citrate. To understand the fate of glucose, we performed stable isotope tracer analysis using GC-MS and $^{13}C_{6}$-glucose as substrates, where we characterised further changes in glycolytic metabolites and lipid phenotypes following EDI3 silencing in MCF7 cells.

4.3 Materials and methods

Cell samples on which the metabolomics analyses were conducted were generated using RNA silencing by our collaborator, Dr. Rosemarie Marchan (Leibniz Research Centre, Dortmund) in the laboratory of Prof. Jan Hengstler (Leibniz Research Centre for Working Environment and Human Factors, Dortmund). I was solely responsible for performing the analytical part of the GC-MS experiments and data analysis, as well as the acquisition of the ^{1}H NMR data, Dr. James Ellis, Gabriel Valbuena and Shyam Solanki (Imperial College London) and myself were all involved in the NMR sample preparation. Part of these data (GPC/PC determinations) has been published in (Stewart *et al*. 2012). I am solely responsible for the analysis of the ^{1}H NMR data presented here.

4.3.1 Cell culture and maintenance

MCF7, AN3-CA and MDA-MB-231 cells were purchased from the *German Collection of Microorganisms and Cell Cultures*. Their authenticities were confirmed by DNA fingerprinting. MCF7 was maintained in Dulbecco's modified medium (DMEM) supplemented with 10% heat-inactivated fetal bovine serum (Pan-Biotech), 1% sodium pyruvate (Sigma), 0.5% non-essential amino acids (Gibco), and 0.1% insulin (Sigma). The cells were passaged at 70-80% confluency.

4.3.2 RNA silencing

For EDI3 silencing, cells were transfected with Stealth RNAi siRNA specific for human EDI3 (Invitrogen). At the start of the experiment, half a million cells were suspended in 2.5 ml of medium before they were added to each well in a six-well plate containing 5 μl of Lipofectamine RNAiMAX (Invitrogen), 500 μl of Opti-MEM, and 20nM siRNA oligos. Stealth RNAi siRNA negative controls (Invitrogen) were used to account for off-target effects of the RNAi. The two negative controls are two different RNAi siRNA with independent target sequences. Cells were incubated for 72hrs before they were used for metabolic profiling experiments, to ensure good knockdown efficiency at the RNA and at the protein level.

4.3.3 Metabolomics experiment

For the stable isotope glucose labelling experiment, glucose-free, glutamine-free, pyruvate-free DMEM medium was used. This was then supplemented with 10% dialysed FBS, pen/strep, 2mM glutamine and 5.6mM $^{13}C_6$-glucose. The experimental media were refreshed at '0hr' and were incubated for 5 or 24 hours. Both media and cells were collected at the time of harvest; and approximately 1 million cells were harvested from each well on a 6-well plate. Four technical replicates were used in the experiment. A representative well from each condition was used for cell counting, and to confirm knockdown efficiency.

For ^{1}H NMR analysis, MCF7, MDA-MB-231, and AN3-CA cells were cultured in DMEM medium, supplemented with 10% dialysed FBS, pen/strep, 2mM glutamine and 5.6mM glucose. The cells were cultured on 6-well plates; the media were refreshed at '0hr', and cells were harvested at 24 hours. Cells from multiple wells were pooled together to make up NMR samples each containing approximately 3 million cells.

Sample extraction, methods and protocols for ^{1}H NMR and GC-MS analysis were described in section 2.4.

4.4 Results

4.4.1 ^{1}H NMR spectroscopy analysis of intracellular aqueous metabolite level following EDI3 silencing

Three cancer cell lines transfected with EDI3 siRNA, MCF7 (breast), MDA-MB-231 (breast), and AN3-CA (endometrial), were analysed with ^{1}H NMR spectroscopy. Knockdown efficiencies in these cell models were determined to be > 50% (Stewart *et al.* 2012). After the raw NMR spectra were normalised using median fold change, we generated an overview of the differences between the two treatment groups (Figure 4.1, Figure 4.2). Intensity differences between the mean spectra measured for EDI3 control and EDI3 knockdown samples in each cell line were illustrated in Figure 4.1 and Figure 4.2, with each data point coloured according to the significance of the difference in the mean at that point. Figure 4.3 illustrates the same data as in Figure 4.1 but with the plots expanded to show the congested aliphatic region between 2-4 ppm more clearly. Several consistent differences in metabolite signals were observed. GPC levels, as expected, were elevated in all cell lines upon EDI3 silencing. Phosphocholine levels were typically reduced, while the levels of choline present were difficult to assess due to low abundance. In addition to changes in choline metabolism, levels of lactate, alanine, citrate and glycine were also consistently decreased in cells transfected with EDI3 siRNA. Next, we quantified metabolite resonances that were consistently different between the two treatment groups (Figure 4.3). This analysis confirmed that in all three lines, cell samples transfected with EDI3 siRNA exhibited significantly higher GPC levels ($p < 0.005$), consistent with its proposed glycerophosphodiester phosphodiesterase function. In support of this finding, PCho levels were not found to be significantly different between the knockdown and control, while GPC/PCho ratios were found to be considerably higher ($p < 0.005$) when EDI3 expression was silenced (Figure 4.3). In addition, the trend towards decreased citrate, alanine, and lactate levels following EDI3 silencing reached significance in some models (Figure 4.3). This supported the hypothesis that EDI3 has an impact across the wider metabolome. Since all three metabolites are predominantly generated by metabolism of pyruvate downstream of glycolysis, we analysed the fate of stable isotope labelled $^{13}C_6$-glucose in the MCF7 cells.

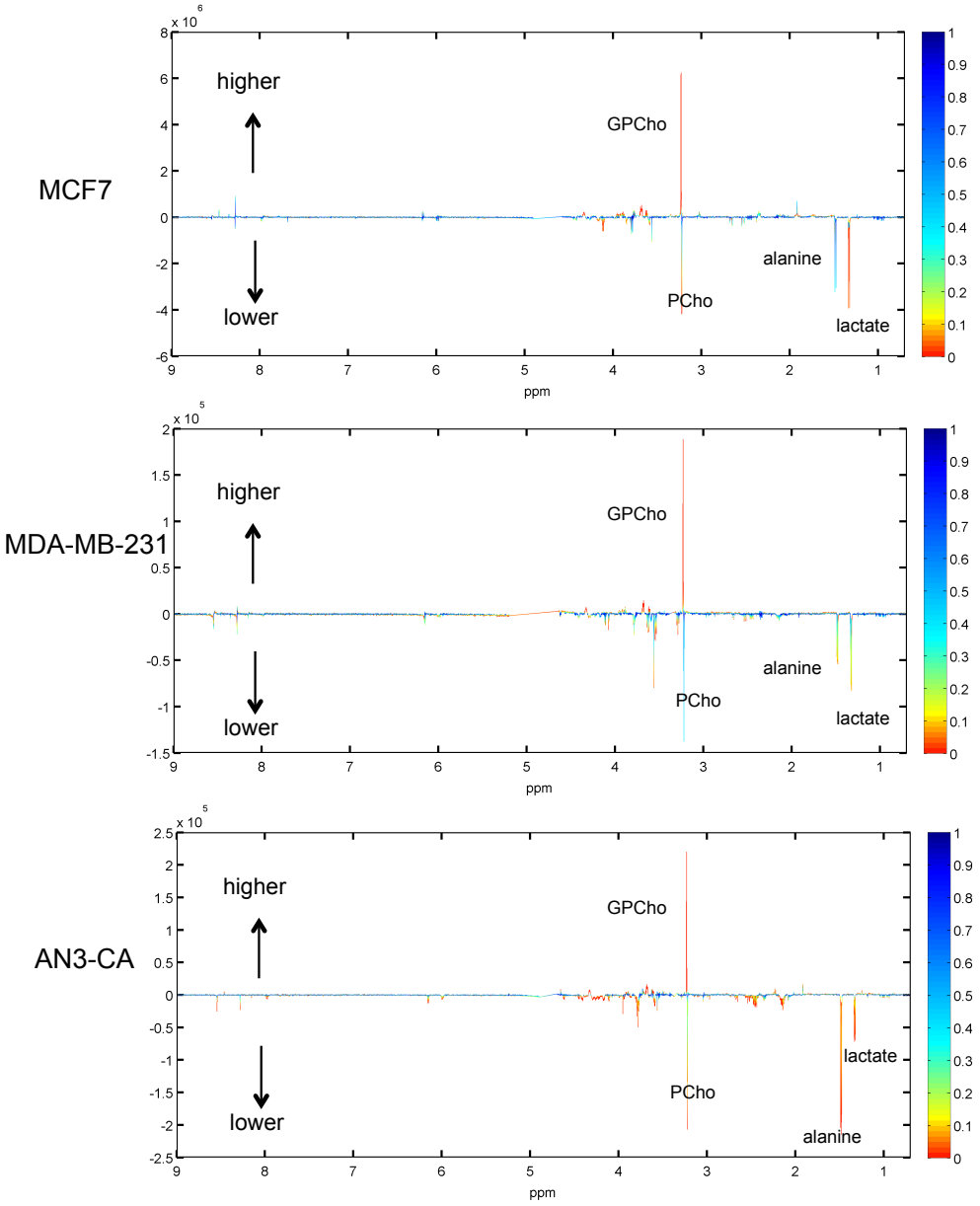

Figure 4.1 EDI3 silencing modulates ^{1}H NMR-detectable intracellular metabolome

NMR difference spectra of MCF7, MDA-MB-231, and AN3-CA above demonstrate consistent changes in metabolite levels across a number of resonance peaks. The difference spectra were calculated by subtracting the intensities of mean siEDI3 sample spectra from the mean negative control sample spectra; and thus peak resonances elevated in EDI3 siRNA samples have positive magnitudes and peak resonances decreased lowered in EDI3 siRNA samples acquire negative magnitudes. The colour bars represent Student's T-test p values and indicate statistical significance of the peak intensity differences at each data point on the chemical shift axis. The sample data of each biological group represent six replicates from two independent biological batches.

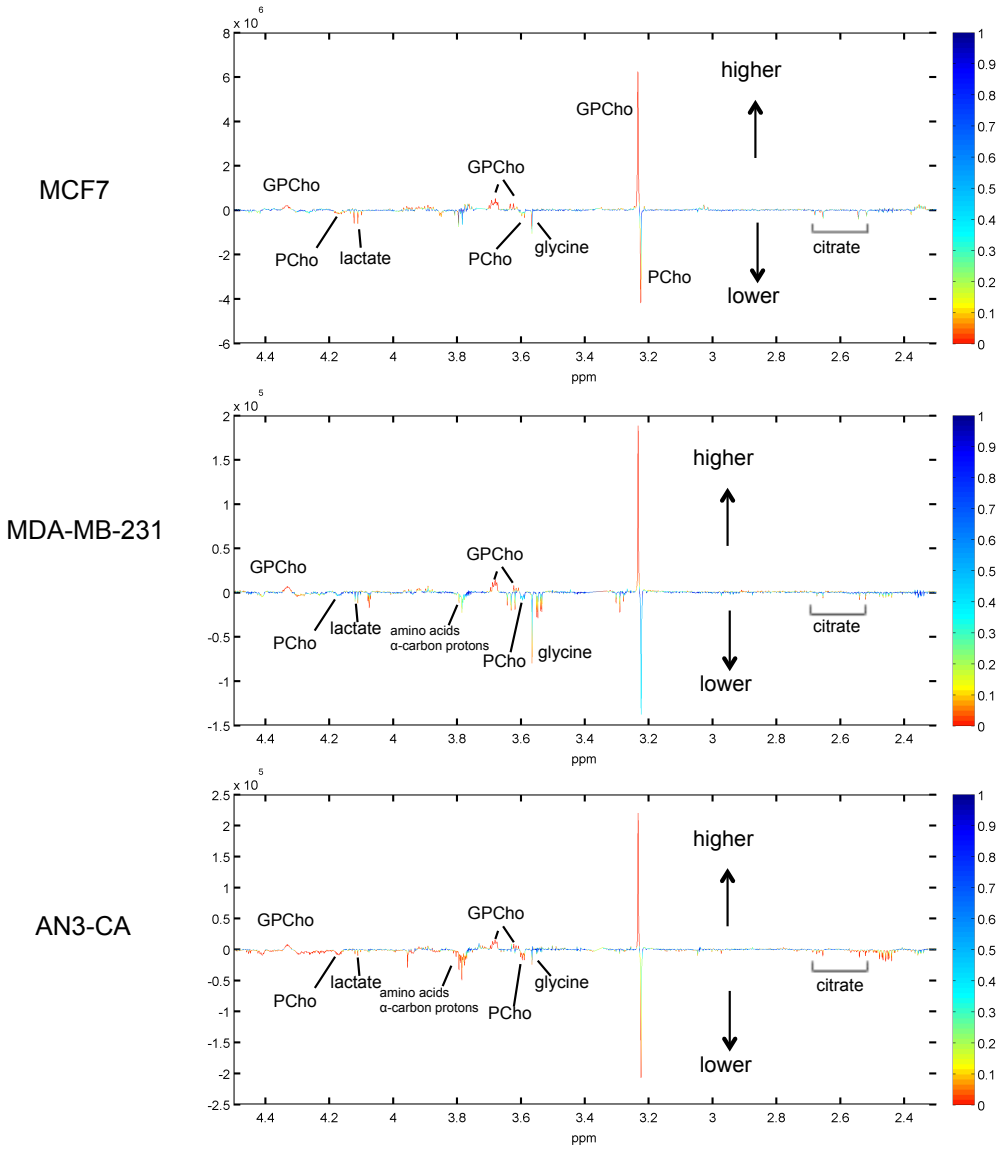

Figure 4.2 EDI3 silencing modulates ^{1}H NMR-detectable intracellular metabolic profile in the 2.4 - 4.5 ppm resonance region

NMR difference spectra (2.4ppm to 4.5ppm) of MCF7, MDA-MB-231, and AN3-CA above demonstrate consistent changes following EDI3 silencing across a number of resonance peaks, including in GPC, PCho, lactate, glycine, citrate and amino acids alpha–carbon proton signal resonances. Peak resonances elevated in EDI3 siRNA samples have positive magnitudes and peak resonances lowered in EDI3 siRNA samples acquire negative magnitudes. The colour bars represent Student's t-test p values and indicate statistical significance of the intensity differences at each data point on the chemical shift axis. The sample data of each biological group represent six replicates from two independent biological batches.

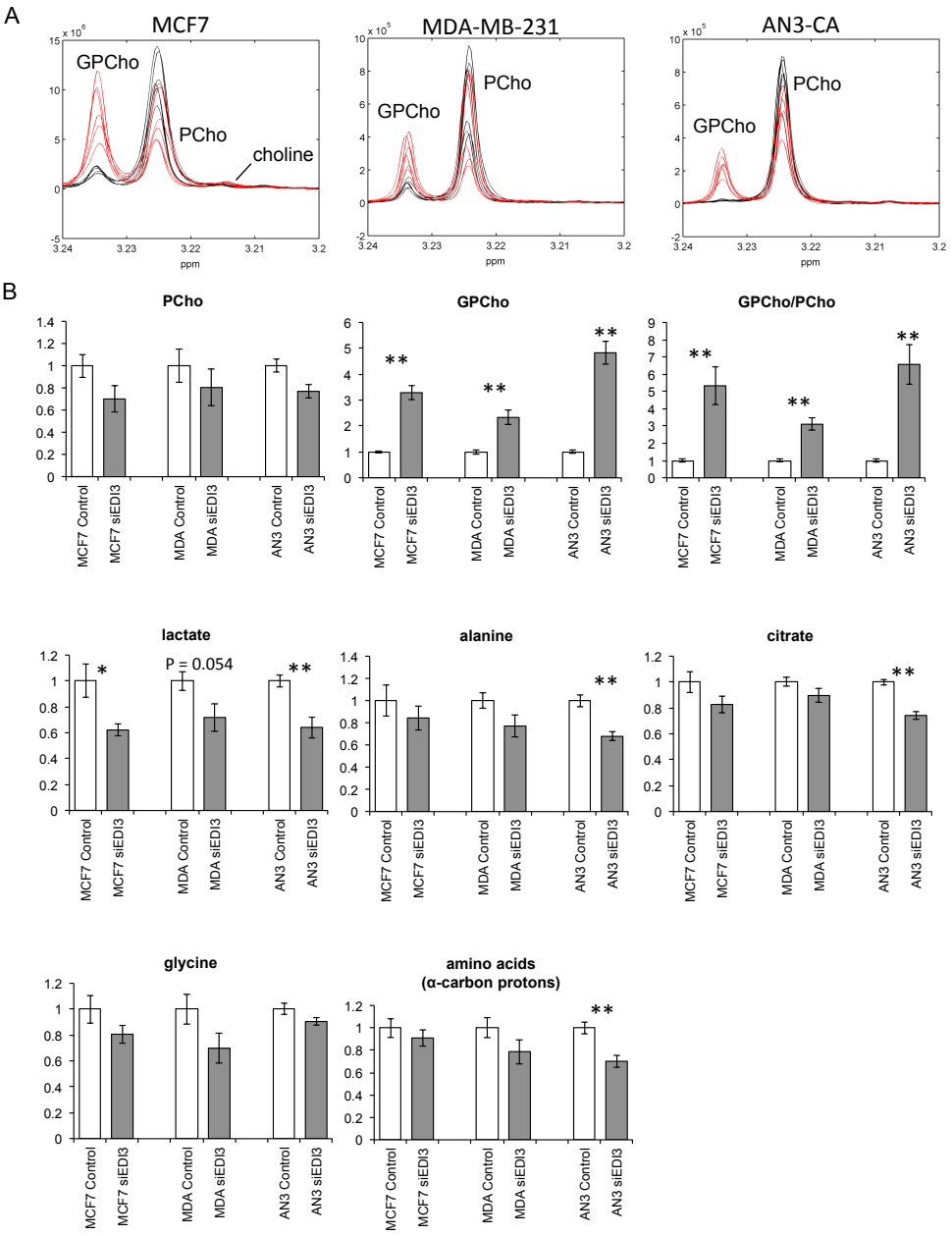

Figure 4.3 ^{1}H NMR analysis of intracellular aqueous metabolite level following EDI3 silencing

A) Comparison of GPC and PCho ^{1}H NMR resonance intensities between EDI3 siRNA (shown in red) and negative control samples (shown in black) in 3 cell lines. B) Relative changes in metabolite signals following EDI3 silencing. Metabolite resonances showing consistent changes across the 3 cell lines were quantified. Bar charts represent mean ± SEM of six replicates from two independent biological batches, and spectral data were normalised using median fold change. ** represents Student's t-test p value < 0.005 and * represents Student's t-test p value < 0.05.

4.4.2 Analysis of the effect of EDI3 silencing in MCF7 cells cultured in $^{13}C_6$-glucose: metabolite uptake and release

Stable glucose isotope tracer experiments were performed in MCF7 cells by substituting glucose in the media with uniformly labelled $^{13}C_6$-glucose. Media and extracts of cells were analysed to determine the distribution of ^{13}C carbon tracers in metabolites downstream of glucose metabolism. In this experiment, MCF7 cells were transfected with either siRNA targeting EDI3 or one of two independent negative control siRNAs with different scramble sequences. A knockdown efficiency greater than 90% was achieved in this experiment (Figure 4.16). The culture media were analysed using ^{1}H NMR spectroscopy. Cellular uptake of glucose, glutamine, and choline, and net alanine, lactate and glutamate production were detected over the 24-hour culture period (Figure 4.4). During the 24-hour period, $^{13}C_6$-glucose consumption and ^{13}C labelled lactate production by MCF7 cells transfected with EDI3 siRNA were both reduced by approximately half ($p < 1x10^{-5}$) compared to controls. This was surprising, given that no significant changes in growth were detected between the control and knockdown (Figure 4.15). Despite the big difference in absolute rates, no differences in the ^{13}C lactate release to ^{13}C glucose consumption ratio were observed (Figure 4.5). Other than glycolytic metabolites, an effect on glutamine utilisation upon EDI3 silencing was also seen. Although glucose uptake was diminished in EDI3 siRNA transfected cells, glutamine consumption broadly remained similar in the knockdown and in the controls. However, the molar ratio of glutamine to glucose consumption nearly doubled ($p < 1x10^{-4}$) (Figure 4.5). Furthermore, elevated production ($p < 0.05$) of non-glucose derived glutamate (C-4, CH_2 resonance) (Figure 4.4), and hence higher glutamate release to glutamine consumption ratio ($p < 5x10^{-3}$)(Figure 4.5), were detected in the media of EDI3 siRNA transfected cells. We also measured and compared the uptake of choline, and observed no changes following EDI3 silencing. This was interesting given that EDI3 can modify the intracellular availability of choline (Figure 4.4). Collectively, these observations suggest that silencing EDI3 suppresses glycolysis and increases glutamate production in the MCF7 cells.

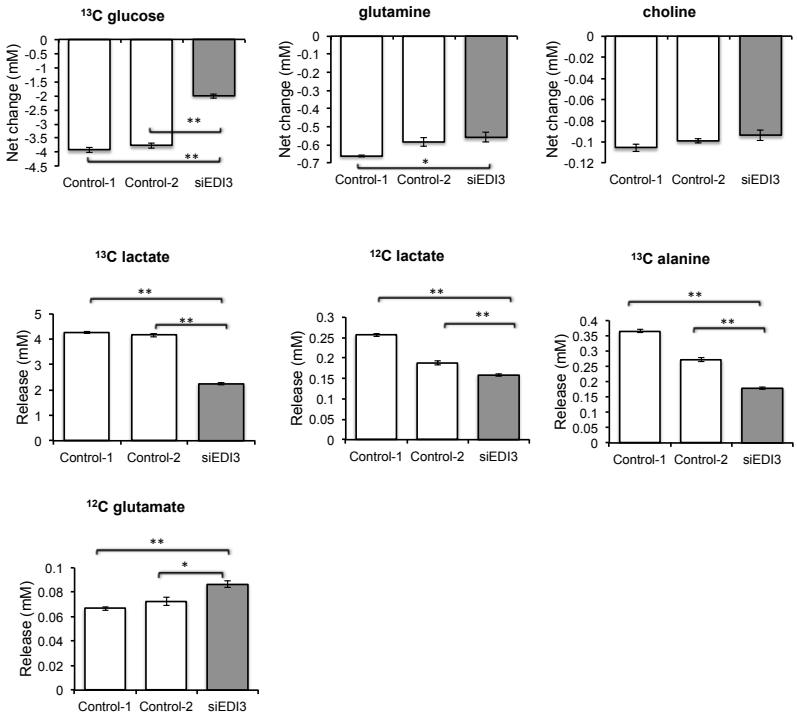

Figure 4.4 NMR measurement of medium metabolite consumption and release profile in MCF7 cells transfected with EDI3 siRNA

MCF7 transfected with EDI3 siRNA was compared to MCF7 cells transfected with the two independent negative control scramble vector sequences (i.e. control-1, control-2). The bar graphs represent the mean ± SEM from four technical replicates and * represents comparisons with Student's t-test p value < 0.05 and ** represents comparisons with Student's t-test p value < 0.005.

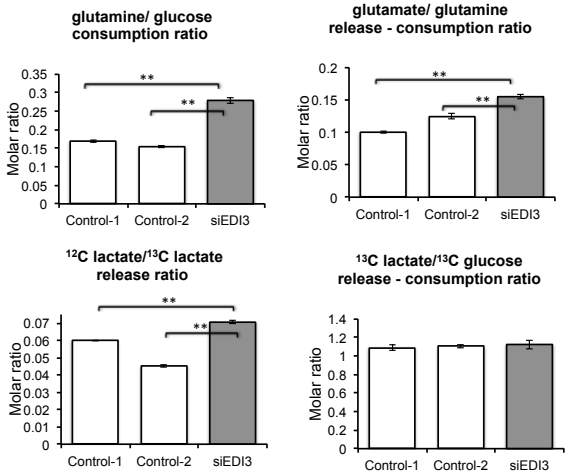

Figure 4.5 Key substrate medium consumption and release ratios

The bar graphs above represent the mean ± SEM from four technical replicates and ** represents comparisons with Student's t-test p value < 0.005.

4.4.3 Analysis of the effect of EDI3 silencing in MCF7 cells cultured in $^{13}C_6$-glucose: changes in aqueous cell extracts

The intracellular metabolites of MCF7 cells cultured with U-$^{13}C_6$ glucose were analysed using GC-MS; the relative abundance of metabolites and their ^{13}C mass isotopomer distributions were both examined. Global analysis of the metabolite abundance profile indicated that the levels of glycolytic products and direct metabolites of pyruvate such as alanine and lactate were all ($p < 0.005$) significantly reduced in cells transfected with EDI3 siRNA (Figure 4.6). Alanine and pyruvate are inter-convertible via transamination reactions (Beuster *et al.* 2011). The levels of citrate and malate were also lowered ($p < 0.005$) after the transient silencing of EDI3. Overall, this set of results were in agreement with the NMR data previously described in section 4.4.1, where decreases of citrate, lactate and alanine were also found in the MCF7 cells using samples from independent biological replicate experiments (Figure 4.3). While silencing EDI3 appeared to suppress glycolysis, its effects on the TCA cycle were less apparent. Thus, to help understand if the flux through the TCA cycle might have been altered by EDI3 knockdown, the mass isotopomer distributions of metabolites in the TCA cycle were analysed. However, we found that EDI3 silencing did not significantly alter the contribution of $^{13}C_6$ glucose into the carbon skeleton of TCA cycle intermediates (Figure 4.7), and that the ^{13}C mass isotopomer distribution of citrate and malate remained unchanged (Figure 4.8).

Furthermore, a substantial increase ($p < 1x10^{-5}$) in [glycerol-3 phosphate + glycerophosphocholine] ([G3P + GPC]) was observed in cells transfected with EDI3 siRNA (Figure 4.6). As described in Chapter 3 section (3.4.4) the derivatisation method did not discriminate well between G3P and GPC. Through running standards we did however arrive at a GPC-specific ion fragment (m/z: 325, RT: 17.8min), and with the small subset of data acquired using the full scan mode, we confirmed that the increase in [G3P + GPC] in the EDI3 knockdown cells was likely due to changes in GPC (Figure 4.9). Additionally, the ^{13}C mass isotopomer distribution data of GPC indicates that GPC accumulation in the EDI3 knockdown cells was due to the rise in the unlabelled isotopomer population (m_0), consistent with the notion that most GPC is derived from the degradation of choline phospholipids, which typically have

slower turnover rate compared to metabolic substrates involved in glycolysis, the TCA cycle or the pentose phosphate pathway.

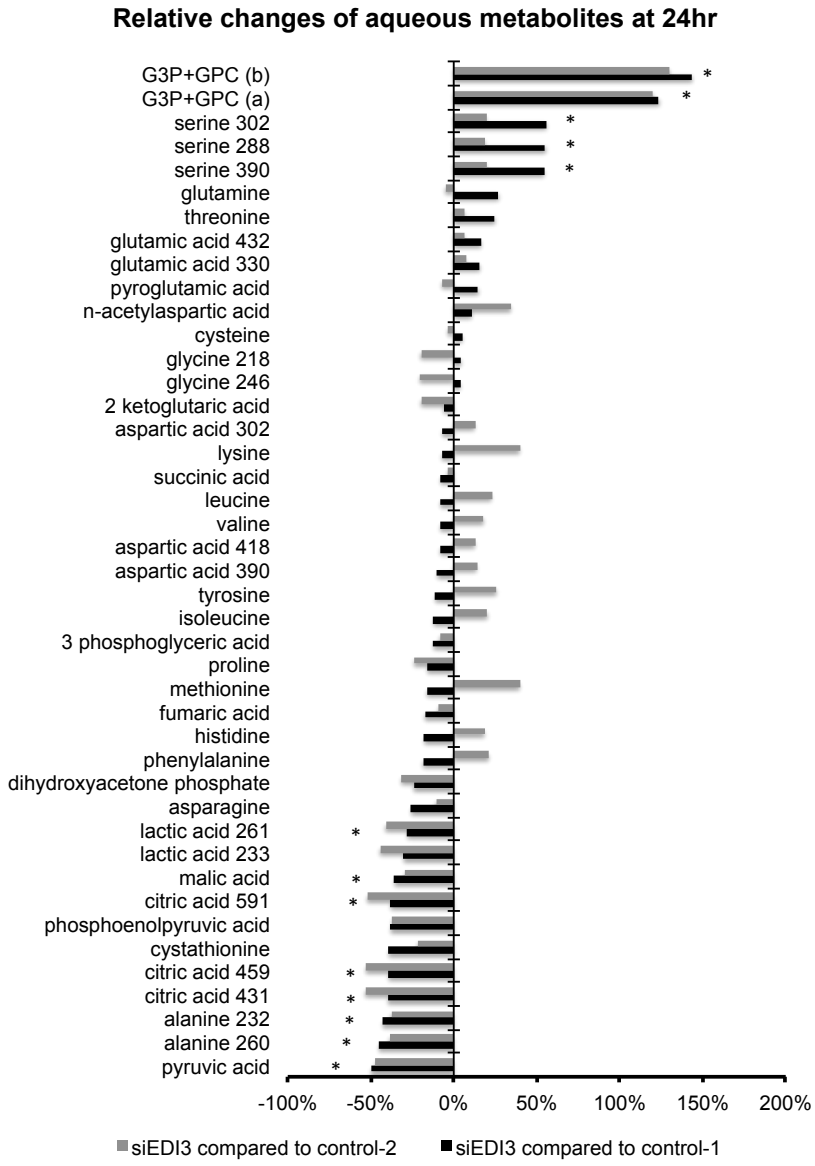

Figure 4.6 EDI3 silencing modulates global intracellular metabolome

MCF7 transfected with EDI3 siRNA was compared to MCF7 cells transfected with the two independent negative control scramble vector sequences (i.e. control-1, control-2). GC-MS integrals were normalized by median fold change. Metabolites in the data table were ranked by relative changes where a positive change represents an increase in siEDI3 compared to the control. The bar graphs represent the mean from four technical replicates and * represents metabolite comparisons with Student's t-test p value < 0.005 against both control 1 and control 2.

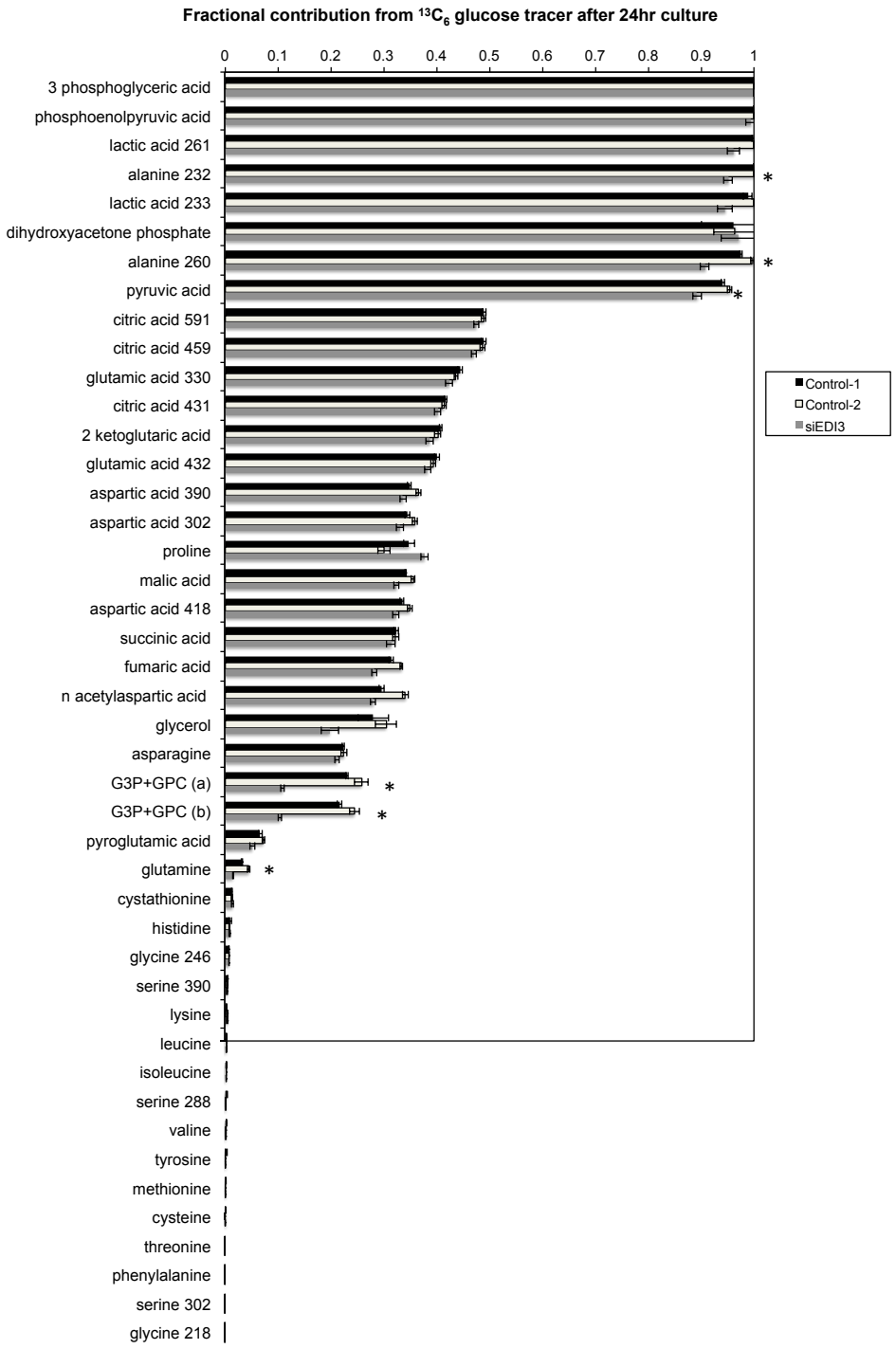

Figure 4.7 Effect of EDI3 on glucose's carbon incorporation into intracellular metabolome in MCF7 after 24hr of glucose labelled culture

The bar graphs represent the mean ± SD from four technical replicates and * represents metabolite comparisons with Student's t-test p value < 0.005 against both control 1 and control 2

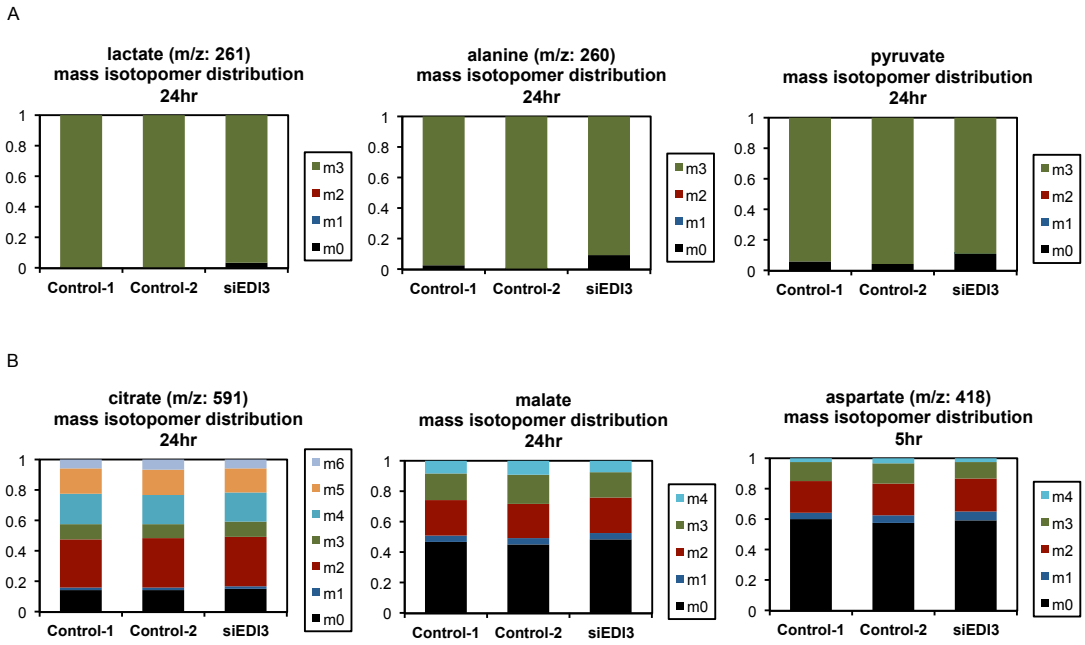

Figure 4.8 Effect of EDI3 silencing on mass isotopomer distribution (MID) of intracellular metabolites

(A) Non-glucose contribution into glycolytic metabolites upon EDI3 silencing was prominent. (B) No obvious changes in the MID were observed in the TCA cycle intermediates upon EDI3 silencing. Bar graphs represent the mean from four technical replicates.

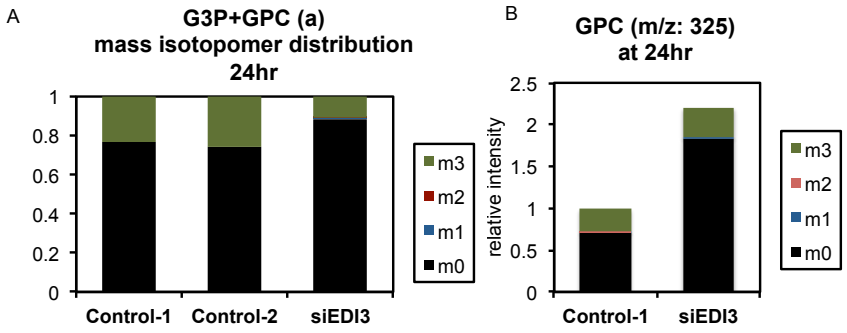

Figure 4.9 EDI3 silencing leads to an accumulation of the non-labelled GPC pool

(A) In MCF7 cells, the proportion of labelled GPC mass fragments was reduced upon EDI3 silencing. Bar graphs represent the mean from four technical replicate. (B) The increase in the relative intensity of GPC mass fragment upon EDI3 silencing was largely accounted for by the rise in the non-labelled GPC pool. The bar graphs represent data analysed under the full scan mode from a single sample.

4.4.4 EDI3 silencing alters fatty acid profile in MCF7 cells

The non-polar lipid-containing extracts from the $^{13}C_6$-glucose culture experiment were also analysed using GC-MS; free fatty acids were derivatised through silylation, while fatty acid chains as parts of other structural or signalling lipids were transesterified during the extraction process. Through performing Isotopomer Spectral Analysis (ISA) on the fatty acid ^{13}C mass isotopomer distribution data, we examined the effects of transient EDI3 knockdown on the glucose-labelled lipogenic acetyl-CoA pool, the synthetic rate of fatty acid *de novo*, and on fatty acid elongation in the MCF7 cells (Figure 4.10, Figure 4.11, Figure 4.12). After 24 hours of $^{13}C_6$ glucose culture, lowered *de novo* synthesis of transesterified myristate, palmitate, palmitoleate and stearate (all $p < 0.005$) were observed in cells transfected with EDI3 siRNA (Figure 4.11), and the contribution of labelled glucose into the lipogenic acetyl-CoA pool was also found to be marginally decreased (Figure 4.12).

Furthermore, analysis of the lipid intensity data also revealed that silencing EDI3 might have affected the relative abundance of a subset of lipid species (Figure 4.13). In particular, transesterified palmitoleate detected at both 5 hours (p value < 0.05) and at 24 hours (p value < 0.01) were lowered by approximately one-fifth, and the ratio of transesterified palmitoleate to palmitate (p value < 0.005) also dropped by approximately the same amount in cells transfected with EDI3 siRNA (Figure 4.14). It was unclear whether this was due to lower desaturase activity, changes in palmitoleate recycling or extracellular uptake. However overall, our data suggest EDI3 silencing altered the profile of fatty acid chains in lipids.

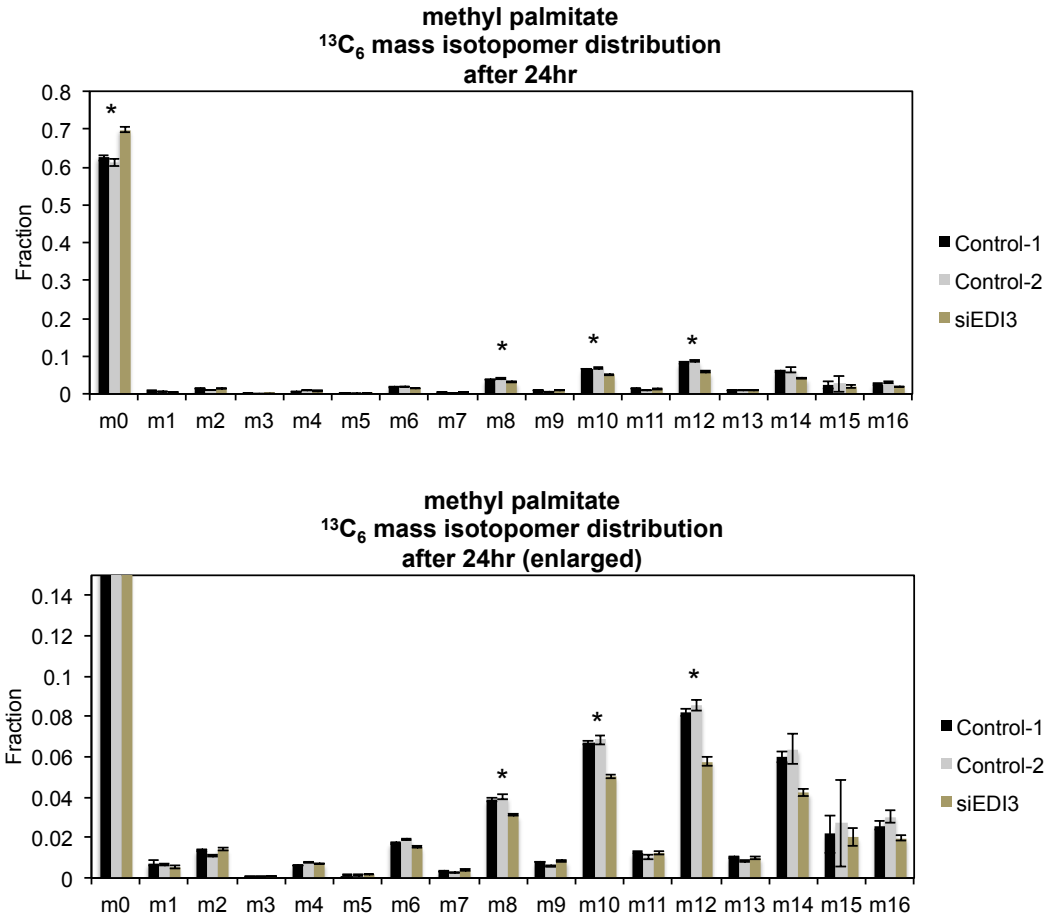

Figure 4.10 The effect of EDI3 on ^{13}C-glucose labelled mass isotopomer distribution of lipid metabolites

The methyl palmitate MID is representative of the pattern observed in other lipid species. The bar graphs represent the mean ± SD from four technical replicates. * represents feautres with Student's t-test p values < 0.001 against both control groups.

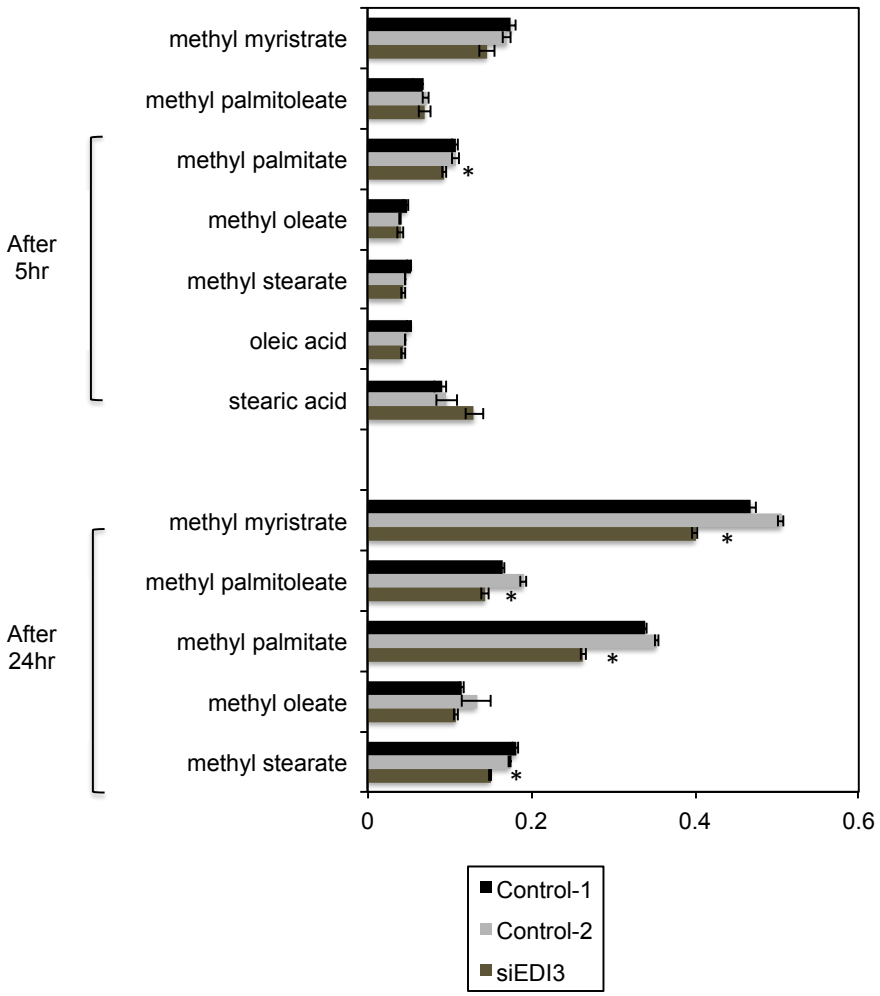

Figure 4.11 EDI3 silencing suppresses *de novo* fatty acid synthesis

The rate of *de novo* fatty acid synthesis is a parameter derived using the 3-parameters ISA model, and is based on the raw mass isotopomer distribution data of the individual lipid species. Bar graphs represent the means ± SEM from four technical replicates and * represents lipid metabolite comparisons with Student's t-test p value <0.05 against both control 1 and control 2

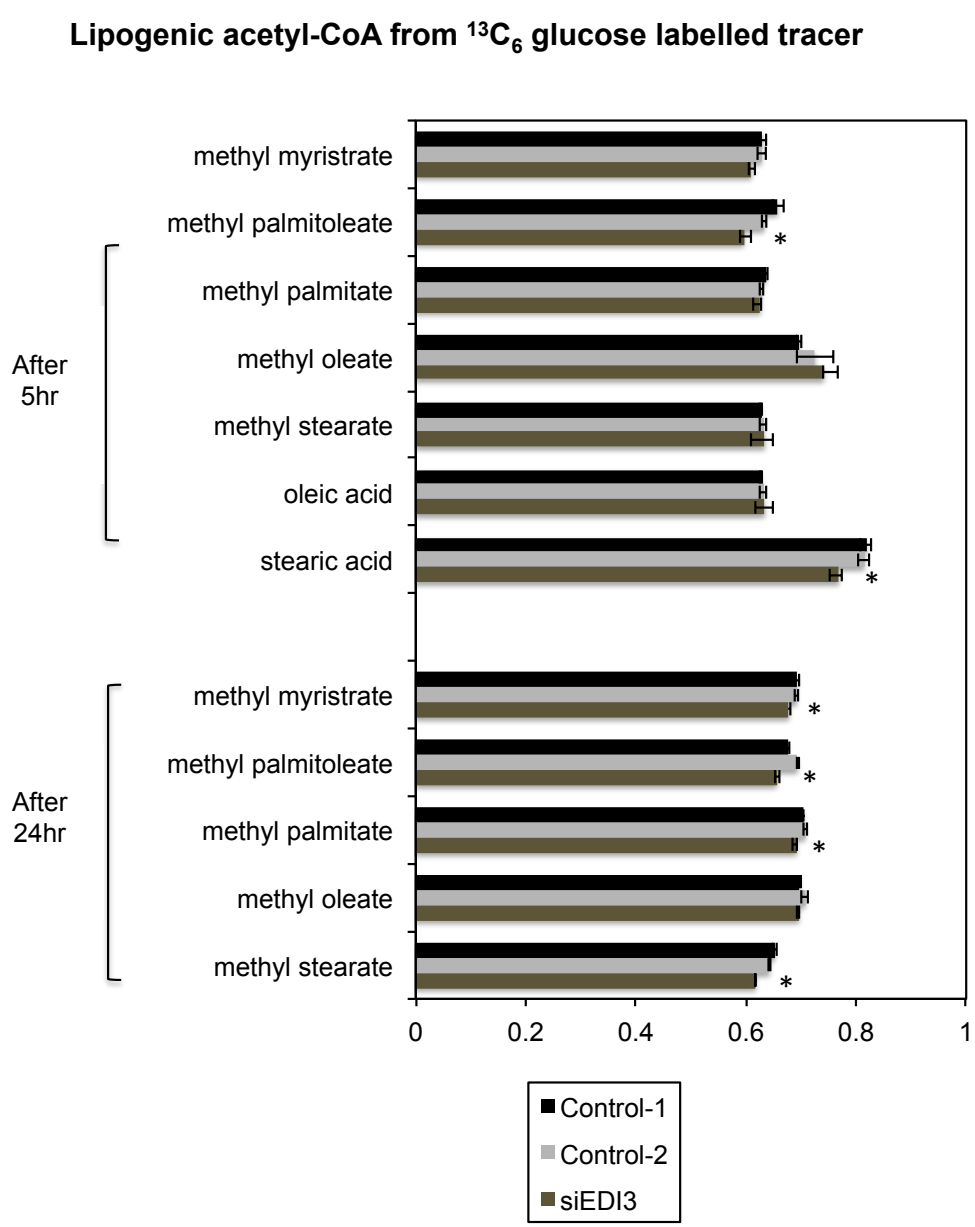

Figure 4.12 Effect of EDI3 silencing on labelled lipogenic acetyl-CoA pool

This is another parameter derived from the same 3-parameters ISA model. The bar graphs represent the means ± SEM from four technical replicates and * represents lipid metabolite comparisons with Student's t-test p value < 0.05 against both control 1 and control 2.

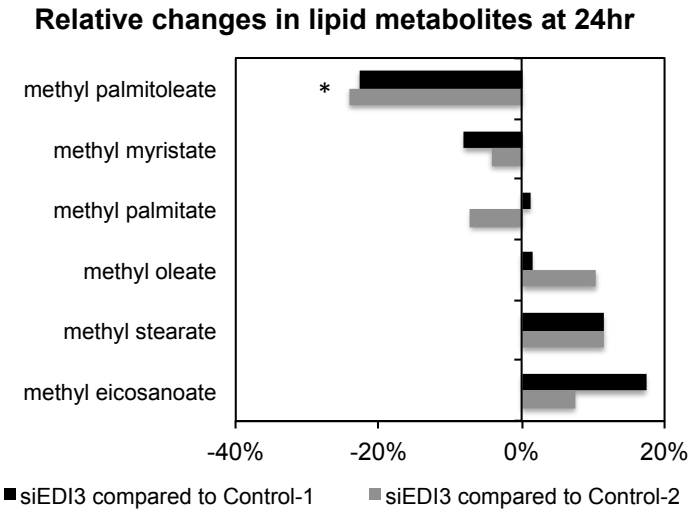

Figure 4.13 EDI3 alters lipid metabolic profile

The GC-MS integrals were median fold normalized, and the lipid metabolite species were ranked according to relative changes where a negative change represents a decrease in siEDI3 compared to the control. The bar graphs represent the mean from four technical replicates and * represents comparisons with Student t-test p value < 0.05 against both control 1 and control 2.

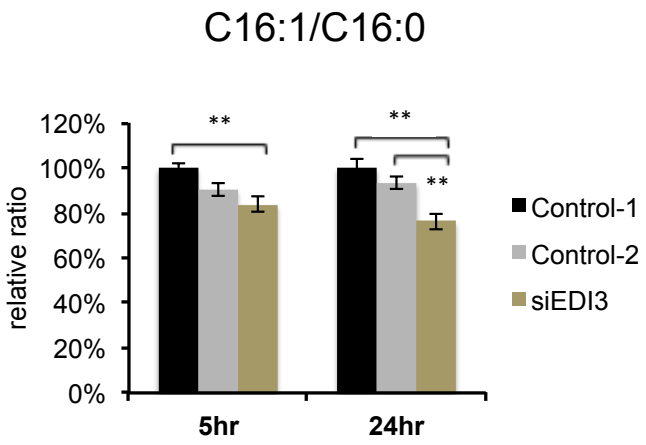

Figure 4.14 EDI3 silencing lowers palmitoleate to palmitate (C16:1/C16:0) ratio

The bar graphs represent the mean and SEM from four technical replicates; * represents comparisons with Student's t-test p value <0.05, and ** represents comparisons with Student's t-test p value < 0.005.

4.5 Discussion

Using multiple cell models, the experiments presented in this chapter validated the role of EDI3 in regulating glycerophosphocholine (GPC) levels and GPC:PCho ratio, consistent with observations made when other glycerophosphodiester phosphodiesterases were targeted in breast tumour xenografts (Wijnen *et al.* 2014). However, this study has also revealed previously unknown interactions between central carbon metabolism and EDI3 function, namely that silencing EDI3 with siRNA suppresses glycolysis and fatty acid synthesis, elevates glutamate production, and reduces the relative abundance of transesterified palmitoleate compared to other fatty acids in the MCF7 cells.

The links between EDI3 activity and regulation of metabolic pathways beyond GPC metabolism are unclear. GPC is converted by EDI3 into choline and glycerol-3 phosphate (G3P) (Stewart *et al.* 2012), hence downstream metabolic effects are likely directly related to levels of GPC, choline or G3P. Apart from being described as an osmolyte in the kidney (Burg 1996, Gallazzini *et al.* 2008), there are no obvious metabolic routes that rationalise accumulation of GPC with the effects that were observed. While we did not directly observe a decrease in choline or G3P, it is plausible that inhibition of GPC activity could contribute to a reduction in the supply of either of these metabolites. Choline oxidation could potentially link choline availability to mitochondrial metabolism, and hence other metabolic pathways such as lipogenesis (Katz-Brull *et al.* 2002). However, choline uptake did not increase upon EDI3 silencing (Figure 4.5), suggesting that choline availability was not likely an important factor. Glycerol-3 phosphate is a substrate for glycerol-3 phosphate dehydrogenase and glycerol-3 phosphate acyltransferase, respectively involved in glycerol-3 phosphate shuttle and lipid biosynthesis (Turyn *et al.* 2003). Glycerol-3 phosphate acyltransferase is the rate limiting step in glycerolipid and glycerophospholipid biosynthesis (Wendel *et al.* 2009), and requires both glycerol-3 phosphate and acyl-CoA as substrates. It has been shown that restriction in lipogenic glycerol-3 phosphate availability limits glycerol-3 phosphate acyltransferase activity, and could lead to a build up of acyl-CoA. Glycerol-3 phosphate acyltransferase-1 (GPAT1) knockout mice have been shown to result in an almost two-fold increase of acyl-CoA in the liver, as well as lower hepatic triacylglycerol and diacylglycerol

levels (Hammond *et al.* 2005, Neschen *et al.* 2005). Acyl-CoA species can inhibit activity of hexokinases (Tippett and Neet 1982), (Thompson and Cooney 2000) and citrate synthase (Hsu and Powell 1975, Hansel and Powell 1984). However direct confirmation of G3P depletion and acyl-CoA accumulation downstream of EDI3 would be required to support this hypothesis.

4.5.1 Limitations and Future work

By demonstrating changes in GPC levels and the GPC/PCho ratios and presenting evidence for changes in alanine, lactate, and citrate levels across several cell models, we illustrated that silencing EDI3 has widespread implications on the cellular metabolome. However, we acknowledge that repeated measurements on extracellular culture media and lipid profile using additional cell model systems would be beneficial in allowing us to generalise our observations beyond MCF7 cells. Although MCF7 cells were used as a convenient model for transfection, little is known about the specific relevance of EDI3 to breast cancer, and it would be useful in future work to repeat these experiments in endometrial and ovarian cancer models where there is a clearer association to disease progression.

Another limitation in this current study is that choline and glycerol-3 phosphate, the two major metabolites of interest, could not be quantified using the described ^{1}H NMR/ GC-MS metabolomics method. An alternative MS based method inclusive of these two major analytes would enable changes in metabolic profiles to be better contextualised. Also, some discrepancies were observed e.g. between the enrichment of lactate in extracellular (NMR) and intracellular (GC-MS) pools (Figure 4.4 and Figure 4.8A), which could be due to mass detector saturation, specific interferences or low signal/noise for some analytes. A more sensitive assay would allow for a more accurate determination of fractional ^{13}C enrichment. It would also be important in future work to use metabolic modelling to calculate the alterations in metabolic flux explicitly, since the differences in isotopomer distributions – although statistically significant – were often small in magnitude and therefore difficult to interpret biologically.

It is worth noting that the importance of EDI3 expression in relation to other glycerophosphodiester phosphodiesterase (GDE) isoforms remains poorly defined. It is plausible that enzymatic activities of other GDE isoforms may be influential in determining changes to the metabolic profile upon EDI3 silencing, and future experiments could be directed to address the extent to which changes in metabolic profiles may be associated with basal EDI3 and/or other GDE isoform expression levels. For example, GDE2, coded for by the *GDPD5* gene, has also been reported to be important for GPC cleavage in breast tumours (Cao *et al.* 2012a). Stewart *et. al* reported that EDI3 knockdown did not affect GDE2 mRNA expression, however, it is not yet clear if GDE2 activities might compensate for the loss of EDI3 function at the substrate level. One approach could be to compare changes in metabolic profiles in a panel of cell lines with varying background of EDI3 and other GDE isoform expressions. This would allow us to at least partially address if EDI3 background expression/ other GDE isoform co-expression play a role in determining the metabolic outcome of EDI3 interference.

4.5.2 Conclusion

In conclusion, this study demonstrates that silencing glycerophosphodiester phosphodiesterase EDI3 increases GPC level and GPC/PCho ratio in tumour cells. Also, silencing EDI3 has broader effects on tumour metabolism, as exemplified by the decrease in glucose uptake and fatty acid synthesis in MCF7 cells.

4.6 Supplementary data

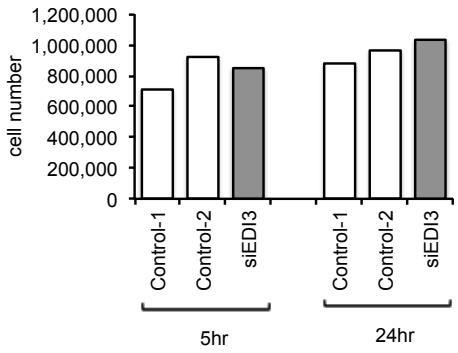

Figure 4.15 Cell numbers in MCF7 cells transfected with EDI3 siRNA

The figure above shows cell numbers from representative wells in the U-$^{13}C_6$ glucose labelled metabolomics experiment. These data were provided by our collaborator Dr. Rosemarie Marchan (Leibniz Research Centre, Dortmund)

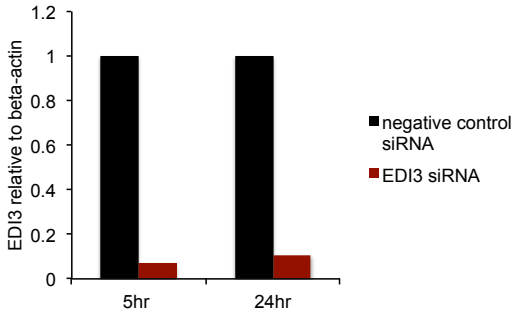

Figure 4.16 EDI3 siRNA knockdown efficiency in the U-$^{13}C_6$ glucose labelled culture metabolomics experiment in MCF7 cells.

The EDI3 protein levels were normalised to β-actin levels and to the negative control. These data were provided by our collaborator, Dr. Rosemarie Marchan.

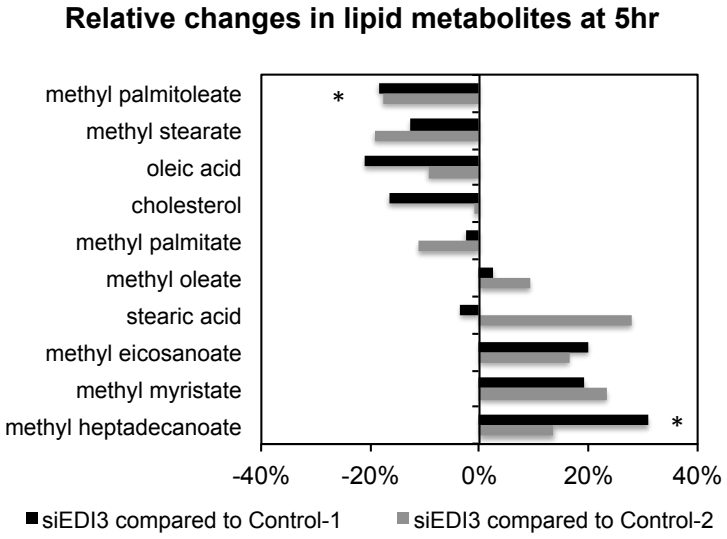

Figure 4.17 EDI3 knockdown on the relative lipid pools at the 5-hour timepoint

The GC-MS integrals were normalized by median fold change. The lipid species in the data table were ranked according to the relative changes, where a negative change represents a decrease in siEDI3 compared to the control. The bar graphs represent the mean from four technical replicates and * represents feature comparisons with Student's t-test p value < 0.05 against both control 1 and control 2.

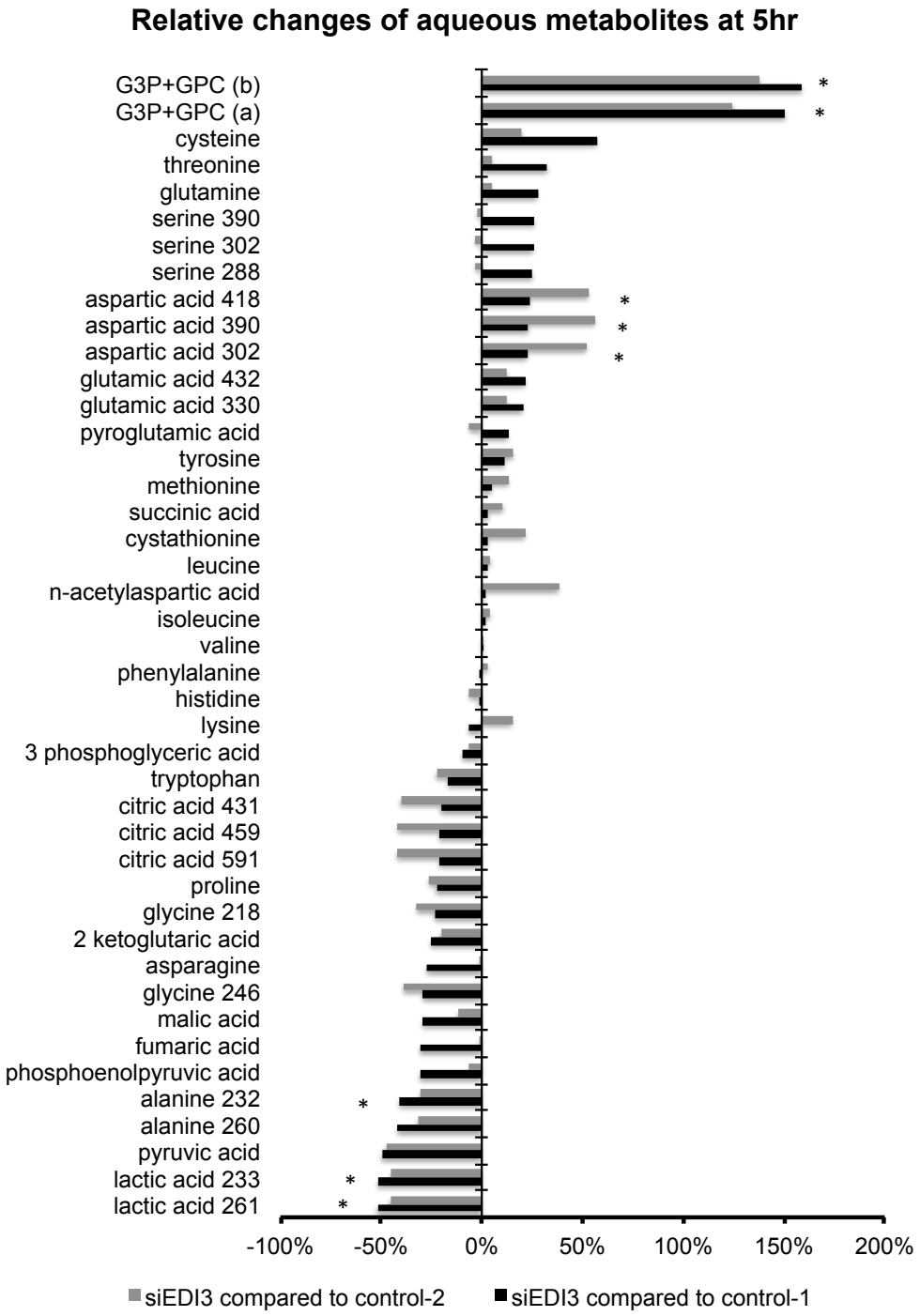

Figure 4.18 Effect of EDI3 on intracellular metabolome at the 5-hour timepoint

MCF7 cells transfected with EDI3 siRNA were compared to MCF7 cells transfected with the two independent negative control scramble vector sequences (i.e. control-1, control-2). The GC-MS integrals were normalized by median fold change, and the metabolite features in the graph was ranked by the relative changes. A positive change represents an increase in siEDI3 compared to the control. Bar graphs represent the mean from four technical replicates and * represents feature comparisons with Student's t-test p value < 0.005 against both control 1 and control 2.

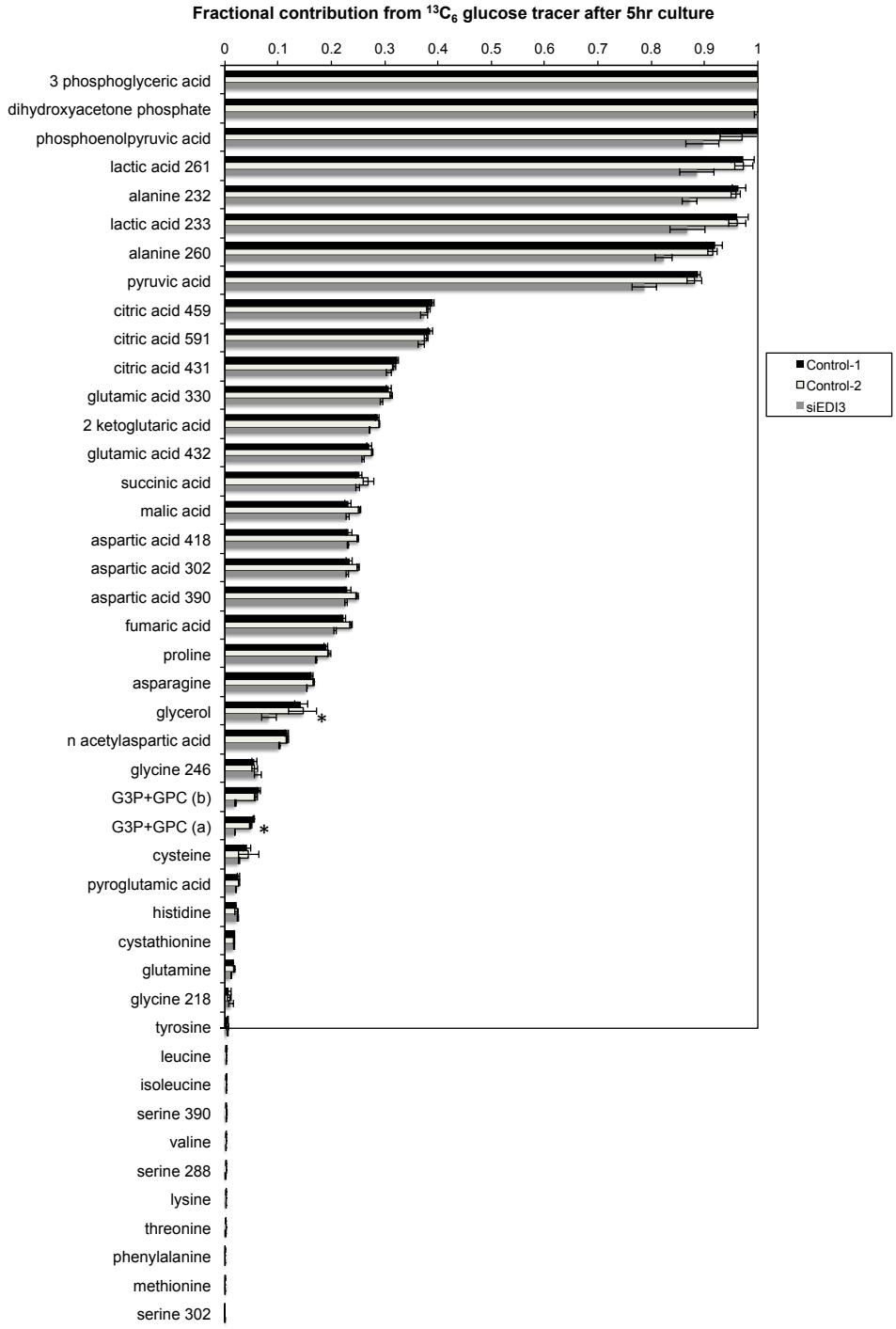

Figure 4.19 Fractional contribution of labelled glucose after 5 hours of U-$^{13}C_6$ glucose culture

Bar graphs represent the mean ± SD from four technical replicates and * represents feature comparisons with Student's t-test p value < 0.005 against both control 1 and control 2

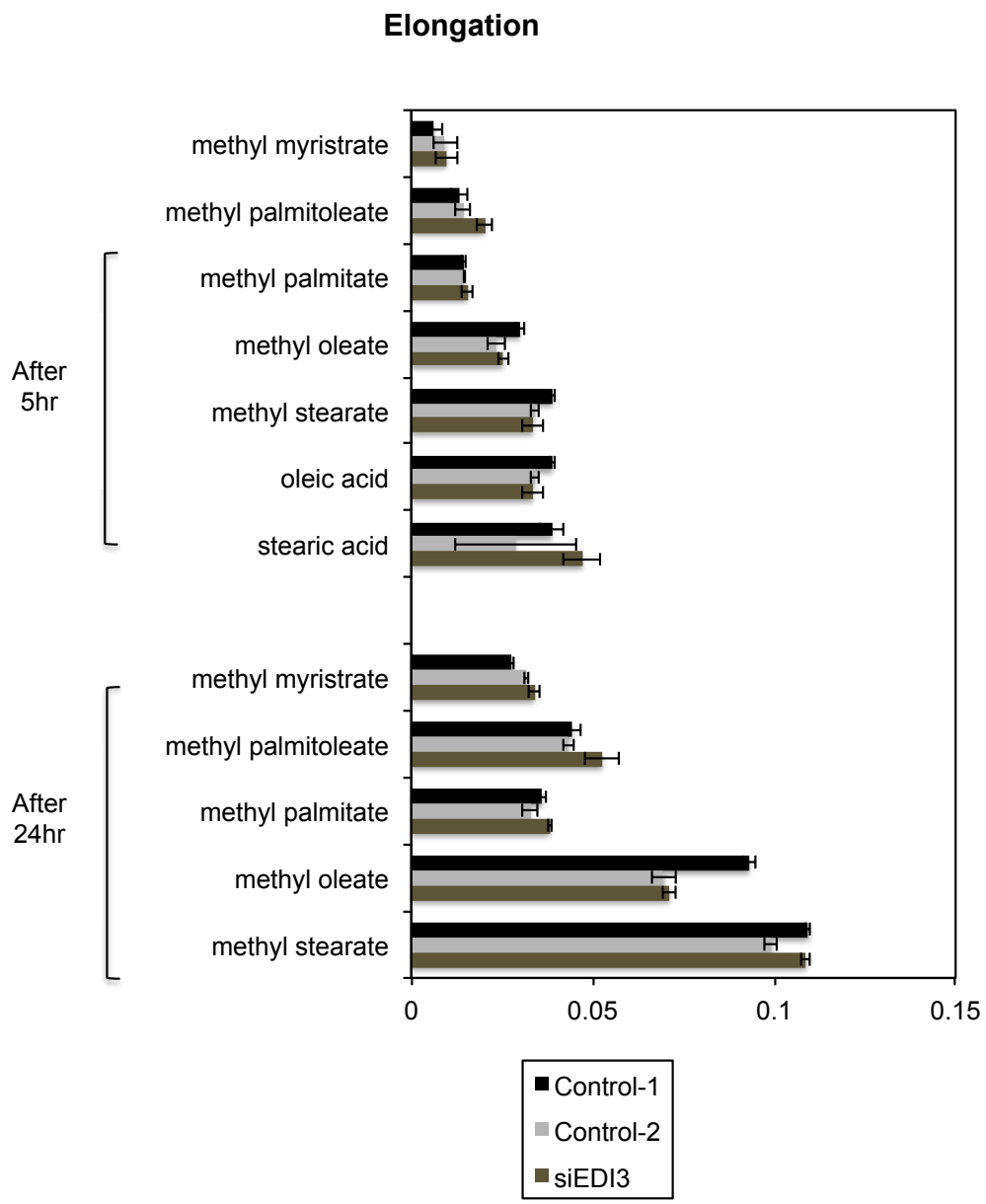

Figure 4.20 Fatty acid elongation in MCF7

The elongation parameter is derived using a 3-parameter ISA model. The bar graphs above represent the means ± SEM from four technical replicates.

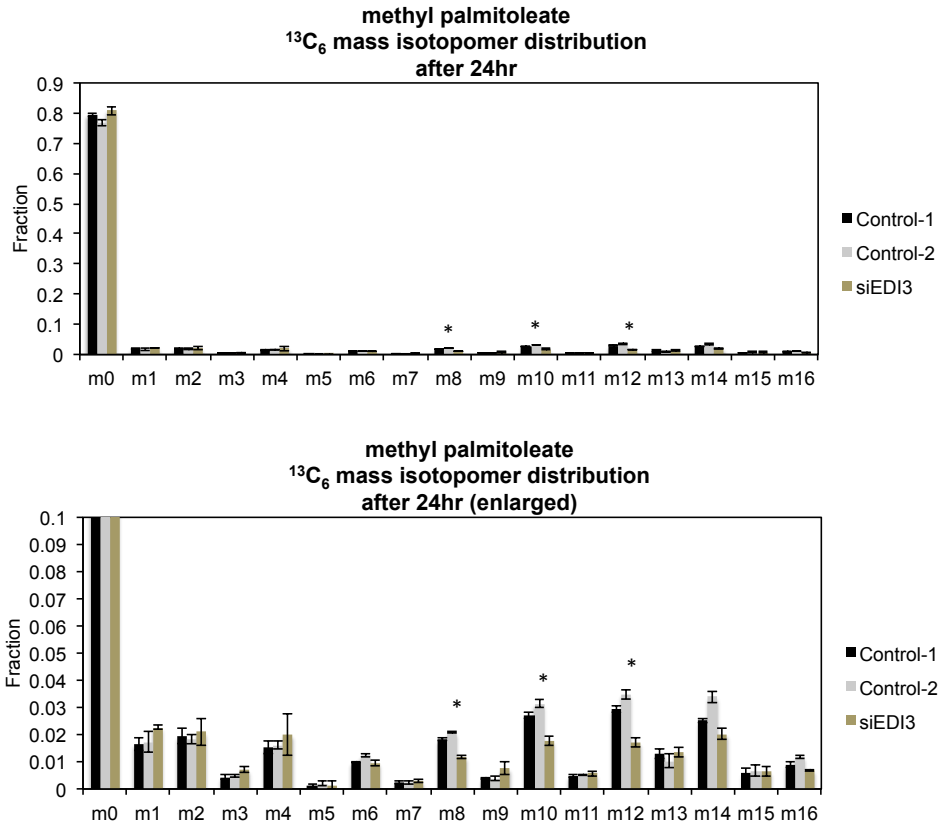

Figure 4.21 ^{13}C mass isotopomer distribution of transesterified palmitoleate after 24 culture

* represents feature comparisons with Student's t-test p values < 0.001 when comparing siEDI3 against both control groups.

Chapter 5 Targeting CSF1R mediated macrophage infiltration modulates choline metabolism in a mouse model of pancreatic cancer

5.1 Abstract

Pancreatic Ductal Adenocarcinoma (PDAC) is highly lethal in humans, and is often only possible to be diagnosed at late stages. The discovery and development of effective therapeutic solutions are urgently required, and targeting CSF1R mediated macrophage infiltration has recently emerged as a means of inhibiting malignant progression. Metabolic parameters are amongst the most tractable, reliable and practical therapeutic biomarkers in clinic, yet to date, metabolomic responses to CSF1R therapy in PDAC remain unknown. Intact pancreatic tissues and blood plasma samples from *Pdx-1-Cre, LSL-KRAS*$^{+/-}$ (KP), *Pdx1-Cre, LSL-Kras*$^{G12D/+}$ (KC) and *LSL-Kras*$^{G12D/+}$ *LSL-Trp53*$^{R172H/+}$ (KPC) mice, and KPC mice treated with a small molecular CSF1R inhibitor, AZD7507, or gemcitabine (a nucleoside analogue) were analysed by high-resolution ^{1}H nuclear magnetic resonance spectroscopy (NMR). Progressive alterations in metabolic profile were observed in the wild type, *Kras* mutant, and *Kras* and *p53* mutant (KPC) mouse tissue samples, which were then reversed with drug treatments. Increases in choline and decreases in phosphocholine levels were amongst the main phenotypic changes associated with disease progression. Also, we found that the increase in phosphocholine to taurine ratio was specific only to AZD7507, and not to gemcitabine treatment. Targeting CSF1R-mediated macrophage infiltration of the tumour microenvironment altered metabolite levels in tumours, in particular choline metabolites, in a manner that is distinct from using the conventional chemotherapeutic gemcitabine. The study implies a potential role for macrophage-tumour interactions in the regulation of choline metabolism, and highlights the potential of metabolomics for identifying pharmacodynamic biomarkers for monitoring anti-CSF1R therapy in human disease.

5.2 Introduction

The incidence of pancreatic cancer is on the rise (Hezel *et al.* 2006), and it currently accounts for approximately 3% of all cancers in Europe and in the US. The prognosis is poor, with approximately 85% of cases developing distant metastasis; overall patients have a 5-year survival rate of < 5% (Hidalgo 2010). Thus, there is a strong impetus to identify new and better therapeutic regimes. In recent years, it has emerged that chronic immune responses play important roles in promoting tumour progression (Olefsky and Glass 2010, Strelko *et al.* 2011, Biswas and Mantovani 2012, Papatriantafyllou 2012, Panni *et al.* 2013). In pancreatic cancer, targeting tumour infiltrating macrophages has been found to reduce the number of tumour-initiating cells, relieve immunosuppression, and improve chemotherapeutic responses (Bayne *et al.* 2012, Mitchem *et al.* 2013). In particular, targeting macrophage colony stimulating factor 1 receptor (CSF1R/CSF-1R) has been shown to be effective in modulating signalling and polarization of immune cells in tumours (Hamilton 1997, Priceman *et al.* 2010, Pyonteck *et al.* 2013). AZD7507 is an ATP competitive small molecule tyrosine kinase inhibitor to CSF1R developed by AstraZeneca (Scott *et al.* 2013) while several other inhibitor candidates are also currently in development (Irvine *et al.* 2006, Manthey *et al.* 2009, Patel and Player 2009, Scott *et al.* 2013).

Pancreatic ductal adenocarcinoma (PDAC) is the most common type of pancreatic malignancy. Oncogenic mutations of *KRAS* (Collins *et al.* 2012) and loss of functional tumour suppressor p53 (Morton *et al.* 2010) are highly prevalent in PDAC, and are considered important in the progression to malignancy. *KRAS* is mutated in nearly all PDAC human specimens (Almoguera *et al.* 1988), while *TP53* is mutated in > 50% of PDAC (Rozenblum *et al.* 1997). *Pdx1-Cre, LSL-Kras*$^{G12D/+}$, *LSL-Trp53*$^{R172H/+}$(KPC) and *Pdx1-Cre, LSL-Kras*$^{G12D/+}$ (KC) transgenic mice are widely used to study cell signalling and therapeutic responses in PDAC (Hingorani *et al.* 2003, Hingorani *et al.* 2005, Herreros-Villanueva *et al.* 2012). Whereas KC mice represent the pancreatic intraepithelial neoplasia (PanIN) disease spectrum, KPC animals develop PDAC with high penetrance.

Metabolic reprogramming has been reported to be important in PDAC (Tesiram *et al.* 2012, Ying *et al.* 2012, Son *et al.* 2013, Zhang *et al.* 2013), and thus understanding metabolic phenotypes in this model offers therapeutic as well as diagnostic opportunities. Here, we compare the HR-MAS NMR detectable metabolic consequences of CSF1R inhibition and gemcitabine treatment - the first-line chemotherapeutics in pancreatic cancer (Hidalgo 2010), in the transgenic *Pdx1-Cre, LSL-Kras*$^{G12D/+}$*, LSL-Trp53*$^{R172H/+}$ mouse model. Our data suggest a previously unreported role for macrophage infiltration in determining the metabolic phenotype in PDAC. In particular, we observed effects on choline metabolism, a critical pathway for tumour cell proliferation as well as an important resource for clinical biomarker discovery.

5.3 Materials and methods

Genetically modified mice, treatment and harvesting

- WT mice: *LSL-Kras*$^{G12D/+}$, *LSL-Trp53*$^{R172H/+}$ (commonly referred to as KP)
- *Kras*^{G12D} mice: *Pdx1-Cre, LSL-Kras*$^{G12D/+}$ (commonly referred to as KC)
- *Kras*^{G12D} *p53*^{R172H} mice: *Pdx1-Cre, LSL-Kras*$^{G12D/+}$, *LSL-Trp53*$^{R172H/+}$ (commonly referred to as KPC)

The protocols for generating the genetically modified heterozygous *Kras* mutant KC, and heterozygous *Kras* and heterozygous p53 mutant KPC mice have previously been described (Hingorani *et al.* 2003). The KP wild type mice were established as a control to the KPC mice, and did not express *Cre.* KP wild type mice were healthy animals that do not normally develop tumours. The *LSL-Kras*$^{G12D/+}$, *LSL-Trp53*$^{R172H/+}$ (KPC) mice were dosed with 100 mg/kg of gemcitabine (Gemzar® by Eli Lilly and Co.) or/and 100 mg/kg of AZD7507. The structure of AZD7507 has recently been described (Scott *et al.* 2013), and it has been found effective in inhibiting CSF1R activity at low dose (Figure 5.9). Tissues were harvested 5 days after treatment by flash freezing in liquid nitrogen. I was responsible for the acquisitions and the analysis of the ^{1}H NMR data. Mouse husbandry, treatments, sample harvesting and immunohistochemical staining were performed by our collaborator, Dr. Juliana Candido, who is based at the Barts Cancer Institute, London.

NMR sample preparation, acquisitions and data processing for tissue analysis

Tissue samples were kept on ice during the preparation process. 6 animals per biological group were analysed. An average of 15-20 mg of intact tissue was packed into a 4 mm/ 65 µl zirconia rotor insert. D_2O/saline solution (containing 0.9g NaCl in 100 ml D_2O) was added to the insert to maintain near-physiological conditions, as well as to provide for lock signal and to avoid the formation of air bubbles. Spectra were acquired on a 14.1 Tesla Bruker Avance III spectrometer equipped with a HR-MAS probe. Samples were spun at 5 kHz, and temperature was set at 300 degree Kelvin. Shimming was performed first using an automated Bruker gradient

shimming algorithm and signal lineshapes were then subsequently individually optimised on the methyl signal of alanine on a per sample basis. Samples were analysed using a Carr–Purcell–Meiboom–Gill (CPMG) pulse sequence with a total spin echo time of 240 ms (loop number = 300, τ = 400 μs). 128 scans were accumulated for each experiment and the data were acquired with 64k data points. The relaxation delay was set at 2 seconds and a water presaturation pulse was applied to attenuate the water signal. The total acquisition time was around 15 minutes per sample, and the total experimental time including sample preparation, spectrometer setup and shimming was around 40 minutes per sample. Preliminary experimental data from series of CPMG experiments taken over a 1-hour period suggested that metabolite signals in the tissue samples were broadly stable during the analysis. The Bruker software package Topspin 2.2 and MATLAB® (MathWorks) were used to process the spectra, and the methyl signal of alanine was used for chemical shift calibration (1.48 ppm). The following spectral resonances were removed before spectral normalisation: 0.86-0.97 ppm (lipid), 1.26-1.44 ppm (lipid), 1.17-1.21 ppm (ethanol), 1.55-1.73 ppm, 2.01-2.14 ppm (lipid), 2.23-2.33 ppm (lipid), 3.36-3.37ppm (methanol), 3.64-3.69 ppm (ethanol), 4.84-5.04 ppm (water), 5.22-5.42 ppm (lipid). The area normalisation factors were back-projected on the full data spectra to aid data visualisation. The metabolite signal integrals were then extracted and integral data were normalised using median fold change to allow for comparison across the sample set.

NMR sample preparation and data acquisitions for the analysis of mouse plasma

Aliquots of 200 μl of plasma were diluted with 300 μl of isotonic saline (0.9g NaCl in 100 ml of 80%: 20% H_2O: D_2O solution) before they were pipetted into standard 5 mm NMR tubes. High-resolution ^1H NMR spectra were acquired using a 5mm broadband-inverse tube probehead using a 14.1T Bruker AVANCE 600 spectrometer (Bruker Biospin). Carr- Purcell-Meilboom-Gill (CPMG) spectra were acquired using a standard presat pulse sequence, with the fixed echo time (τ) set at 400 μs and a total spin echo time set at 64 ms. Spectra were recorded with 64 transient scans, following 16 dummy scans. The relaxation delay was set at 3 seconds, and gradient shimming

was used before all spectral acquisitions to improve magnetic field homogeneity across the detected sample volume.

5.4 Results

5.4.1 Analysis of animal pancreatic tissues

To assess the global impact on metabolic profiles, pancreatic tissues of $Kras^{G12D}p53^{R172H}$ (KPC) mice treated with gemcitabine and/or CSF1R inhibitor were analysed by ^{1}H HR-MAS NMR, and their metabolic profiles were compared to those of the less aggressive $Kras^{G12D}$ (KC) and healthy WT mice. We were able to identify and integrate signals from the most abundant metabolites (Figure 5.3; representative spectra are illustrated in Figure 5.1), and the integral data were modelled using principal component analysis (first principal component R^2: 0.35) to provide for an unsupervised ('unbiased') multivariate summary of the global NMR metabolic profiles of the animals. The variations in metabolic profile between the animals from the different genotype/treatment groups were illustrated in Figure 5.2A, and our data model suggests that the global metabolic profiles of individual animals appear to be different between the genotype ($p < 0.05$) and the treatment groups. Although substantial variations existed within animal groups, as illustrated by the spread of the principal component analysis (PCA) scores (Figure 5.2), we observed a progressive trend in the scores, from low values for the WT mice, to intermediate values for the $Kras^{G12D}$ mice, to high values for the $Kras^{G12D}p53^{R172H}$ mice. Thus, the changes in the metabolic profile coincided with the sequential activation of oncogenic *Kras* and mutant *TP53,* which are characteristics of PDAC disease progression. Furthermore, we observed that the model scores of the $Kras^{G12D}p53^{R172H}$ mice were reversed upon treatment with the CSF1R inhibitor (AZD7507). While mice treated with gemcitabine retained similar profile scores as the untreated $Kras^{G12D}p53^{R172H}$ animals, $Kras^{G12D}p53^{R172H}$ animals that were treated with CSF1R inhibitor (AZD7507), either as a single agent or in combination with gemcitabine were found to have attained scores that were more akin to the WT and $Kras^{G12D}$ mice ($p < 0.05$ in mice treated with both gemcitabine and CSF1R inhibitor). The model loadings (Figure 5.2), which define the relative contributions of individual metabolites to the model scores, revealed that the overall variations in the HR-MAS-NMR-detectable metabolic profiles could mainly be attributed to changes in phosphocholine, glycerophosphocholine, taurine, lactate, choline and creatine levels. In our PCA data model, the presence of phosphocholine and glycerophosphocholine were associated

with low component scores, i.e. lower in the healthy WT mice, whereas high levels of taurine, lactate and choline were associated with high scores, i.e. higher in the *Kras*^{G12D} *p53*^{R172H} mice (Figure 5.2B). Scores and loadings of 2nd and subsequent principal components were also examined, however, they do not contain additional clustering information.

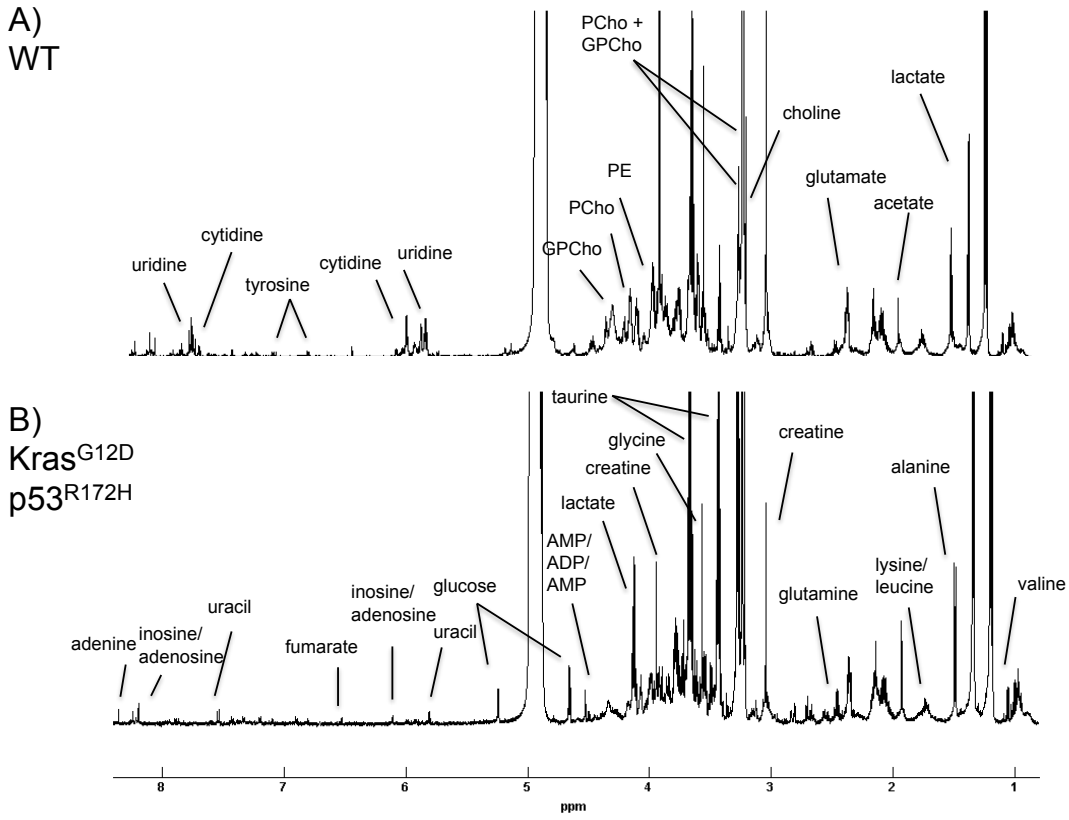

Figure 5.1 Representative high-resolution magic angle spinning proton magnetic resonance spectra of pancreatic tissues

(A) Wild type healthy mice and (B) *Kras*^{G12D} *p53*^{R172H} (KPC) mice with PDAC

A)

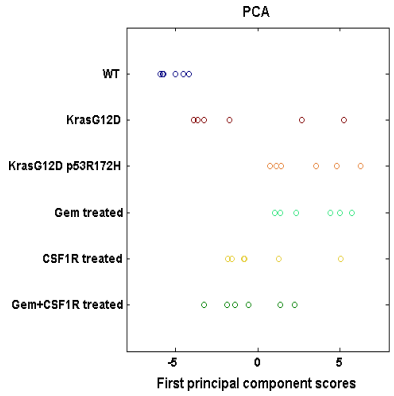

B)

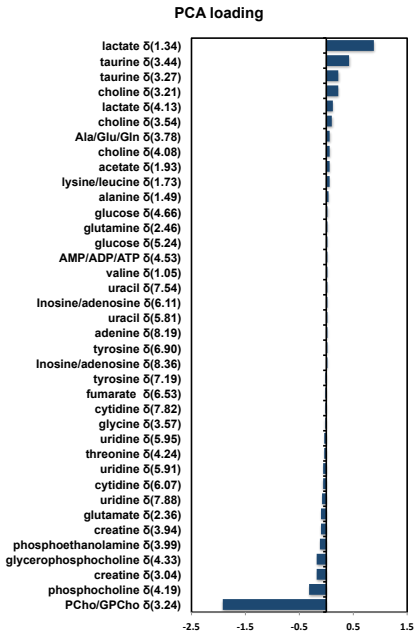

Figure 5.2 Principal component analysis of MAS-NMR spectra of pancreatic tissues from WT, *Kras*^{G12D} (KC) mice, *Kras*^{G12D}*p53*^{R172H} (KPC) mice, and KPC mice treated with gemcitabine and small molecule CSF1R inhibitor

The WT mice were healthy animals and the KPC mice were models for PDAC. The metabolite integrals were mean-centred and UV-scaled prior to Principal Component Analysis (A) the score plot and (B) the loading plot of the first principal component (R^2 = 0.35). Each data point on the score plot represents a different animal, and 6 animals per group were analysed. PCho /GPCho (δ3.24) represents the integral sum of the two overlapping singlet resonance peaks from PCho and GPC; the PCho /GPCho (δ3.24) signal contributed significantly more towards the model loading compared to the PCho (δ4.19) and GPC (δ4.33) multiplet signals separately. This was likely because the PCho /GPCho (δ3.24) signals were more intense (higher signal to noise) compared to the two multiplet signals, leading to lower analytical variability and stronger correlation/covariance with other metabolite signal peaks.

1H MAS NMR metabolic profile of pancreatic tumor tissues

		Profile of disease progression (relative change to WT mice)		Effect of treatment on KrasG12D p53R172H (KPC) mice (relative change to KPC mice)		
Metabolite signal	**δ, ppm**	**Kras G12D (KC)**	**KrasG12D p53R172H (KPC)**	**Gemcitabine**	**CSF1Ri**	**Gemcitabine and CSF1Ri**
choline	3.54	303%	532% **	-7%	-24%	-37%
choline	3.21	155% *	447% **	-19%	-34%	-59% **
AMP/ADP/ATP	4.53	271% *	293% **	27%	-12%	-27%
choline	4.08	61%	252% **	-26%	-32%	-58% **
lactate	1.34	72% *	174% *	45%	-13%	-30%
tyrosine	6.90	75%	154% *	-55% *	-53%	-46%
glucose	4.66	167%	151%	-15%	-27%	8%
Inosine/adenosine	6.11	-10%	151%	-29%	-42%	-40%
glucose	5.24	188%	139%	31%	16%	87%
taurine	3.44	104% *	135% *	9%	-15%	-29%
uracil	7.54	114%	131%	62%	-8%	-24%
adenine	8.19	55%	55%	-7%	-11%	-20%
glutamine	2.46	2%	40%	-17%	-30%	-29%
uracil	5.81	-12%	35%	5%	-1%	0%
glycine	3.57	28%	34%	-18%	-2%	7%
acetate	1.93	70%	22%	193%	146%	394%
valine	1.05	-1%	22%	1%	-28%	-18%
taurine	3.27	22%	19%	11%	1%	-17%
lactate	4.13	-10%	19%	14%	-12%	-31%
tyrosine	7.19	-13%	17%	-40%	-34%	-33%
Inosine/adenosine	8.36	-11%	5%	-24%	-12%	15%
lysine/leucine	1.73	-10%	5%	54%	-40%	21%
alanine	1.49	2%	-7%	38%	-5%	-8%
Ala/Glu/Gln	3.78	-11%	-9%	28%	0%	1%
glutamate	2.36	-22%	-31%	17%	19%	16%
phosphoethanolamine	3.99	-12%	-39%	46%	21%	53%
fumarate	6.53	-37%	-46%	-5%	63%	9%
glycerophosphocholine	4.33	-24%	-51%	40%	61%	78%
PCho/GPCho	3.24	-30%	-57% *	6%	41%	45%
cytidine	7.82	-26%	-57% *	-49%	63%	124% **
uridine	5.91	-53%	-62%	-30%	40%	86% *
threonine	4.24	-44%	-64%	-37%	44%	53%
phosphocholine	4.19	-34%	-67% **	-12%	85%	79%
creatine	3.94	-64% **	-73% **	27%	46%	13%
creatine	3.04	-65% **	-75% **	23%	52%	21%
cytidine	6.07	-48%	-76% **	-10%	71%	121% *
uridine	5.95	-41%	-77% **	-3%	104%	137% *
uridine	7.88	-59% *	-79% **	-42%	64%	126% **

Figure 5.3 Relative metabolite profile of WT, *Kras*^{G12D}, *Kras*^{G12D}*p53*^{R172H} mice (KPC) and KPC mice treated with gemcitabine and small molecule CSF1R inhibitor in pancreatic tissues

The metabolites in the table are ranked according to the relative changes between the WT and the *Kras*^{G12D} *p53*^{R172H} mice. The WT were healthy mice and the KPC mice were models for PDAC. Significant differences were determined using one-way ANOVA and Student's t-test statistics (n =6). Data were normalized to the median fold change from the median spectrum (Dieterle *et al.* 2006) based on the extracted integrals. * denotes one-way ANOVA $p < 0.05$ and Student's t-test p value < 0.05, ** denotes one-way ANOVA $p < 0.05$ and Student's t-test p value < 0.005.

Analysis of the individual metabolite integrals reinforced our findings that disease progression in the $Kras^{G12D}$ (KC) and $Kras^{G12D}$ $p53^{R172H}$ (KPC) mice was significantly associated with elevated choline, AMP/ADP/ATP, lactate, and taurine levels, and reduced levels of phosphocholine, creatine and the nucleosides uridine and cytidine (Figure 5.3). Significantly, effects associated with disease progression on choline, uridine and cytidine were reversed when $Kras^{G12D}p53^{R172H}$ (KPC) mice were treated with gemcitabine and CSF1R inhibitor (AZD7507) in combination, suggesting a subset of metabolites could potentially be used as biomarkers for evaluating treatment efficacy in PDAC.

When the pattern and the direction of metabolite modulations were examined (Figure 5.4), we noted remarkable similarities between levels of phosphocholine, uridine and cytidine, and also between choline, taurine, AMP/ADP/ATP and lactate, indicating that changes may be consequences to alterations to only a small handful of common systemic processes. Modulation in phosphocholine and nucleoside (uridine/cytidine) levels might imply changes in cellular replicative potentials, while differences in choline, taurine, lactate, and AMP/ADP/ATP levels may hint at changes in energy balance, nutrient transport and osmotic regulations.

CSF1R expression is specific to macrophages, and CSF1R inhibitors specifically target macrophage populations in the tumour microenvironment. We observed contrasts in the metabolite profile between mice treated with the nucleoside analogue gemcitabine and those on AZD7507 treatment, with the latter appearing to be more effective in reversing the change in metabolite patterns associated with disease progression in the $Kras^{G12D}p53^{R172H}$ (KPC) mouse model (Figure 5.2, Figure 5.3, Figure 5.4). However, as individual animal variations were generally large within treatment groups, no single metabolite feature was found to be significant in demonstrating anti-CSF1R treatment responses. To enhance the statistical power of detection, signal-ratio between metabolites with contrasting pattern of variations in the dataset were instead considered (Figure 5.5). Taking signal-ratio measurements between highly abundant metabolites can sometimes be advantageous as it avoids errors from low S/N integrals. Phosphocholine ratios to lactate, taurine, and choline were calculated, with the phosphocholine: taurine ratio particularly valuable in

demonstrating treatment effects (Figure 5.5). The Phosphocholine: taurine ratio significantly decreased with disease progression ($p < 0.005$), which was then reversed when $Kras^{G12D}$ $p53^{R172H}$ (KPC) mice were treated with AZD7507 or in combination with gemcitabine (both $p < 0.05$). No changes in the phosphocholine: taurine ratio were seen with KPC mice on gemcitabine treatment, and responses between gemcitabine and CSF1R inhibitor treatments were significantly different ($p < 0.05$), indicating that CSF1R inhibitor (AZD7507) generated a distinct metabolic response to conventional chemotherapy in the $Kras^{G12D}$ $p53^{R172H}$ (KPC) mice.

The contrasting pattern of response in choline and phosphocholine we observed was striking. Both choline and phosphocholine are precursor metabolites to phosphatidylcholine biosynthesis; choline kinase is responsible for the enzymatic conversion of choline to phosphocholine, and has been frequently implicated in cancer signalling (Glunde *et al.* 2011). Thus, through our collaborators at the Barts Cancer Institute (London), we further explored if choline kinase expression was modulated, and if so, how choline kinase expression might be related to the presence of macrophages in the mice pancreas using immunohistochemical staining. Preliminary results from immunohistochemical staining appeared to show that mice treated with CSF1R inhibitor expressed a higher level of choline kinase α, compared to mice treated with gemcitabine and untreated mice (Figure 5.6) however these data were not quantitative or sufficiently replicated. Also, the data indicate that choline kinase-α and the macrophage marker (F4/80) did not co-localise, suggesting that choline kinase α expression may be due to other cell types in the tumour (Figure 5.6).

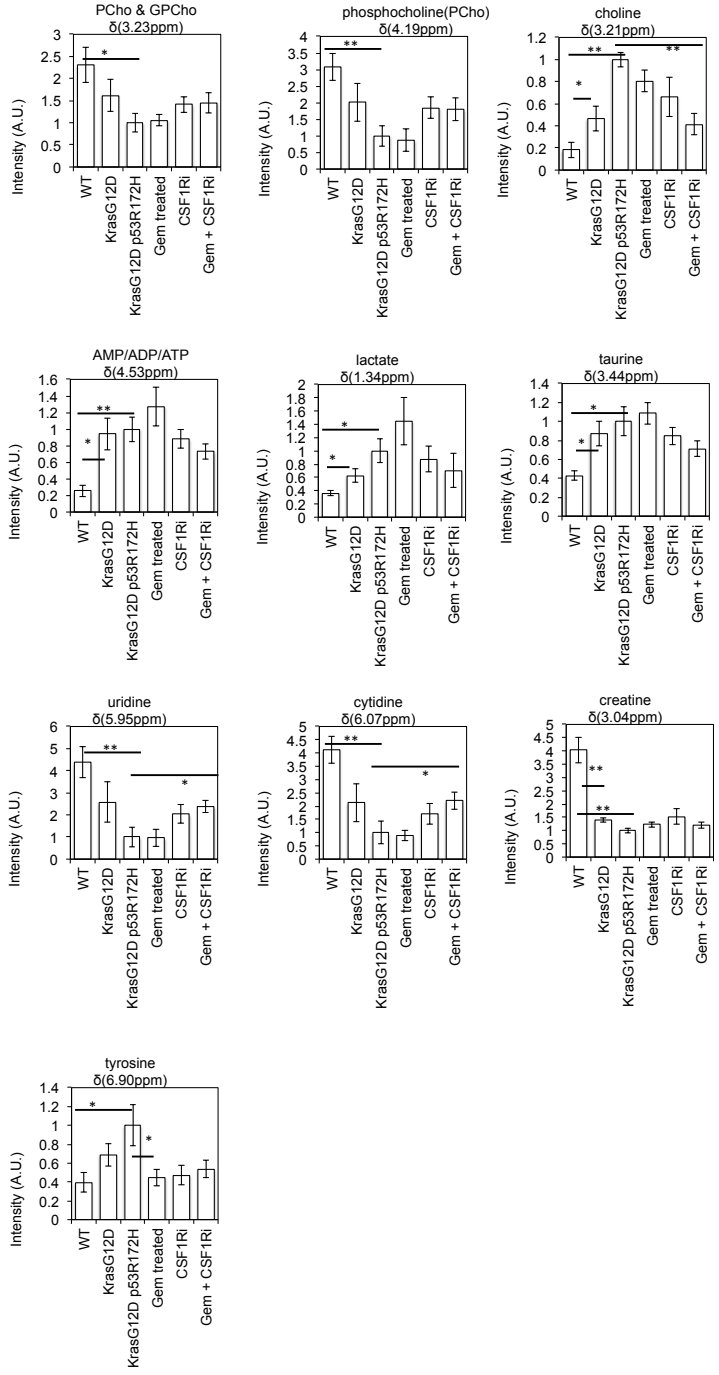

Figure 5.4 Cancer progression and treatments significantly altered abundance of a number of metabolite features in pancreatic tissues

The abundance of metabolites is presented relative to the $Kras^{G12D}p53^{R172H}$ (KPC) mice. The wild type (WT) mice were healthy animals. $Kras^{G12D}p53^{R172H}$ (KPC) mice, models for PDAC, were treated with gemcitabine (Gem), AZD7507 (CSF1Ri) or in combination (Gem + CSF1Ri). The bar graphs show the mean ± SEM of measurements from 6 animals. Significant differences were determined using one-way ANOVA and Student's t-test statistics. * denotes one-way ANOVA $p < 0.05$ and Student's t-test $p < 0.05$, ** denotes one-way ANOVA $p < 0.05$ and Student's t-test $p < 0.005$.

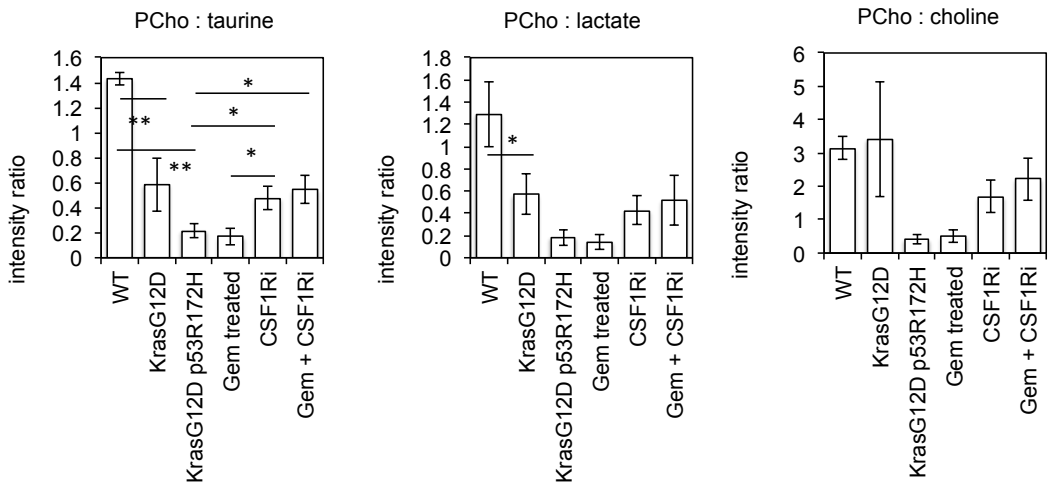

Figure 5.5 Phosphocholine (PCho) to taurine signal ratio in tissues is a potential therapeutic marker for anti-CSF1R treatment

PCho: taurine, PCho: lactate and PCho: choline signal ratios were calculated. The wild type (WT) mice were healthy animals. $Kras^{G12D}p53^{R172H}$ (KPC) mice, models for PDAC, were treated with gemcitabine (Gem), AZD7507 (CSF1Ri) or in combination (Gem + CSF1Ri). The bar graphs show the mean ± SEM of measurements from 6 different animals. Significant differences were determined using one-way ANOVA and Student's t-test statistics. * denotes one-way ANOVA $p < 0.05$ and Student's t-test p value < 0.05, ** denotes one-way ANOVA $p < 0.05$ and Student's t-test p value <0.005.

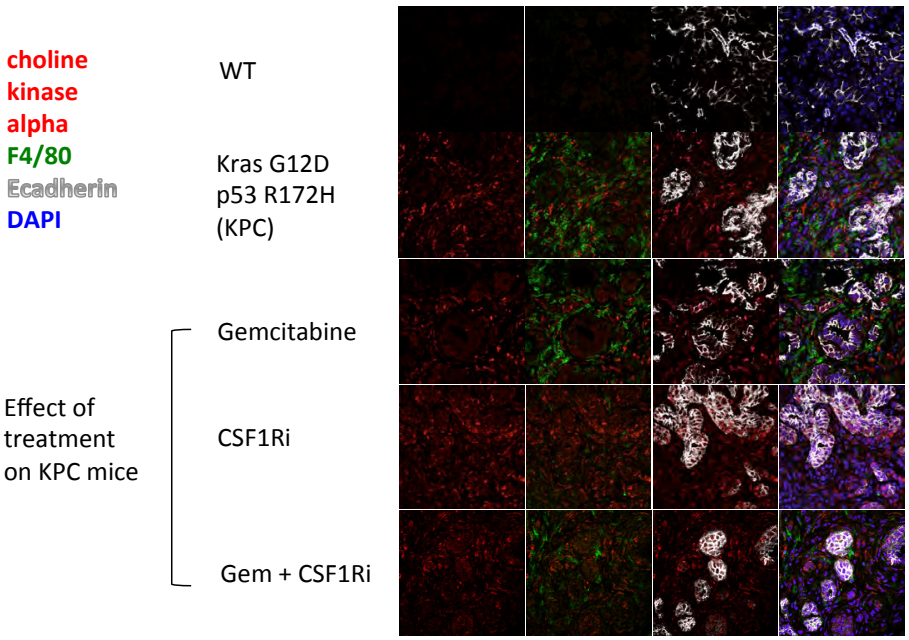

Figure 5.6 Treatments induce changes in choline kinase-α expression and macrophage population responses in the KrasG12Dp53R172H (KPC) mice pancreas tissues

Immunohistochemical staining of choline kinase-α and F4/80, a marker of macrophages in mice, were performed on representative pancreatic tissue samples. These data demonstrate that (i) AZD7507 (CSF1Ri) was more effective than gemcitabine (Gem) in reducing macrophage population; (ii) CSF1Ri appeared to have increased choline kinas-α expressions in pancreatic tissues; (iii) choline kinas-α and macrophage marker did not co-localise and suggest that the presence of choline kinase-α expression is likely associated with other cell types in the tumour. These were data provided by our collaborator, Dr. Juliana Candido.

5.4.2 Analysis of animal blood plasma samples

Animal blood plasma samples were analysed using 1H NMR spectroscopy in conventional 5mm tubes, metabolite resonances were annotated and quantified, and the metabolite levels between the genotype/treatment groups were compared (Figure 5.7). Plasma glucose was observed to be different between the genotype models (Figure 5.8): glucose levels were found highest in the wild type (WT) mice, and lowest in the $Kras^{G12D}$ $p53^{R172H}$ (KPC) mice (Figure 5.8). Also glucose concentrations in the $Kras^{G12D}$ $p53^{R172H}$ (KPC) animals were elevated upon drug treatments ($p < 0.05$ for CSF1R treatment and combinatorial treatment). The reasons behind the modulation in plasma glucose are unclear, however it is possible that the systemic behavioural and physiological changes the mice underwent as the disease progressed may play a role. Also, we found that $Kras^{G12D}$ mice had significantly higher level of lactate ($p < 0.05$) when compared to the wild type (WT) healthy mice, and two of the three $Kras^{G12D}$ $p53^{R172H}$ mice (KPC) had high levels of lipids (Figure 5.8). However, we did not observe significant differences in plasma metabolites that discriminate between mice treated with CSF1R inhibitor (AZD7507) and those on gemcitabine treatment.

In addition, we noted that intensities of an unassigned doublet resonance (at 7.82ppm), were statistically correlated to both citrate levels and to another unassigned multiplet resonance (at 7.37ppm). We found that these resonance signals were elevated (2-fold higher) in the $Kras^{G12D}$ mice compared to the WT healthy mice ($p < 0.05$) (Figure 5.8). While we are unclear of the origin of these signal resonances, it is possible that these might be artefacts of adding anticoagulant during sample collection (Barton *et al.* 2010).

1H NMR metabolic profile of blood plasma

		Profile of disease progression (relative change to WT mice)		Effect of treatment on KrasG12D p53R172H (KPC) mice (relative change to KPC mice)		
Metabolite signal	**δ, ppm**	**Kras G12D (KC)**	**KrasG12D p53R172H (KPC)**	**Gemcitabine**	**CSF1Ri**	**Gemcitabine and CSF1Ri**
fatty acid (CH=CH-CH2-CH=CH)n	2.81	61%	381%	-86%	-83%	-73%
fatty acid (CO-CH2-CH2)	1.59	11%	359%	-92%	-91%	-87%
fatty acid (CH=CH)	5.32	-4%	332%	-93%	-82%	-76%
fatty acid (-CO-CH2)	2.25	-8%	197%	-80%	-75%	-74%
fatty acid (CH2)n	1.32	45%	169%	-74%	-57%	-64%
creatine	3.95	-30%	130%	-61%	-46%	-54%
glutamate	2.42	-63%	86%	-19%	-58%	-67%
methionine + fatty acid (CH-CH=)	2.07	14%	81%	-51%	-42%	-42%
glutamine	2.47	29%	58%	-13%	-38%	-49%
alanine	1.49	71%	44%	3%	8%	-29%
fatty acid (CH3)	0.87	11%	32%	-32%	4%	-4%
lactate	1.35	110% *	26%	-6%	30%	-31%
valine	1.09	-43%	23%	-23%	-7%	-33%
isoleuine	1.06	36%	22%	-7%	6%	-16%
lactate	4.12	70%	17%	-6%	24%	-22%
glycerol	3.59	141%	15%	-31%	99%	26%
pyruvate	2.39	31%	4%	-25%	9%	-8%
formate	8.47	-41%	1%	-44%	-10%	-20%
histidine	7.07	19%	-1%	-20%	9%	-20%
tyrosine	6.92	121%	-8%	-18%	-53%	-1%
branched chain amino acids	1.02	173%	-21%	5%	106%	-4%
glycerol	3.68	27%	-30%	41%	83%	46%
acetate	1.94	34%	-30%	101%	-3%	-51%
glucose	3.27	10%	-33%	25%	4%	-27%
glucose	3.77	-21%	-36%	26%	31%	26%
theonine	1.21	-14%	-37%	54%	37%	32%
glucose	3.43	-24% *	-41% *	31%	46%	36%
glucose	3.56	-25%	-42%	31%	39%	37%
glucose	3.92	-25% *	-44%	39%	48% *	43%
phospholipids	3.23	-3%	-46%	73%	136%	100%
glucose	3.48	-27% *	-47% *	44%	50% *	48%
glucose	4.67	1%	-48%	28%	22%	35%
glucose	5.25	-26% *	-49% **	54%	64% *	61% *
glucose	3.85	-30% *	-50% *	39%	53%	49%
glucose	3.52	-37%	-50%	42%	39%	51%
unassigned multiplet	7.37	192%	-59%	-82%	-98%	-93%
citrate	2.55	102%	-62%	-62%	-27%	-62%
unassigned doublet	7.82	324% *	-62%	-100%	10%	-8%
citrate	2.68	110%	-62%	-48%	-10%	-54%
citrate	2.70	65%	-69%	27%	47%	33%

Figure 5.7 Relative blood plasma profile of WT, *Kras*^{G12D}, *Kras*^{G12D} *p53*^{R172H} mice (KPC) and KPC mice treated with gemcitabine and small molecule CSF1R inhibitor

Integrals were extracted from data acquired using CPMG pulse sequence experiments. Wild type mice (WT) were healthy animals. *Kras*^{G12D}*p53*^{R172H} (KPC) mice, models for PDAC, were treated with gemcitabine (Gem), AZD7507 (CSF1Ri) or in combination (Gem + CSF1Ri). Metabolites are ranked according to the magnitudes of relative change between the WT and the *Kras*^{G12D}p53^{R172H} mice. Significance was determined using one-way ANOVA and Student's t-test statistics (n =3). * denotes one-way ANOVA $p < 0.05$ and Student's t-test p value < 0.05, ** denotes one-way ANOVA $p < 0.05$ and Student's t-test p value < 0.005.

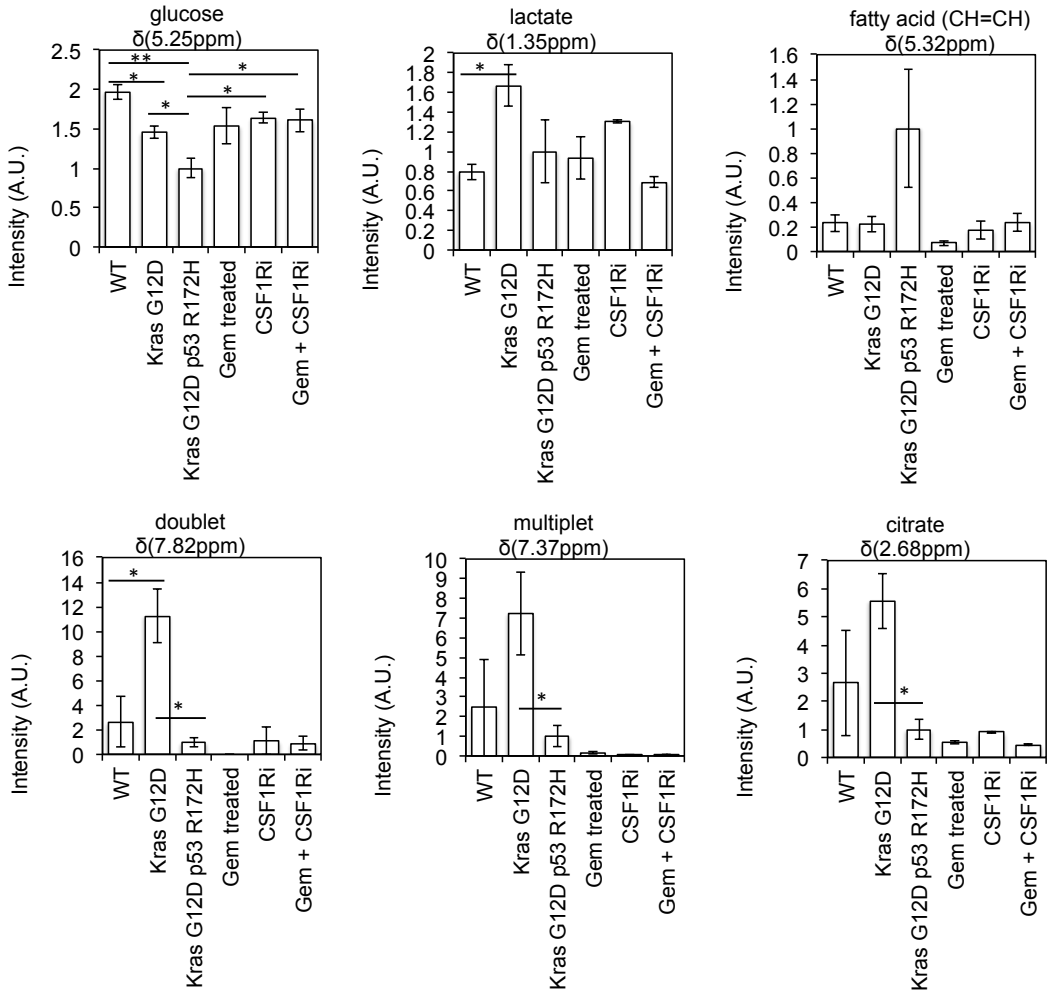

Figure 5.8 Genotype and disease progression significantly affected relative abundances of common blood plasma metabolites such as glucose, lactate and citrate detected

The wild type (WT) mice were healthy animals. $Kras^{G12D}p53^{R172H}$ (KPC) mice, models for PDAC, were treated with gemcitabine (Gem), AZD7507 (CSF1Ri) or in combination (Gem + CSF1Ri). Averages from three different animals were represented and error bars represent SEM. Significant differences were determined using one-way ANOVA and Student's t-test statistics (n =6). * denotes one-way ANOVA $p < 0.05$ and Student's t-test p value < 0.05, ** denotes one-way ANOVA $p < 0.05$ and Student's t-test $p < 0.005$.

5.5 Discussion

5.5.1 Metabolic profiles of pancreatic cancer progression and treatment efficacy

The transgenic *Pdx1-Cre, LSL-Kras$^{G12D/+}$, LSL-Trp53$^{R172H/+}$ (KPC)* and *Pdx1-Cre, LSL-Kras$^{G12D/+}$ (KC)* animal models have been widely used in pancreatic cancer studies, and our analysis of pancreatic tissue showed that metabolic profiles of the mouse models broadly mirrored the changes in tumour aggressiveness. A number of studies have already demonstrated the utility of metabolomics in identifying diagnostic markers of disease stage in a range of sample types, including blood serum/plasma, urine, bile and saliva (Di Gangi *et al.* 2014). However, studies with pancreatic tissue samples remain few. To our knowledge, there is only one other published metabolic profiling study examining progression phenotypes using transgenic animal models in pancreatic cancer, and it identified decreased palmitoleate in the *Kras(G12V)* induced PDAC rat model compared to the control (Yabushita *et al.* 2013). Another mouse xenograft model study reported that mice with pancreatic cancer had higher levels of choline, taurine, and lactate, and lower levels of phosphocholine compared to normal nude mouse pancreas (He *et al.* 2013). Furthermore, with a small sample set of cancerous and matched normal human pancreas, Kaur *et. al* found that levels of nicotinamide adenine dinucleotide and uridine were lower, while the level of taurine was higher in the cancerous tissues (Kaur *et al.* 2012). These reported findings were consistent with the phenotype we observed in the *Kras*^{G12D} (KC) and *Kras*^{G12D}p53^{R172H} (KPC) disease progression model, highlighting the translational relevance of these specific transgenic models. Our study demonstrates the potentials for assessing disease staging and therapeutic efficacy using metabolic information from the pancreatic tumours.

5.5.2 Anti-CSF1R and gemcitabine treatments resulted in dissimilar responses

Our results show that CSF1R inhibition and gemcitabine were capable of producing differential outcomes in reversing the choline phospholipid metabolite levels associated with pancreatic tumour progression in the (KPC) *Pdx1-Cre, LSL-Kras$^{G12D/+}$, LSL-Trp53$^{R172H/+}$* mouse model. For example, we showed that only anti-

CSF1R treatment elevated phosphocholine levels in the pancreas, and this is supported by another recent study using an identical mouse model (KPC) showing that gemcitabine treatment also did not alter phosphocholine or glycerophosphocholine levels (Bapiro *et al.* 2014). This may reflect the fact that conventional chemotherapy and CSF1R inhibition treatments differ significantly in their mechanisms of action as well as the cell types they target. While gemcitabine disrupts DNA replication and thereby causes equivocal growth arrest (Hertel *et al.* 1990), the CSF1R inhibitor blocks kinase signalling critical to proliferation, differentiation and survival in monocytes and macrophages (Imamura *et al.* 1990, Hamilton 1997). CSF1R is specific to tumour-associated macrophages (TAMs) and related myeloid cells; PDAC tumours have been shown not to express a significant level of CSF1R *in vivo* and *in vitro* (Mitchem *et al.* 2013). And while CSF1R inhibition blocks growth of TAMs, gemcitabine has been shown to increase macrophage infiltration into PDAC tumours (Mitchem *et al.* 2013). Furthermore, we also know that macrophage population in the pancreas, as measured by F4/80 expression, rises with increasing tumourigenicity of the transgenic models (unpublished data from the laboratory of Prof. Hagemann). Hence, the change in metabolic phenotype we observed here could reflect variation in macrophage populations and their metabolic functions. Importantly, our results could imply that it would be possible to differentiate conventional chemotherapy and treatments targeting immune cells through their metabolic consequences, potentially enabling the monitoring of specific therapeutic regimes in patients.

5.5.3 Choline phospholipid metabolites, tumour cells and macrophages

One of the interesting findings concerns the directionality of changes in phosphocholine and choline levels, and the extent to which these may be translated to clinical and diagnostic settings in humans. Phosphocholine is a precursor to the most abundant membrane phospholipid phosphatidylcholine (Ridgway 2013), and its synthesis and turnover is critical for cellular proliferation and maintenance. While lower phosphocholine levels in cancerous tissues were observed in our model as well as several other animal models of pancreatic cancer, phosphocholine levels have been widely reported to be elevated in a range of cancers (Ackerstaff *et al.* 2003,

Glunde *et al.* 2011). Changes in phosphocholine have previously been attributed to increases in choline kinase-α and HIF1α activities (Iorio *et al.* 2005, Janardhan *et al.* 2006, Glunde *et al.* 2008). However, this is far from universal, and decreases in phosphocholine levels has also been reported in the TRAMP prostate cancer mouse model (Teichert *et al.* 2008, Raina *et al.* 2009, Raina *et al.* 2013), where Teichert *et al.* found no differences in choline kinase expression between malignant and normal tissues. Furthermore, von Forstner *et al.* also found no significant changes in CHKA and CHKB gene expression in pancreatic tumours (von Forstner *et al.* 2008). It is possible that phosphocholine levels are influenced by other factors, such as acidosis (Galons *et al.* 1995), or it might not reflect PdtCho level (Raina *et al.* 2009, Raina *et al.* 2013). Also, CTP:Phosphocholine Cytidylyltransferase (CCT), a rate-limiting enzyme that converts phosphocholine to CDP-choline, could be induced by *ras* to stimulate PdtCho synthesis in tumour cells (Arsenault *et al.* 2013) or free-cholesterols in macrophages through post-translational regulation (Shiratori *et al.* 1994). Increased CCT activity would also explain the decrease in phosphocholine level with cancer progression we observed. Moreover, according to a recent study in a swine chronic pancreatitis model, a decrease in phosphocholine could also be associated with immune response (Sun *et al.* 2014). Macrophages have distinctive metabolic characteristics (Biswas and Mantovani 2012), and actively regulate cholesterol and phospholipid metabolism (Tabas 2000, Spann *et al.* 2012). In addition, lysophosphatidylcholine (LysoPC) could also act as signalling molecules in the recruitment of primary macrophages and monocytes. As mentioned in the introduction (Section 5.2), apart from pancreatic cancer, targeting CSF1R-mediated tumour-infiltrating macrophages and myeloid cells has also shown promise in glioma (Pyonteck *et al.* 2013), leukaemia (Aikawa *et al.* 2010), prostate (Xu *et al.* 2013) and breast (DeNardo *et al.* 2011) cancers. Further mechanistic insights would help to untangle both tumour-macrophage metabolic signalling, and help determine the context and translational value of using choline- PET and MRS imaging probes in clinical biomarker studies, particularly in tumours where inflammatory response is important.

5.5.4 Limitations and Future work

Our study implies a potential role for macrophage-tumour interactions in the regulation of choline phospholipid metabolites, however the mechanism by which anti-CSF1R treatment led to the changes in choline and phosphocholine levels is currently unclear. While anti-CSF1R treatment reduced macrophage populations in the tumour, it has been reported that CSF1R blockage can lead to enhanced anti-tumour responses from myeloid cells and T-cells (Zhu *et al.* 2014). Dynamics of other immune cell types and tumour cells may be important to the regulation of choline phospholipid metabolites in tumour tissues. Further work could involve metabolic analysis of CSF1R inhibition using tumour, T-cell and macrophage cell culture models to ascertain which specific cell type may be responsible for change in regulation of choline kinase activity and choline phospholipid metabolites in the tumour microenvironment upon CSF1R inhibition.

In the chapter, we mentioned that ^{1}H NMR-detectable choline, phosphocholine, and glycerophosphocholine resonances could potentially be utilised to monitor tumour progression and anti-CSF1R treatment in clinics. However, it is worth noting that our analysis was performed with a MAS probe in a 14.1T spectrometer, whilst most MR spectrometers currently in clinical use typically operate at a lower magnetic field strength (1.5T or 3T), where choline, phosphocholine, and glycerophosphocholine resonances at 3.2 ppm are not readily resolved; they are instead reported together as 'total choline' (Stanwell *et al.* 2005). In our study, anti-CSF1R treatment simultaneously led to higher phosphocholine and lower choline levels. Since phosphocholine resonance was on average 3 - 4 times more intense as that of choline, variations in phosphocholine level would dominate the overall choline, phosphocholine, and glycerophosphocholine resonance profile at 3.2 ppm, potentially leading to the loss of specific metabolic information. Further work could focus on understanding the variations in choline level in this tumour model, and the extent to which variations in choline might be related to choline uptake. Ideally, concentration data should be presented in molar quantity per unit mass (i.e. μmol/gram), however in the current work samples were analysed in the absence of an appropriate internal or external concentration reference, which could be applied in future studies (Wider and Dreier 2006). If alterations to choline metabolism are

confirmed then choline-PET imaging could also be used in addition to MR approaches to track choline uptake *in vivo* and monitor anti-CSF1R treatment efficacy.

5.5.5 Conclusion

In conclusion, this study demonstrates that disease progression in the *Pdx1-Cre, LSL-Kras$^{G12D/+}$ LSL-Trp53$^{R172H/+}$* (KPC) mice is associated with ^{1}H NMR detectable choline phospholipid metabolites. Targeting macrophage infiltration in KPC tumours with CSF1R inhibitor altered phosphocholine levels, providing a potential pharmacodynamic marker *in vivo*.

5.6 Supplementary Data

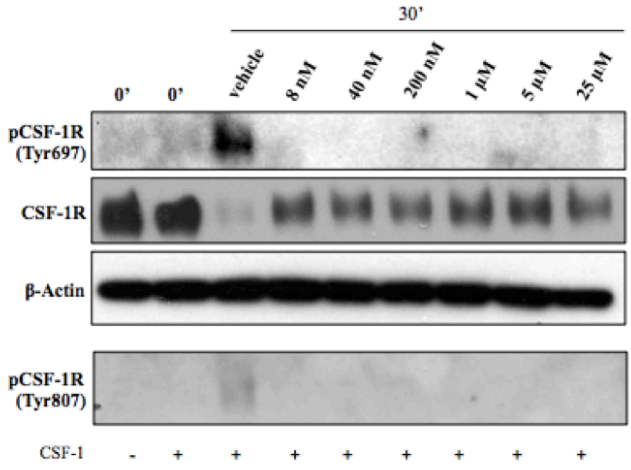

Figure 5.9 Effect of AZD7507 treatment on phosphorylation status of CSF1R in macrophage cells in culture.

Western blot data showing phosphorylation of CSF1R (Tyr807 and Tyr697) were effectively inhibited by AZD7507 at low dose (8nM) in BMDM macrophage cells. Cell lysates were collected 30 minutes after treatment with either AZD7507 or the vehicle control. β -Actin was used as the loading control. These data were provided by our collaborator Dr Juliana Candido, and this figure is reproduced from Dr Juliana Candido's PhD thesis with her permission.

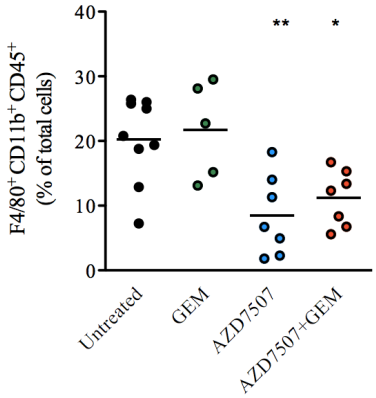

Figure 5.10 Effect of treatments on macrophage population in the KPC mice pancreas

$F4/80^{+}CD11b^{+}CD45^{+}$ are markers for macrophages, and percentages of tumour-associated macrophage population were quantified by flow cytometry. Dots represent values from individual mice and lines represent averages of the biological groups. ** represents p value < 0.01 and * represents p value < 0.05 using Mann-Whitney tests in comparison with the untreated mice. These data were provided by our collaborator Dr Juliana Candido, and this figure is reproduced from Dr Juliana Candido's PhD thesis with her permission.

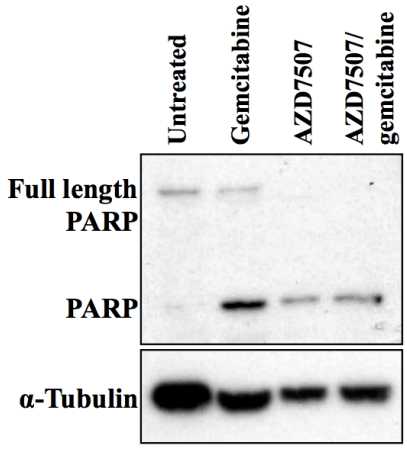

Figure 5.11 Effect of treatments on PARP activity in KPC mice pancreatic tissues

Western blot analysis of KPC mice pancreas protein lysates shows that PARP responses to treatments. Poly ADP ribose polymerase (PARP) is associated with DNA damage response and cell death. α- Tubulin was used as loading control. These data were provided by our collaborator Dr Juliana Candido, and this figure is reproduced from Dr Juliana Candido's PhD thesis with her permission.

Chapter 6 Final Discussion

Alteration in choline phospholipid metabolism is an important hallmark of tumour development. Biosynthesis of membrane phospholipids must be accelerated in tumour cells in order to meet the demand of rapid proliferation, thus rendering the choline phospholipid biosynthesis pathway an attractive target for drug and biomarker discovery (Glunde *et al.* 2011). Phosphatidylcholine (PtdCho) is a major membrane constituent in mammalian cells. PtdCho regulates diverse structural and signalling functions, for examples the abundance of PtdCho has been known to oscillate during the cell cycle (Jackowski 1994) and it is also involved in the regulation of Akt membrane binding (Koeberle *et al.* 2013). PtdCho is primarily synthesised from precursor molecules phosphocholine (PCho) and choline in mammalian cells (Kennedy and Weiss 1956). The characteristics of the choline phospholipid metabolite levels in breast tumour cells are relatively well documented. Studies in the past have indicated that a high PCho to glycerophosphocholine (GPC) ratio could reflect tumour aggressiveness (Aboagye and Bhujwalla 1999), and choline transporters are up-regulated in breast cancer (Eliyahu *et al.* 2007). It was shown that elevation of PCho levels could mainly be attributed to the regulation of choline kinase and PtdCho phospholipase C activities in tumour cells (Iorio *et al.* 2010). Furthermore choline kinase could be activated by hypoxia-inducible factors (HIFs) or through Ras and PI3K signalling (de Molina *et al.* 2002), thus changes to PCho and choline phospholipid phenotype could be dynamically regulated by signalling events in cancer.

By examining the effects on metabolism resulting from oncogenic *PIK3CA* mutation in the MCF10A breast epithelial cells, we provided evidence of reduction in GPC levels following oncogenic transformation. GPC is a product of phosphatidylcholine degradation (Dawson 1955) and reduction in GPC could potentially indicate enhanced survival signalling. It has been shown that apoptotic signalling can stimulate calcium-independent phospholipase A_2, an enzyme which catalyses the first step of phosphatidylcholine degradation into GPC and fatty acids (Lauber *et al.* 2003).

Interestingly, the role of GPC as a metabolic substrate in the context of tumour metabolism remains largely ignored. Glycerophosphodiester phosphodiesterases (GDE) are the only class of enzymes that metabolise GPC. GDE2 and GDE5/EDI3 are both highly specific in breaking down GPC into choline and glycerol-3 phosphate (G3P) (Ridgway 2013). GDE1 knockout has been reported to affect metabolic profiles and serine levels in mice, highlighting the importance of GDE in maintaining metabolic homeostasis. Through analysis of tumour cells transfected with EDI3 siRNA, we report previously unknown consequences of EDI3 in modulating tumour metabolism. We found that silencing EDI3 elevates the level of intracellular GPC, while restricting glucose uptake, lipogenesis and the size of intracellular citrate pool. A recent MRS study has demonstrated that silencing GDE5 results in GPC accumulation in a *in vivo* mouse xenograft model (Wijnen *et al.* 2014); the role of EDI3 in regulating metabolism could be very relevant in the clinical settings. The effects of silencing EDI3 on glucose uptake, lipogenesis and intracellular citrate could be mediated by restriction on G3P and choline availability. It has been reported that long chain acyl-CoA could inhibit hexokinase and citrate synthase (Board *et al.* 1995). Moreover, G3P levels are found to be up-regulated in breast tumours (Brockmoeller *et al.* 2012), and it has been reported that increased glycerol-3 phosphate dehydrogenase activity could also be found in bladder cancer (Turyn *et al.* 2003), underlining the importance of G3P as metabolic substrates in cancer. It is also possible that metabolites downstream of G3P, such as lysophosphatidic acid (LPA), might influence metabolism via cellular signalling circuits. LPA has been reported to display growth-factor-like activities that directly influence G-protein signalling (Van Corven *et al.* 1989, Mills and Moolenaar 2003). Also regulation of glycerophosphodiester phosphodiesterases could have implications for upstream metabolic processes through GPC accumulation. GPC has been reported as an important osmotic regulator; *GDPD5*/GDE2 is rapidly inhibited by urea and NaCl (Gallazzini *et al.* 2008). GPC accumulation may affect the rate of hydrolysis of PtdCho through phospholipase A_1 and phospholipase A_2 activity. The constant turnover of PtdCho serves functional roles in maintaining cellular signalling, and in remodelling membrane lipids to provide for lipid diversity and membrane balance (Nishizuka 1992). It has been shown that lysophosphatidylcholine acyltransferase 1, an enzyme that facilitate the remodelling of PtdCho, is

overexpressed in human tumours (Mansilla *et al.* 2009). Glycerophosphodiester phosphodiesterases could be very important in cancer through directly altering G3P and choline availability, or through regulating other upstream and downstream metabolic activities. Glycerophosphodiester phosphodiesterases could thus be particularly important in conditions where supply of G3P is tight, and may be a potential therapeutic target.

Furthermore the biomarker value of GPC for disease progression remains controversial. GPC is difficult to resolve using *in vivo* MRS at clinical field strength, and there is a lack of consistency in the literature in the interpretation of changes in GPC levels in tumours. While GPC levels have been reported to be lower in ovarian and breast cancer cells (Glunde *et al.* 2004, Iorio *et al.* 2005), they have also been reported to be higher in human prostate, lung and breast tumours (Swanson *et al.* 2008, Giskeodegard *et al.* 2010, Rocha *et al.* 2010, Cao *et al.* 2012b). Understanding the intricate balance between PLA_1/PLA_2 and glycerophosphodiester phosphodiesterases activities may be important (Ridgway 2013). Additionally, cell culture conditions do not mimic the tumour microenvironment, and this may be a significant source of discrepancy between the choline phospholipid phenotype observed in culture and *in vivo*. MRS has already shown potential in monitoring therapies targeting choline kinase (Al-Saffar *et al.* 2006), Ras (Ronen *et al.* 2001) and PI3K (Al-Saffar *et al.* 2010). In the final part of the thesis we demonstrated that anti-CSF1R inhibitor targeting macrophage infiltration alters the phosphocholine phenotype, implying that its therapeutic efficacies could also potentially be monitored *in vivo*. CSF1 is a specific growth factor for macrophages, and CSF1 has previously been shown to elevate CTP:phosphocholine cytidylytransferase (CCT) mRNA by four-fold in just 15 minutes (Tessner *et al.* 1991). In addition, macrophages may also have distinctive choline phospholipid metabolic regulation compared to tumour cells. Choline phospholipid metabolite profiles have the potential to be exploited for monitoring therapies targeting macrophage infiltration, and better mechanistic insights into how macrophage-tumour interactions impact upon the choline phospholipid phenotype could have profound translational applications.

6.1 General study limitations

Our study approach focused heavily on analysis at the metabolite level using metabolomics platforms, which inherently came with its own set of challenges. Metabolite regulations and feedback are rapid and dynamic at the enzyme, metabolic substrate and compartmental levels, thus potentially limiting the size effect of metabolite accumulation or depletion. Depending on context, a small percentage change in metabolite flux or pool size may have knock-on consequences on multiple cellular processes. Also, changes in the ^{13}C mass isotopomer distribution data are often small; inferring the biological significance through metabolite data alone is sometimes difficult. In future, a more integrated metabolic approach that includes probing for enzymatic regulation directly may help provide the added confidence to support our observations.

Data from metabolomics experiments, including those presented here, are generally only semi-quantitative; concentration estimates are usually informative within the context of specific sample sets, but are generally not robust enough for the purpose of cross-study comparison. For example, absolute quantification using NMR spectroscopy typically requires longer recovery delay than the 2 or 3 seconds that were implemented in the studies presented here. To quantify metabolites using mass spectrometry based assays normally require a series of calibration samples to be analysed alongside the sample set, which is generally not practical unless metabolites of interest are pre-defined before the start of the analysis. In future, targeted and validated methods that focus on quantifying a subset of metabolites should be considered.

6.2 Final conclusion

Our metabolomic investigations into several tumour model systems all indicate choline phospholipid phenotype to be profoundly altered through disease transformation. Within the context of choline phospholipid metabolism, the therapeutic and diagnostic implications of previously unknown glycerophosphodiester phosphodiesterase functions and macrophage-tumour interactions were discussed.

Bibliography

Aboagye, E. O. and Bhujwalla, Z. M. (1999) 'Malignant transformation alters membrane choline phospholipid metabolism of human mammary epithelial cells', *Cancer Research*, 59(1), 80-84.

Ackerstaff, E., Glunde, K. and Bhujwalla, Z. M. (2003) 'Choline phospholipid metabolism: A target in cancer cells?', *Journal of Cellular Biochemistry*, 90(3), 525-533.

Aikawa, Y., Katsumoto, T., Zhang, P., Shima, H., Shino, M., Terui, K., Ito, E., Ohno, H., Stanley, E. R., Singh, H., Tenen, D. G. and Kitabayashi, I. (2010) 'PU.1-mediated upregulation of CSF1R is crucial for leukemia stem cell potential induced by MOZ-TIF2', *Nature Medicine*, 16(5), 580-U115.

Al-Saffar, N. M. S., Jackson, L. E., Raynaud, F. I., Clarke, P. A., de Molina, A. R., Lacal, J. C., Workman, P. and Leach, M. O. (2010) 'The Phosphoinositide 3-Kinase Inhibitor PI-103 Downregulates Choline Kinase a Leading to Phosphocholine and Total Choline Decrease Detected by Magnetic Resonance Spectroscopy', *Cancer Research*, 70(13), 5507-5517.

Al-Saffar, N. M. S., Troy, H., Ramirez de Molina, A., Jackson, L. E., Madhu, B., Griffiths, J. R., Leach, M. O., Workman, P., Lacal, J. C., Judson, I. R. and Chung, Y. L. (2006) 'Noninvasive magnetic resonance spectroscopic pharmacodynamic markers of the choline kinase inhibitor MN58b in human carcinoma models', *Cancer Research*, 66(1), 427-434.

Almoguera, C., Shibata, D., Forrester, K., Martin, J., Arnheim, N. and Perucho, M. (1988) 'MOST HUMAN CARCINOMAS OF THE EXOCRINE PANCREAS CONTAIN MUTANT C-K-RAS GENES', *Cell*, 53(4), 549-554.

Alum, M. F., Shaw, P. A., Sweatman, B. C., Ubhi, B. K., Haselden, J. N. and Connor, S. C. (2008) '4,4-dimethyl-4-silapentane-1-ammonium trifluoroacetate (DSA), a promising universal internal standard for NMR-based metabolic profiling studies of biofluids, including blood plasma and serum', *Metabolomics*, 4(2), 122-127.

Anastas, J. N. and Moon, R. T. (2013) 'WNT signalling pathways as therapeutic targets in cancer', *Nature Reviews Cancer*, 13(1), 11-26.

Appleton, A. V., Olivia Lim, Ming Yeong (2013) *Metabolism and nutrition*, 3rd ed., Edinburgh : Mosby Elsevier

Argaud, D., Kirby, T. L., Newgard, C. B. and Lange, A. J. (1997) 'Stimulation of glucose-6-phosphatase gene expression by glucose and fructose-2,6-bisphosphate', *Journal of Biological Chemistry*, 272(19), 12854-12861.

Arsenault, D. J., Yoo, B. H., Rosen, K. V. and Ridgway, N. D. (2013) 'ras-induced Up-regulation of CTP:Phosphocholine Cytidylyltransferase alpha Contributes to Malignant Transformation of Intestinal Epithelial Cells', *Journal of Biological Chemistry*, 288(1), 633-643.

Bapiro, T. E., Frese, K. K., Courtin, A., Bramhall, J. L., Madhu, B., Cook, N., Neesse, A., Griffiths, J. R., Tuveson, D. A., Jodrell, D. I. and Richards, F. M. (2014) 'Gemcitabine diphosphate choline is a major metabolite linked to the Kennedy pathway in pancreatic cancer models in vivo', *British Journal of Cancer*, 111(2), 318-325.

Barton, R. H., Waterman, D., Bonner, F. W., Holmes, E., Clarke, R., Nicholson, J. K., Lindon, J. C. and Consortium, P. (2010) 'The influence of EDTA and citrate anticoagulant addition to human plasma on information recovery from NMR-based metabolic profiling studies', *Molecular Biosystems*, 6(1), 215-224.

Bayne, L. J., Beatty, G. L., Jhala, N., Clark, C. E., Rhim, A. D., Stanger, B. Z. and Vonderheide, R. H. (2012) 'Tumor-Derived Granulocyte-Macrophage Colony-Stimulating Factor Regulates Myeloid Inflammation and T Cell Immunity in Pancreatic Cancer', *Cancer Cell*, 21(6), 822-835.

Beckonert, O., Coen, M., Keun, H. C., Wang, Y., Ebbels, T. M. D., Holmes, E., Lindon, J. C. and Nicholson, J. K. (2010) 'High-resolution magic-angle-spinning NMR spectroscopy for metabolic profiling of intact tissues', *Nat. Protocols*, 5(6), 1019-1032.

Behrends, V., Tredwell, G. D. and Bundy, J. G. (2011) 'A software complement to AMDIS for processing GC-MS metabolomic data', *Anal Biochem*, 415(2), 206-8.

Beloueche-Babari, M., Jackson, L. E., Al-Saffar, N. M. S., Eccles, S. A., Raynaud, F. I., Workman, P., Leach, M. O. and Ronen, S. M. (2006) 'Identification of magnetic resonance detectable metabolic changes associated with inhibition of phosphoinositide 3-kinase signaling in human breast cancer cells', *Molecular Cancer Therapeutics*, 5(1), 187-196.

Berwick, D. C., Hers, I., Heesom, K. J., Moule, S. K. and Tavare, J. M. (2002) 'The identification of ATP-citrate lyase as a protein kinase B (Akt) substrate in primary adipocytes', *Journal of Biological Chemistry*, 277(37), 33895-33900.

Beuster, G., Zarse, K., Kaleta, C., Thierbach, R., Kiehntopf, M., Steinberg, P., Schuster, S. and Ristow, M. (2011) 'Inhibition of Alanine Aminotransferase in Silico and in Vivo Promotes Mitochondrial Metabolism to Impair Malignant Growth', *Journal of Biological Chemistry*, 286(25), 22323-22330.

Biswas, S. K. and Mantovani, A. (2012) 'Orchestration of Metabolism by Macrophages', *Cell Metabolism*, 15(4), 432-437.

Board, M., Colquhoun, A. and Newsholme, E. A. (1995) 'HIGH K-M GLUCOSE-PHOSPHORYLATING (GLUCOKINASE) ACTIVITIES IN A RANGE OF

TUMOR-CELL LINES AND INHIBITION OF RATES OF TUMOR-GROWTH BY THE SPECIFIC ENZYME-INHIBITOR MANNOHEPTULOSE', *Cancer Research*, 55(15), 3278-3285.

Brockmoeller, S. F., Bucher, E., Mueller, B. M., Budczies, J., Hilvo, M., Griffin, J. L., Oresic, M., Kallioniemi, O., Iljin, K., Loibl, S., Darb-Esfahani, S., Sinn, B. V., Klauschen, F., Prinzler, J., Bangemann, N., Ismaeel, F., Fiehn, O., Dietel, M. and Denkert, C. (2012) 'Integration of Metabolomics and Expression of Glycerol-3-phosphate Acyltransferase (GPAM) in Breast Cancer-Link to Patient Survival, Hormone Receptor Status, and Metabolic Profiling', *Journal of Proteome Research*, 11(2), 850-860.

Bruhn, H., Frahm, J., Gyngell, M. L., Merboldt, K. D., Hanicke, W., Sauter, R. and Hamburger, C. (1989) 'NONINVASIVE DIFFERENTIATION OF TUMORS WITH USE OF LOCALIZED H-1 MR SPECTROSCOPY INVIVO - INITIAL EXPERIENCE IN PATIENTS WITH CEREBRAL-TUMORS', *Radiology*, 172(2), 541-548.

Bundy, J. G., Davey, M. P. and Viant, M. R. (2009) 'Environmental metabolomics: a critical review and future perspectives', *Metabolomics*, 5(1), 3-21.

Burg, M. B. (1996) 'Coordinate regulation of organic osmolytes in renal cells', *Kidney International*, 49(6), 1684-1685.

Cao, M. D., Doepkens, M., Krishnamachary, B., Vesuna, F., Gadiya, M. M., Lonning, P. E., Bhujwalla, Z. M., Gribbestad, I. S. and Glunde, K. (2012a) 'Glycerophosphodiester phosphodiesterase domain containing 5 (GDPD5) expression correlates with malignant choline phospholipid metabolite profiles in human breast cancer', *Nmr in Biomedicine*, 25(9), 1033-1042.

Cao, M. D., Sitter, B., Bathen, T. F., Bofin, A., Lonning, P. E., Lundgren, S. and Gribbestad, I. S. (2012b) 'Predicting long-term survival and treatment response in breast cancer patients receiving neoadjuvant chemotherapy by MR metabolic profiling', *Nmr in Biomedicine*, 25(2), 369-378.

Carr, H. Y. and Purcell, E. M. (1954) 'Effects of Diffusion on Free Precession in Nuclear Magnetic Resonance Experiments', *Physical Review*, 94(3), 630-638.

Caulin, A. F. and Maley, C. C. (2011) 'Peto's Paradox: evolution's prescription for cancer prevention', *Trends in Ecology & Evolution*, 26(4), 175-182.

Clem, B. F., Clem, A. L., Yalcin, A., Goswami, U., Arumugam, S., Telang, S., Trent, J. O. and Chesney, J. (2011) 'A novel small molecule antagonist of choline kinase-α that simultaneously suppresses MAPK and PI3K/AKT signaling', *Oncogene*, 30(30), 3370-80.

Collins, M. A., Bednar, F., Zhang, Y., Brisset, J.-C., Galban, S., Galban, C. J., Rakshit, S., Flannagan, K. S., Adsay, N. V. and di Magliano, M. P. (2012)

'Oncogenic Kras is required for both the initiation and maintenance of pancreatic cancer in mice', *Journal of Clinical Investigation*, 122(2), 639-653.

Coore, H. G., Denton, R. M., Martin, B. R. and Randle, P. J. (1971) 'REGULATION OF ADIPOSE TISSUE PYRUVATE DEHYDROGENASE BY INSULIN AND OTHER HORMONES', *Biochemical Journal*, 125(1), 115-&.

Corda, D., Mosca, M. G., Ohshima, N., Grauso, L., Yanaka, N. and Mariggio, S. (2014) 'The emerging physiological roles of the glycerophosphodiesterase family', *Febs Journal*, 281(4), 998-1016.

Cully, M., You, H., Levine, A. J. and Mak, T. W. (2006) 'Beyond PTEN mutations: the PI3K pathway as an integrator of multiple inputs during tumorigenesis', *Nature Reviews Cancer*, 6(3), 184-192.

Dang, C. V. (2012) 'Links between metabolism and cancer', *Genes & Development*, 26(9), 877-890.

Dang, L., White, D. W., Gross, S., Bennett, B. D., Bittinger, M. A., Driggers, E. M., Fantin, V. R., Jang, H. G., Jin, S., Keenan, M. C., Marks, K. M., Prins, R. M., Ward, P. S., Yen, K. E., Liau, L. M., Rabinowitz, J. D., Cantley, L. C., Thompson, C. B., Heiden, M. G. V. and Su, S. M. (2009) 'Cancer-associated IDH1 mutations produce 2-hydroxyglutarate', *Nature*, 462(7274), 739-U52.

Dawson, P. J., Wolman, S. R., Tait, L., Heppner, G. H. and Miller, F. R. (1996) 'MCF10AT: A model for the evolution of cancer from proliferative breast disease', *American Journal of Pathology*, 148(1), 313-319.

Dawson, R. M. (1955) 'The role of glycerylphosphorylcholine and glycerylphosphorylethanolamine in liver phospholipid metabolism', *The Biochemical journal*, 59(1), 5-8.

de Molina, A. R., Penalva, V., Lucas, L. and Lacal, J. C. (2002) 'Regulation of choline kinase activity by Ras proteins involves Ral-GDS and PI3K', *Oncogene*, 21(6), 937-946.

DeBerardinis, R., Lum, J., Hatzivassiliou, G. and Thompson, C. (2008) 'The biology of cancer: metabolic reprogramming fuels cell growth and proliferation', *Cell metabolism*, 7(1), 11-20.

DeBerardinis, R. J., Mancuso, A., Daikhin, E., Nissim, I., Yudkoff, M., Wehrli, S. and Thompson, C. B. (2007) 'Beyond aerobic glycolysis: Transformed cells can engage in glutamine metabolism that exceeds the requirement for protein and nucleotide synthesis', *Proceedings of the National Academy of Sciences*, 104(49), 19345-19350.

Debnath, J., Muthuswamy, S. K. and Brugge, J. S. (2003) 'Morphogenesis and oncogenesis of MCF-10A mammary epithelial acini grown in three-dimensional basement membrane cultures', *Methods*, 30(3), 256-268.

DeLaBarre, B., Gross, S., Fang, C., Gao, Y., Jha, A., Jiang, F., Song, J. J., Wei, W. and Hurov, J. B. (2011) 'Full-Length Human Glutaminase in Complex with an Allosteric Inhibitor', *Biochemistry*, 50(50), 10764-10770.

DeNardo, D. G., Brennan, D. J., Rexhepaj, E., Ruffell, B., Shiao, S. L., Madden, S. F., Gallagher, W. M., Wadhwani, N., Keil, S. D., Junaid, S. A., Rugo, H. S., Hwang, E. S., Jirstrom, K., West, B. L. and Coussens, L. M. (2011) 'Leukocyte Complexity Predicts Breast Cancer Survival and Functionally Regulates Response to Chemotherapy', *Cancer Discovery*, 1(1), 54-67.

Dettmer, K., Aronov, P. A. and Hammock, B. D. (2007) 'Mass spectrometry-based metabolomics', *Mass Spectrometry Reviews*, 26(1), 51-78.

Di Gangi, I. M., Vrhovsek, U., Pazienza, V. and Mattivi, F. (2014) 'Analytical metabolomics-based approaches to pancreatic cancer', *Trac-Trends in Analytical Chemistry*, 55, 94-116.

Dieterle, F., Ross, A., Schlotterbeck, G. t. and Senn, H. (2006) 'Probabilistic Quotient Normalization as Robust Method to Account for Dilution of Complex Biological Mixtures. Application in 1H NMR Metabonomics', *Analytical Chemistry*, 78(13), 4281-4290.

Eliyahu, G., Kreizman, T. and Degani, H. (2007) 'Phosphocholine as a biomarker of breast cancer: Molecular and biochemical studies', *International Journal of Cancer*, 120(8), 1721-1730.

Elstrom, R. L., Bauer, D. E., Buzzai, M., Karnauskas, R., Harris, M. H., Plas, D. R., Zhuang, H. M., Cinalli, R. M., Alavi, A., Rudin, C. M. and Thompson, C. B. (2004) 'Akt stimulates aerobic glycolysis in cancer cells', *Cancer Research*, 64(11), 3892-3899.

Engelman, J. A., Luo, J. and Cantley, L. C. (2006) 'The evolution of phosphatidylinositol 3-kinases as regulators of growth and metabolism', *Nat Rev Genet*, 7(8), 606-619.

Fernandez-Murray, J. P. and McMaster, C. R. (2005) 'Glycerophosphocholine catabolism as a new route for choline formation for phosphatidylcholine synthesis by the Kennedy pathway', *Journal of Biological Chemistry*, 280(46), 38290-38296.

Fiehn, O. (2002) 'Metabolomics - the link between genotypes and phenotypes', *Plant Mol Biol*, 48(1-2), 155 - 171.

Fillmore, C. M. and Kuperwasser, C. (2008) 'Human breast cancer cell lines contain stem-like cells that self-renew, give rise to phenotypically diverse progeny and survive chemotherapy', *Breast Cancer Research*, 10(2).

Foster, R., Griffin, S., Grooby, S., Feltell, R., Christopherson, C., Chang, M., Sninsky, J., Kwok, S. and Torrance, C. (2012) 'Multiple Metabolic Alterations Exist

in Mutant PI3K Cancers, but Only Glucose Is Essential as a Nutrient Source', *PloS one*, 7(9), e45061.

Fruman, D. A. and Rommel, C. (2014) 'PI3K and cancer: lessons, challenges and opportunities', *Nature Reviews Drug Discovery*, 13(2), 140-156.

Gallazzini, M., Ferraris, J. D. and Burg, M. B. (2008) 'GDPD5 is a glycerophosphocholine phosphodiesterase that osmotically regulates the osmoprotective organic osmolyte GPC', *Proceedings of the National Academy of Sciences of the United States of America*, 105(31), 11026-11031.

Galluzzi, L., Kepp, O., Vander Heiden, M. G. and Kroemer, G. (2013) 'Metabolic targets for cancer therapy', *Nature Reviews Drug Discovery*, 12(11), 829-846.

Galons, J. P., Job, C. and Gillies, R. J. (1995) 'INCREASE OF GPC LEVELS IN CULTURED-MAMMALIAN-CELLS DURING ACIDOSIS - A P-31 MR SPECTROSCOPY STUDY USING A CONTINUOUS BIOREACTOR SYSTEM', *Magnetic Resonance in Medicine*, 33(3), 422-426.

Gambhir, S. S. (2002) 'Molecular imaging of cancer with positron emission tomography', *Nature Reviews Cancer*, 2(9), 683-693.

Gao, Z. Y., Li, G., Najafi, H., Wolf, B. A. and Matschinsky, F. M. (1999) 'Glucose regulation of glutaminolysis and its role in insulin secretion', *Diabetes*, 48(8), 1535-42.

Garcia-Cao, I., Song, M. S., Hobbs, R. M., Laurent, G., Giorgi, C., de Boer, V. C., Anastasiou, D., Ito, K., Sasaki, A. T., Rameh, L., Carracedo, A., Vander Heiden, M. G., Cantley, L. C., Pinton, P., Haigis, M. C. and Pandolfi, P. P. (2012) 'Systemic elevation of PTEN induces a tumor-suppressive metabolic state', *Cell*, 149(1), 49-62.

Giskeodegard, G. F., Grinde, M. T., Sitter, B., Axelson, D. E., Lundgren, S., Fjosne, H. E., Dahl, S., Gribbestad, I. S. and Bathen, T. F. (2010) 'Multivariate Modeling and Prediction of Breast Cancer Prognostic Factors Using MR Metabolomics', *Journal of Proteome Research*, 9(2), 972-979.

Glunde, K. and Bhujwalla, Z. M. (2011) 'Metabolic Tumor Imaging Using Magnetic Resonance Spectroscopy', *Seminars in Oncology*, 38(1), 26-41.

Glunde, K., Bhujwalla, Z. M. and Ronen, S. M. (2011) 'Choline metabolism in malignant transformation', *Nature Reviews Cancer*, 11(12), 835-848.

Glunde, K., Jie, C. and Bhujwalla, Z. M. (2004) 'Molecular causes of the aberrant choline phospholipid metabolism in breast cancer', *Cancer Research*, 64(12), 4270-4276.

Glunde, K., Shah, T., Winnard, P. T., Jr., Raman, V., Takagi, T., Vesuna, F., Artemov, D. and Bhujwalla, Z. M. (2008) 'Hypoxia regulates choline kinase

expression through hypoxia-inducible factor-lot signaling in a human prostate cancer model', *Cancer Research*, 68(1), 172-180.

Grassian, A. R., Metallo, C. M., Coloff, J. L., Stephanopoulos, G. and Brugge, J. S. (2011) 'Erk regulation of pyruvate dehydrogenase flux through PDK4 modulates cell proliferation', *Genes & Development*, 25(16), 1716-1733.

Griffiths, W. J. (2007) *Metabolomics, Metabonomics and Metabolite Profiling*.

Gustin, J. P., Karakas, B., Weiss, M. B., Abukhdeir, A. M., Lauring, J., Garay, J. P., Cosgrove, D., Tamaki, A., Konishi, H., Konishi, Y., Mohseni, M., Wang, G., Rosen, D. M., Denmeade, S. R., Higgins, M. J., Vitolo, M. I., Bachman, K. E. and Park, B. H. (2009) 'Knockin of mutant PIK3CA activates multiple oncogenic pathways', *Proc Natl Acad Sci U S A*, 106(8), 2835-40.

Hamilton, J. A. (1997) 'CSF-1 signal transduction', *Journal of Leukocyte Biology*, 62(2), 145-155.

Hammond, L. E., Neschen, S., Romanelli, A. J., Cline, G. W., Ilkayeva, O. R., Shulman, G. I., Muoio, D. M. and Coleman, R. A. (2005) 'Mitochondrial glycerol-3-phosphate acyltransferase-1 is essential in liver for the metabolism of excess acyl-CoAs', *Journal of Biological Chemistry*, 280(27), 25629-25636.

Hammond, M. E. H., Hayes, D. F., Dowsett, M., Allred, D. C., Hagerty, K. L., Badve, S., Fitzgibbons, P. L., Francis, G., Goldstein, N. S., Hayes, M., Hicks, D. G., Lester, S., Love, R., Mangu, P. B., McShane, L., Miller, K., Osborne, C. K., Paik, S., Perlmutter, J., Rhodes, A., Sasano, H., Schwartz, J. N., Sweep, F. C. G., Taube, S., Torlakovic, E. E., Valenstein, P., Viale, G., Visscher, D., Wheeler, T., Williams, R. B., Wittliff, J. L. and Wolff, A. C. (2010) 'American Society of Clinical Oncology/College of American Pathologists Guideline Recommendations for Immunohistochemical Testing of Estrogen and Progesterone Receptors in Breast Cancer', *Journal of Clinical Oncology*, 28(16), 2784-2795.

Hansel, B. C. and Powell, G. L. (1984) 'REGULATION OF ENZYMES BY FATTY ACYL COENZYME-A - INTERACTIONS OF SHORT AND LONG-CHAIN SPIN-LABELED ACYL-COA WITH THE ACETYL-COA SITE ON PIG-HEART CITRATE SYNTHASE', *Journal of Biological Chemistry*, 259(3), 1423-1430.

He, X.-H., Li, W.-T., Gu, Y.-J., Yang, B.-F., Deng, H.-W., Yu, Y.-H. and Peng, W.-J. (2013) 'Metabonomic studies of pancreatic cancer response to radiotherapy in a mouse xenograft model using magnetic resonance spectroscopy and principal components analysis', *World Journal of Gastroenterology*, 19(26), 4200-4208.

Herreros-Villanueva, M., Hijona, E., Cosme, A. and Bujanda, L. (2012) 'Mouse models of pancreatic cancer', *World Journal of Gastroenterology*, 18(12), 1286-1294.

Hertel, L. W., Boder, G. B., Kroin, J. S., Rinzel, S. M., Poore, G. A., Todd, G. C. and Grindey, G. B. (1990) 'EVALUATION OF THE ANTITUMOR-ACTIVITY OF

GEMCITABINE (2',2'-DIFLUORO-2'-DEOXYCYTIDINE)', *Cancer Research*, 50(14), 4417-4422.

Hezel, A. F., Kimmelman, A. C., Stanger, B. Z., Bardeesy, N. and DePinho, R. A. (2006) 'Genetics and biology of pancreatic ductal adenocarcinoma', *Genes & Development*, 20(10), 1218-1249.

Hidalgo, M. (2010) 'Pancreatic Cancer', *New England Journal of Medicine*, 362(17), 1605-1617.

Hingorani, S. R., Petricoin, E. F., Maitra, A., Rajapakse, V., King, C., Jacobetz, M. A., Ross, S., Conrads, T. P., Veenstra, T. D., Hitt, B. A., Kawaguchi, Y., Johann, D., Liotta, L. A., Crawford, H. C., Putt, M. E., Jacks, T., Wright, C. V. E., Hruban, R. H., Lowy, A. M. and Tuveson, D. A. (2003) 'Preinvasive and invasive ductal pancreatic cancer and its early detection in the mouse', *Cancer Cell*, 4(6), 437-450.

Hingorani, S. R., Wang, L. F., Multani, A. S., Combs, C., Deramaudt, T. B., Hruban, R. H., Rustgi, A. K., Chang, S. and Tuveson, D. A. (2005) 'Trp53(R172H) and KraS(G12D) cooperate to promote chromosomal instability and widely metastatic pancreatic ductal adenocarcinoma in mice', *Cancer Cell*, 7(5), 469-483.

Holmes, E. and Antti, H. (2002) 'Chemometric contributions to the evolution of metabonomics: mathematical solutions to characterising and interpreting complex biological NMR spectra', *Analyst*, 127(12), 1549 - 1557.

Hsu, K. H. L. and Powell, G. L. (1975) 'INHIBITION OF CITRATE SYNTHASE BY OLEOYL-COA - REGULATORY PHENOMENON', *Proceedings of the National Academy of Sciences of the United States of America*, 72(12), 4729-4733.

Husarik, D. B., Miralbell, R., Dubs, M., John, H., Giger, O. T., Gelet, A., Cservenyak, T. and Hany, T. F. (2008) 'Evaluation of F-18 -choline PET/CT for staging and restaging of prostate cancer', *European Journal of Nuclear Medicine and Molecular Imaging*, 35(2), 253-263.

Imamura, K., Dianoux, A., Nakamura, T. and Kufe, D. (1990) 'COLONY-STIMULATING FACTOR-I ACTIVATES PROTEIN KINASE-C IN HUMAN MONOCYTES', *Embo Journal*, 9(8), 2423-2429.

Iorio, E., Mezzanzanica, D., Alberti, P., Spadaro, F., Ramoni, C., D'Ascenzo, S., Millimaggi, D., Pavan, A., Dolo, V., Canevari, S. and Podo, F. (2005) 'Alterations of choline phospholipid metabolism in ovarian tumor progression', *Cancer Research*, 65(20), 9369-9376.

Iorio, E., Ricci, A., Bagnoli, M., Pisanu, M. E., Castellano, G., Di Vito, M., Venturini, E., Glunde, K., Bhujwalla, Z. M., Mezzanzanica, D., Canevari, S. and Podo, F. (2010) 'Activation of Phosphatidylcholine Cycle Enzymes in Human Epithelial Ovarian Cancer Cells', *Cancer Research*, 70(5), 2126-2135.

Irvine, K. M., Burns, C. J., Wilks, A. F., Su, S., Hume, D. A. and Sweet, M. J. (2006) 'A CSF-1 receptor kinase inhibitor targets effector functions and inhibits pro-inflammatory cytokine production from murine macrophage populations', *Faseb Journal*, 20(11), 1921-+.

Isakoff, S. J., Engelman, J. A., Irie, H. Y., Luo, J., Brachmann, S. M., Pearline, R. V., Cantley, L. C. and Brugge, J. S. (2005) 'Breast cancer-associated PIK3CA mutations are oncogenic in mammary epithelial cells', *Cancer Res*, 65(23), 10992-1000.

Iyer, V. V., Yang, H., Ierapetritou, M. G. and Roth, C. M. (2010) 'Effects of Glucose and Insulin on HepG2-C3A Cell Metabolism', *Biotechnology and Bioengineering*, 107(2), 347-356.

Jackowski, S. (1994) 'COORDINATION OF MEMBRANE PHOSPHOLIPID-SYNTHESIS WITH THE CELL-CYCLE', *Journal of Biological Chemistry*, 269(5), 3858-3867.

Jain, M., Nilsson, R., Sharma, S., Madhusudhan, N., Kitami, T., Souza, A. L., Kafri, R., Kirschner, M. W., Clish, C. B. and Mootha, V. K. (2012) 'Metabolite Profiling Identifies a Key Role for Glycine in Rapid Cancer Cell Proliferation', *Science*, 336(6084), 1040-1044.

Janardhan, S., Srivani, P. and Sastry, G. N. (2006) 'Choline kinase: An important target for cancer', *Current Medicinal Chemistry*, 13(10), 1169-1186.

Jemal, A., Bray, F., Center, M. M., Ferlay, J., Ward, E. and Forman, D. (2011) 'Global cancer statistics', *CA: a cancer journal for clinicians*, 61(2), 69-90.

Johnson, S. A. and Denton, R. M. (2003) 'Insulin stimulation of pyruvate dehydrogenase in adipocytes involves two distinct signalling pathways', *Biochemical Journal*, 369, 351-356.

Kamphorst, J. J., Cross, J. R., Fan, J., de Stanchina, E., Mathew, R., White, E. P., Thompson, C. B. and Rabinowitz, J. D. (2013) 'Hypoxic and Ras-transformed cells support growth by scavenging unsaturated fatty acids from lysophospholipids', *Proceedings of the National Academy of Sciences of the United States of America*, 110(22), 8882-8887.

Katz-Brull, R., Seger, D., Rivenson-Segal, D., Rushkin, E. and Degani, H. (2002) 'Metabolic markers of breast cancer: Enhanced choline metabolism and reduced choline-ether-phospholipid synthesis', *Cancer Research*, 62(7), 1966-1970.

Kaur, P., Sheikh, K., Kirilyuk, A., Kirilyuk, K., Singh, R., Ressom, H. W. and Cheema, A. K. (2012) 'Metabolomic profiling for biomarker discovery in pancreatic cancer', *International Journal of Mass Spectrometry*, 310, 44-51.

Kell, D. B. (2006) 'Systems biology, metabolic modelling and metabolomics in drug discovery and development', *Drug discovery today*, 11(23-24), 1085.

Kelland, L. (2007) 'The resurgence of platinum-based cancer chemotherapy', *Nature Reviews Cancer*, 7(8), 573-584.

Kelleher, J. K. and Masterson, T. M. (1992) 'Model equations for condensation biosynthesis using stable isotopes and radioisotopes', *Am J Physiol*, 262(1 Pt 1), E118-25.

Kennedy, E. P. and Weiss, S. B. (1956) 'The function of cytidine coenzymes in the biosynthesis of phospholipides', *The Journal of biological chemistry*, 222(1), 193-214.

Kind, T., Wohlgemuth, G., Lee, D. Y., Lu, Y., Palazoglu, M., Shahbaz, S. and Fiehn, O. (2009) 'FiehnLib: Mass Spectral and Retention Index Libraries for Metabolomics Based on Quadrupole and Time-of-Flight Gas Chromatography/Mass Spectrometry', *Analytical Chemistry*, 81(24), 10038-10048.

Koboldt, D. C., Fulton, R. S., McLellan, M. D., Schmidt, H., Kalicki-Veizer, J., McMichael, J. F., Fulton, L. L., Dooling, D. J., Ding, L., Mardis, E. R., Wilson, R. K., Ally, A., Balasundaram, M., Butterfield, Y. S. N., Carlsen, R., Carter, C., Chu, A., Chuah, E., Chun, H.-J. E., Coope, R. J. N., Dhalla, N., Guin, R., Hirst, C., Hirst, M., Holt, R. A., Lee, D., Li, H. I., Mayo, M., Moore, R. A., Mungall, A. J., Pleasance, E., Robertson, A. G., Schein, J. E., Shafiei, A., Sipahimalani, P., Slobodan, J. R., Stoll, D., Tam, A., Thiessen, N., Varhol, R. J., Wye, N., Zeng, T., Zhao, Y., Birol, I., Jones, S. J. M., Marra, M. A., Cherniack, A. D., Saksena, G., Onofrio, R. C., Pho, N. H., Carter, S. L., Schumacher, S. E., Tabak, B., Hernandez, B., Gentry, J., Huy, N., Crenshaw, A., Ardlie, K., Beroukhim, R., Winckler, W., Getz, G., Gabriel, S. B., Meyerson, M., Chin, L., Park, P. J., Kucherlapati, R., Hoadley, K. A., Auman, J. T., Fan, C., Turman, Y. J., Shi, Y., Li, L., Topal, M. D., He, X., Chao, H.-H., Prat, A., Silva, G. O., Iglesia, M. D., Zhao, W., Usary, J., Berg, J. S., Adams, M., Booker, J., Wu, J., Gulabani, A., Bodenheimer, T., Hoyle, A. P., Simons, J. V., Soloway, M. G., Mose, L. E., Jefferys, S. R., Balu, S., Parker, J. S., Hayes, D. N., Perou, C. M., Malik, S., Mahurkar, S., Shen, H., Weisenberger, D. J., Triche, T., Jr*., et al.* (2012) 'Comprehensive molecular portraits of human breast tumours', *Nature*, 490(7418).

Koeberle, A., Shindou, H., Koeberle, S. C., Laufer, S. A., Shimizu, T. and Werz, O. (2013) 'Arachidonoyl-phosphatidylcholine oscillates during the cell cycle and counteracts proliferation by suppressing Akt membrane binding', *Proceedings of the National Academy of Sciences of the United States of America*, 110(7), 2546-2551.

Lappano, R. and Maggiolini, M. (2011) 'G protein-coupled receptors: novel targets for drug discovery in cancer', *Nature Reviews Drug Discovery*, 10(1), 47-60.

Lauber, K., Bohn, E., Krober, S. M., Xiao, Y. J., Blumenthal, S. G., Lindemann, R. K., Marini, P., Wiedig, C., Zobywalski, A., Baksh, S., Xu, Y., Autenrieth, I. B., Schulze-Osthoff, K., Belka, C., Stuhler, G. and Wesselborg, S. (2003) 'Apoptotic cells induce migration of phagocytes via caspase-3-mediated release of a lipid attraction signal', *Cell*, 113(6), 717-730.

Lesjak, M. S., Marchan, R., Stewart, J. D., Rempel, E., Rahnenführer, J. and Hengstler, J. G. (2014) 'EDI3 links choline metabolism to integrin expression, cell adhesion and spreading', *Cell Adh Migr*, 8(4).

Levitt, M. H. (2008) *Spin Dynamics Basics of Nuclear Magnetic Resonance*, 2nd ed., Hoboken : Wiley.

Liu, P., Cheng, H., Roberts, T. M. and Zhao, J. J. (2009) 'Targeting the phosphoinositide 3-kinase pathway in cancer', *Nature Reviews Drug Discovery*, 8(8).

Loi, S., Haibe-Kains, B., Majjaj, S., Lallemand, F., Durbecq, V., Larsimont, D., Gonzalez-Angulo, A. M., Pusztai, L., Symmans, W. F., Bardelli, A., Ellis, P., Tutt, A. N. J., Gillett, C. E., Hennessy, B. T., Mills, G. B., Phillips, W. A., Piccart, M. J., Speed, T. P., McArthur, G. A. and Sotiriou, C. (2010) 'PIK3CA mutations associated with gene signature of low mTORC1 signaling and better outcomes in estrogen receptor-positive breast cancer', *Proceedings of the National Academy of Sciences of the United States of America*, 107(22).

Lowe, I. J. (1959) 'Free Induction Decays of Rotating Solids', *Physical Review Letters*, 2(7), 285-287.

Ludwig, J. A. and Weinstein, J. N. (2005) 'Biomarkers in cancer staging, prognosis and treatment selection', *Nature Reviews Cancer*, 5(11), 845-856.

Lurje, G. and Lenz, H.-J. (2009) 'EGFR Signaling and Drug Discovery', *Oncology*, 77(6), 400-410.

Ma, X. J., Wang, Z. C., Ryan, P. D., Isakoff, S. J., Barmettler, A., Fuller, A., Muir, B., Mohapatra, G., Salunga, R., Tuggle, J. T., Tran, Y., Tran, D., Tassin, A., Amon, P., Wang, W., Enright, E., Stecker, K., Estepa-Sabal, E., Smith, B., Younger, J., Balis, U., Michaelson, J., Bhan, A., Habin, K., Baer, T. M., Brugge, J., Haber, D. A., Erlander, M. G. and Sgroi, D. C. (2004) 'A two-gene expression ratio predicts clinical outcome in breast cancer patients treated with tamoxifen', *Cancer Cell*, 5(6), 607-616.

Mansilla, F., da Costa, K.-A., Wang, S., Kruhoffer, M., Lewin, T. M., Orntoft, T. F., Coleman, R. A. and Birkenkamp-Demtroder, K. (2009) 'Lysophosphatidylcholine acyltransferase 1 (LPCAT1) overexpression in human colorectal cancer', *Journal of Molecular Medicine-Jmm*, 87(1), 85-97.

Manthey, C. L., Johnson, D. L., Illig, C. R., Tuman, R. W., Zhou, Z., Baker, J. F., Chaikin, M. A., Donatelli, R. R., Franks, C. F., Zeng, L., Crysler, C., Chen, Y., Yurkow, E. J., Boczon, L., Meegalla, S. K., Wilson, K. J., Wall, M. J., Chen, J., Ballentine, S. K., Ott, H., Baumann, C., Lawrence, D., Tomczuk, B. E. and Molloy, C. J. (2009) 'JNJ-28312141, a novel orally active colony-stimulating factor-1 receptor/FMS-related receptor tyrosine kinase-3 receptor tyrosine kinase inhibitor with potential utility in solid tumors, bone metastases, and acute myeloid leukemia', *Molecular Cancer Therapeutics*, 8(11), 3151-3161.

Mathews, C., Ahern, K. and Van Holde, K. (2000) *Biochemistry*, 3rd ed., San Francisco ; Harlow : Benjamin Cummings.

Meiboom, S. (1958) 'Modified spin‐echo method for measuring nuclear relaxation times', *Review of scientific instruments*, 29, 688.

Metcalfe, L. D. and Wang, C. N. (1981) 'RAPID PREPARATION OF FATTY-ACID METHYL-ESTERS USING ORGANIC BASE-CATALYZED TRANS-ESTERIFICATION', *Journal of Chromatographic Science*, 19(10), 530-535.

Millard, P., Letisse, F., Sokol, S. and Portais, J. C. (2012) 'IsoCor: correcting MS data in isotope labeling experiments', *Bioinformatics*, 28(9), 1294-6.

Mills, G. B. and Moolenaar, W. H. (2003) 'The emerging role of lysophosphatidic acid in cancer', *Nature Reviews Cancer*, 3(8), 582-591.

Mitchem, J. B., Brennan, D. J., Knolhoff, B. L., Belt, B. A., Zhu, Y., Sanford, D. E., Belaygorod, L., Carpenter, D., Collins, L., Piwnica-Worms, D., Hewitt, S., Udupi, G. M., Gallagher, W. M., Wegner, C., West, B. L., Wang-Gillam, A., Goedegebuure, P., Linehan, D. C. and DeNardo, D. G. (2013) 'Targeting Tumor-Infiltrating Macrophages Decreases Tumor-Initiating Cells, Relieves Immunosuppression, and Improves Chemotherapeutic Responses', *Cancer Research*, 73(3), 1128-1141.

Morton, J. P., Timpson, P., Karim, S. A., Ridgway, R. A., Athineos, D., Doyle, B., Jamieson, N. B., Oien, K. A., Lowy, A. M., Brunton, V. G., Frame, M. C., Evans, T. R. J. and Sansom, O. J. (2010) 'Mutant p53 drives metastasis and overcomes growth arrest/senescence in pancreatic cancer', *Proceedings of the National Academy of Sciences of the United States of America*, 107(1), 246-251.

Nelson, K. M. and Gallagher, P. C. (2014) 'Biosimilars lining up to compete with Herceptin - opportunity knocks', *Expert Opinion on Therapeutic Patents*, 24(11), 1149-1153.

Neschen, S., Morino, K., Hammond, L. E., Zhang, D. Y., Liu, Z. X., Romanelli, A. J., Cline, G. W., Pongratz, R. L., Zhang, X. M., Choi, C. S., Coleman, R. A. and Shulman, G. I. (2005) 'Prevention of hepatic steatosis and hepatic insulin resistance in mitochondrial acyl-CoA : glycerol-sn-3-phosphate acyltransferase 1 knockout mice', *Cell Metabolism*, 2(1), 55-65.

Nicholson, J. K., Lindon, J. C. and Holmes, E. (1999) "Metabonomics': understanding the metabolic responses of living systems to pathophysiological stimuli via multivariate statistical analysis of biological NMR spectroscopic data', *Xenobiotica*, 29(11), 1181 - 1189.

Nishizuka, Y. (1992) 'INTRACELLULAR SIGNALING BY HYDROLYSIS OF PHOSPHOLIPIDS AND ACTIVATION OF PROTEIN-KINASE-C', *Science*, 258(5082), 607-614.

Olefsky, J. M. and Glass, C. K. (2010) 'Macrophages, Inflammation, and Insulin Resistance', *Annual Review of Physiology*, 72, 219-246.

Oliver, S. G., Winson, M. K., Kell, D. B. and Baganz, F. (1998) 'Systematic functional analysis of the yeast genome', *Trends in Biotechnology*, 16(9), 373-378.

Pang, B., Cheng, S., Sun, S.-P., An, C., Liu, Z.-Y., Feng, X. and Liu, G.-J. (2014) 'Prognostic role of PIK3CA mutations and their association with hormone receptor expression in breast cancer: a meta-analysis', *Scientific Reports*, 4.

Panni, R. Z., Linehan, D. C. and DeNardo, D. G. (2013) 'Targeting tumor-infiltrating macrophages to combat cancer', *Immunotherapy*, 5(10), 1075-1087.

Papatriantafyllou, M. (2012) 'Macrophages: Lipid metabolism linked to anti-inflammatory functions', *Nature reviews. Immunology*, 12(11), 747-747.

Patel, S. and Player, M. R. (2009) 'Colony-Stimulating Factor-1 Receptor Inhibitors for the Treatment of Cancer and Inflammatory Disease', *Current Topics in Medicinal Chemistry*, 9(7), 599-610.

Pizer, E. S., Jackisch, C., Wood, F. D., Pasternack, G. R., Davidson, N. E. and Kuhajda, F. P. (1996) 'Inhibition of fatty acid synthesis induces programmed cell death in human breast cancer cells', *Cancer Research*, 56(12), 2745-2747.

Polanski, R., Hodgkinson, C. L., Fusi, A., Nonaka, D., Priest, L., Kelly, P., Trapani, F., Bishop, P. W., White, A., Critchlow, S. E., Smith, P. D., Blackhall, F., Dive, C. and Morrow, C. J. (2014) 'Activity of the Monocarboxylate Transporter 1 Inhibitor AZD3965 in Small Cell Lung Cancer', *Clinical Cancer Research*, 20(4), 926-937.

Porstmann, T., Santos, C. R., Griffiths, B., Cully, M., Wu, M., Leevers, S., Griffiths, J. R., Chung, Y. L. and Schulze, A. (2008) 'SREBP activity is regulated by mTORC1 and contributes to Akt-dependent cell growth', *Cell Metabolism*, 8(3), 224-236.

Price, A. L., Patterson, N. J., Plenge, R. M., Weinblatt, M. E., Shadick, N. A. and Reich, D. (2006) 'Principal components analysis corrects for stratification in genome-wide association studies', *Nature Genetics*, 38(8), 904-909.

Priceman, S. J., Sung, J. L., Shaposhnik, Z., Burton, J. B., Torres-Collado, A. X., Moughon, D. L., Johnson, M., Lusis, A. J., Cohen, D. A., Iruela-Arispe, M. L. and Wu, L. (2010) 'Targeting distinct tumor-infiltrating myeloid cells by inhibiting CSF-1 receptor: combating tumor evasion of antiangiogenic therapy', *Blood*, 115(7), 1461-1471.

Pyonteck, S. M., Akkari, L., Schuhmacher, A. J., Bowman, R. L., Sevenich, L., Quail, D. F., Olson, O. C., Quick, M. L., Huse, J. T., Teijeiro, V., Setty, M., Leslie, C. S., Oei, Y., Pedraza, A., Zhang, J., Brennan, C. W., Sutton, J. C., Holland, E. C., Daniel, D. and Joyce, J. A. (2013) 'CSF-1R inhibition alters macrophage polarization and blocks glioma progression', *Nature Medicine*, 19(10), 1264-+.

Raina, K., Ravichandran, K., Rajamanickam, S., Huber, K. M., Serkova, N. J. and Agarwal, R. (2013) 'Inositol Hexaphosphate Inhibits Tumor Growth, Vascularity, and Metabolism in TRAMP Mice: A Multiparametric Magnetic Resonance Study', *Cancer Prevention Research*, 6(1), 40-50.

Raina, K., Serkova, N. J. and Agarwal, R. (2009) 'Silibinin Feeding Alters the Metabolic Profile in TRAMP Prostatic Tumors: H-1-NMRS-Based Metabolomics Study', *Cancer Research*, 69(9), 3731-3735.

Rao, M. and Sockanathan, S. (2005) 'Transmembrane protein GDE2 induces motor neuron differentiation in vivo', *Science*, 309(5744), 2212-2215.

Ridgway, N. D. (2013) 'The role of phosphatidylcholine and choline metabolites to cell proliferation and survival', *Crit Rev Biochem Mol Biol*, 48(1), 20-38.

Robertson, D. G. (2005) 'Metabonomics in toxicology: A review', *Toxicological Sciences*, 85(2), 809-822.

Rocha, C. M., Barros, A. S., Gil, A. M., Goodfellow, B. J., Humpfer, E., Spraul, M., Carreira, I. M., Melo, J. B., Bernardo, J., Gomes, A., Sousa, V., Carvalho, L. and Duarte, I. F. (2010) 'Metabolic Profiling of Human Lung Cancer Tissue by H-1 High Resolution Magic Angle Spinning (HRMAS) NMR Spectroscopy', *Journal of Proteome Research*, 9(1), 319-332.

Romanska, H. M., Tiziani, S., Howe, R. C., Gunther, U. L., Guizar, Z. and Lalani, E. N. (2009) 'Nuclear Magnetic Resonance Detects Phosphoinositide 3-Kinase/Akt-Independent Traits Common to Pluripotent Murine Embryonic Stem Cells and Their Malignant Counterparts', *Neoplasia*, 11(12), 1301-1308.

Ronen, S. M., Jackson, L. E., Beloueche, M. and Leach, M. O. (2001) 'Magnetic resonance detects changes in phosphocholine associated with Ras activation and inhibition in NIH 3T3 cells', *British Journal of Cancer*, 84(5), 691-696.

Rozenblum, E., Schutte, M., Goggins, M., Hahn, S. A., Panzer, S., Zahurak, M., Goodman, S. N., Sohn, T. A., Hruban, R. H., Yeo, C. J. and Kern, S. E. (1997) 'Tumor-suppressive pathways in pancreatic carcinoma', *Cancer Research*, 57(9), 1731-1734.

Sancak, Y., Peterson, T. R., Shaul, Y. D., Lindquist, R. A., Thoreen, C. C., Bar-Peled, L. and Sabatini, D. M. (2008) 'The Rag GTPases bind raptor and mediate amino acid signaling to mTORC1', *Science*, 320(5882), 1496-1501.

Sarrio, D., Rodriguez-Pinilla, S. M., Hardisson, D., Cano, A., Moreno-Bueno, G. and Palacios, J. (2008) 'Epithelial-mesenchymal transition in breast cancer relates to the basal-like phenotype', *Cancer Research*, 68(4), 989-997.

Sathish, J. G., Sethu, S., Bielsky, M.-C., de Haan, L., French, N. S., Govindappa, K., Green, J., Griffiths, C. E. M., Holgate, S., Jones, D., Kimber, I., Moggs, J., Naisbitt, D. J., Pirmohamed, M., Reichmann, G., Sims, J., Subramanyam, M., Todd, M. D.,

Van der Laan, J. W., Weaver, R. J. and Park, B. K. (2013) 'Challenges and approaches for the development of safer immunomodulatory biologics', *Nature Reviews Drug Discovery*, 12(4), 306-324.

Sawyers, C. L. (2008) 'The cancer biomarker problem', *Nature*, 452(7187), 548-552.

Schafer, Z. T., Grassian, A. R., Song, L., Jiang, Z., Gerhart-Hines, Z., Irie, H. Y., Gao, S., Puigserver, P. and Brugge, J. S. (2009) 'Antioxidant and oncogene rescue of metabolic defects caused by loss of matrix attachment', *Nature*, 461(7260), 109-U118.

Scott, D. A., Dakin, L. A., Daly, K., Del Valle, D. J., Diebold, R. B., Drew, L., Ezhuthachan, J., Gero, T. W., Ogoe, C. A., Omer, C. A., Redmond, S. P., Repik, G., Thakur, K., Ye, Q. and Zheng, X. (2013) 'Mitigation of cardiovascular toxicity in a series of CSF-1R inhibitors, and the identification of AZD7507', *Bioorganic & Medicinal Chemistry Letters*, 23(16), 4591-4596.

Shiratori, Y., Okwu, A. K. and Tabas, I. (1994) 'FREE-CHOLESTEROL LOADING OF MACROPHAGES STIMULATES PHOSPHATIDYLCHOLINE BIOSYNTHESIS AND UP-REGULATION OF CTP - PHOSPHOCHOLINE CYTIDYLYLTRANSFERASE', *Journal of Biological Chemistry*, 269(15), 11337-11348.

Son, J., Lyssiotis, C. A., Ying, H., Wang, X., Hua, S., Ligorio, M., Perera, R. M., Ferrone, C. R., Mullarky, E., Ng, S.-C., Kang, Y. a., Fleming, J. B., Bardeesy, N., Asara, J. M., Haigis, M. C., DePinho, R. A., Cantley, L. C. and Kimmelman, A. C. (2013) 'Glutamine supports pancreatic cancer growth through a KRAS-regulated metabolic pathway', *Nature*, 496(7443), 101-+.

Spann, N. J., Garmire, L. X., McDonald, J. G., Myers, D. S., Milne, S. B., Shibata, N., Reichart, D., Fox, J. N., Shaked, I., Heudobler, D., Raetz, C. R. H., Wang, E. W., Kelly, S. L., Sullards, M. C., Murphy, R. C., Merrill, A. H., Jr., Brown, H. A., Dennis, E. A., Li, A. C., Ley, K., Tsimikas, S., Fahy, E., Subramaniam, S., Quehenberger, O., Russell, D. W. and Glass, C. K. (2012) 'Regulated Accumulation of Desmosterol Integrates Macrophage Lipid Metabolism and Inflammatory Responses', *Cell*, 151(1), 138-152.

Spratlin, J. L., Serkova, N. J. and Eckhardt, S. G. (2009) 'Clinical Applications of Metabolomics in Oncology: A Review', *Clinical Cancer Research*, 15(2), 431-440.

Stanwell, P., Gluch, L., Clark, D., Tomanek, B., Baker, L., Giuffre, B., Lean, C., Malycha, P. and Mountford, C. (2005) 'Specificity of choline metabolites for in vivo diagnosis of breast cancer using H-1 MRS at 1.5 T', *European Radiology*, 15(5), 1037-1043.

Stein, S. E. (1999) 'An integrated method for spectrum extraction and compound identification from gas chromatography/mass spectrometry data', *Journal of the American Society for Mass Spectrometry*, 10(8), 770-781.

Stewart, J. D., Marchan, R., Lesjak, M. S., Lambert, J., Hergenroeder, R., Ellis, J. K., Lau, C.-H., Keun, H. C., Schmitz, G., Schiller, J., Eibisch, M., Hedberg, C., Waldmann, H., Lausch, E., Tanner, B., Sehouli, J., Sagemueller, J., Staude, H., Steiner, E. and Hengstler, J. G. (2012) 'Choline-releasing glycerophosphodiesterase EDI3 drives tumor cell migration and metastasis', *Proceedings of the National Academy of Sciences of the United States of America*, 109(21), 8155-8160.

Strelko, C. L., Lu, W., Dufort, F. J., Seyfried, T. N., Chiles, T. C., Rabinowitz, J. D. and Roberts, M. F. (2011) 'Itaconic Acid Is a Mammalian Metabolite Induced during Macrophage Activation', *Journal of the American Chemical Society*, 133(41), 16386-16389.

Sun, G., Wang, J., Zhang, J., Ma, C., Shao, C., Hao, J., Zheng, J., Feng, X. and Zuo, C. (2014) 'High-resolution magic angle spinning H-1 magnetic resonance spectroscopy detects choline as a biomarker in a swine obstructive chronic pancreatitis model at an early stage', *Molecular Biosystems*, 10(3), 467-474.

Swanson, M. G., Keshari, K. R., Tabatabai, Z. L., Simko, J. P., Shinohara, K., Carroll, P. R., Zektzer, A. S. and Kurhanewicz, J. (2008) 'Quantification of choline- and ethanolamine-containing metabolites in human prostate tissues using 1H HR-MAS total correlation spectroscopy', *Magnetic Resonance in Medicine*, 60(1), 33-40.

Tabas, I. (2000) 'Cholesterol and phospholipid metabolism in macrophages', *Biochimica Et Biophysica Acta-Molecular and Cell Biology of Lipids*, 1529(1-3), 164-174.

Tamura, K., Makino, A., Hullin-Matsuda, F., Kobayashi, T., Furihata, M., Chung, S., Ashida, S., Miki, T., Fujioka, T., Shuin, T., Nakamura, Y. and Nakagawa, H. (2009) 'Novel Lipogenic Enzyme ELOVL7 Is Involved in Prostate Cancer Growth through Saturated Long-Chain Fatty Acid Metabolism', *Cancer Research*, 69(20), 8133-8140.

Teichert, F., Verschoyle, R. D., Greaves, P., Edwards, R. E., Teahan, O., Jones, D. J. L., Wilson, I. D., Farmer, P. B., Steward, W. P., Gant, T. W., Gescher, A. J. and Keun, H. C. (2008) 'Metabolic profiling of Transgenic Adenocarcinoma of Mouse Prostate (TRAMP) tissue by H-1-NMR analysis: Evidence for unusual phospholipid metabolism', *Prostate*, 68(10), 1035-1047.

Tesiram, Y. A., Lerner, M., Stewart, C., Njoku, C. and Brackett, D. J. (2012) 'Utility of Nuclear Magnetic Resonance Spectroscopy for Pancreatic Cancer Studies', *Pancreas*, 41(3), 474-480.

Tessner, T. G., Rock, C. O., Kalmar, G. B., Cornell, R. B. and Jackowski, S. (1991) 'COLONY-STIMULATING FACTOR-I REGULATES CTP-PHOSPHOCHOLINE CYTIDYLYLTRANSFERASE MESSENGER-RNA LEVELS', *Journal of Biological Chemistry*, 266(25), 16261-16264.

Thompson, A. L. and Cooney, G. J. (2000) 'Acyl-CoA inhibition of hexokinase in rat and human skeletal muscle is a potential mechanism of lipid-induced insulin resistance', *Diabetes*, 49(11), 1761-1765.

Tippett, P. S. and Neet, K. E. (1982) 'SPECIFIC-INHIBITION OF GLUCOKINASE BY LONG-CHAIN ACYL CO-ENZYMES-A BELOW THE CRITICAL MICELLE CONCENTRATION', *Journal of Biological Chemistry*, 257(21), 2839-2845.

Tobias, J. S. H., Daniel Souhami, Robert L (2010) *Cancer and its management*, 6th ed., Chichester : Wiley-Blackwell

Topanurak, S., Ferraris, J. D., Li, J., Izumi, Y., Williams, C. K., Gucek, M., Wang, G., Zhou, X. and Burg, M. B. (2013) 'High NaCl- and urea-induced posttranslational modifications that increase glycerophosphocholine by inhibiting GDPD5 phosphodiesterase', *Proceedings of the National Academy of Sciences of the United States of America*, 110(18), 7482-7487.

Turyn, J., Schlichtholz, B., Dettlaff-Pokora, A., Presler, M., Goyke, E., Matuszewski, M., Kmiec, Z., Krajka, K. and Swierczynski, J. (2003) 'Increased activity of glycerol 3-phosphate dehydrogenase and other lipogenic enzymes in human bladder cancer', *Hormone and Metabolic Research*, 35(10), 565-569.

Tönjes, M., Barbus, S., Park, Y. J., Wang, W., Schlotter, M., Lindroth, A. M., Pleier, S. V., Bai, A. H., Karra, D., Piro, R. M., Felsberg, J., Addington, A., Lemke, D., Weibrecht, I., Hovestadt, V., Rolli, C. G., Campos, B., Turcan, S., Sturm, D., Witt, H., Chan, T. A., Herold-Mende, C., Kemkemer, R., König, R., Schmidt, K., Hull, W. E., Pfister, S. M., Jugold, M., Hutson, S. M., Plass, C., Okun, J. G., Reifenberger, G., Lichter, P. and Radlwimmer, B. (2013) 'BCAT1 promotes cell proliferation through amino acid catabolism in gliomas carrying wild-type IDH1', *Nat Med*.

Van Corven, E. J., Groenink, A., Jalink, K., Eichholtz, T. and Moolenaar, W. H. (1989) 'LYSOPHOSPHATIDATE-INDUCED CELL PROLIFERATION IDENTIFICATION AND DISSECTION OF SIGNALING PATHWAYS MEDIATED BY G PROTEINS', *Cell*, 59(1), 45-54.

Vivanco, I. and Sawyers, C. L. (2002) 'The phosphatidylinositol 3-kinase-AKT pathway in human cancer', *Nature Reviews Cancer*, 2(7), 489-501.

von Forstner, C., Egberts, J.-H., Ammerpohl, O., Niedzielska, D., Buchert, R., Mikecz, P., Schumacher, U., Peldschus, K., Adam, G., Pilarsky, C., Grutzmann, R., Kalthoff, H., Henze, E. and Brenner, W. (2008) 'Gene expression patterns and tumor uptake of F-18-FDG, F-18-FLT, and F-18-FEC in PET/MRI of an orthotopic mouse xenotransplantation model of pancreatic cancer', *Journal of Nuclear Medicine*, 49(8), 1362-1370.

Warburg, O. (1956) 'On the Origin of Cancer Cells', *Science*, 123(3191), 309-314.

Ward, J. L., Baker, J. M. and Beale, M. H. (2007) 'Recent applications of NMR spectroscopy in plant metabolomics', *Febs J*, 274(5), 1126 - 1131.

Ward, P. S. and Thompson, C. B. (2012) 'Metabolic Reprogramming: A Cancer Hallmark Even Warburg Did Not Anticipate', *Cancer Cell*, 21(3), 297-308.

Wendel, A. A., Lewin, T. M. and Coleman, R. A. (2009) 'Glycerol-3-phosphate acyltransferases: Rate limiting enzymes of triacylglycerol biosynthesis', *Biochimica Et Biophysica Acta-Molecular and Cell Biology of Lipids*, 1791(6), 501-506.

Wider, G. and Dreier, L. (2006) 'Measuring protein concentrations by NMR spectroscopy', *Journal of the American Chemical Society*, 128(8), 2571-2576.

Wijnen, J. P., Jiang, L., Greenwood, T. R., Cheng, M., Doepkens, M., Cao, M. D., Bhujwalla, Z. M., Krishnamachary, B., Klomp, D. W. J. and Glunde, K. (2014) 'Silencing of the glycerophosphocholine phosphodiesterase GDPD5 alters the phospholipid metabolite profile in a breast cancer model in vivo as monitored by 31P MRS', *Nmr in Biomedicine*, 27(6), 692-699.

Wise, D. R., DeBerardinis, R. J., Mancuso, A., Sayed, N., Zhang, X. Y., Pfeiffer, H. K., Nissim, I., Daikhin, E., Yudkoff, M., McMahon, S. B. and Thompson, C. B. (2008) 'Myc regulates a transcriptional program that stimulates mitochondrial glutaminolysis and leads to glutamine addiction', *Proceedings of the National Academy of Sciences of the United States of America*, 105(48), 18782-18787.

Wold, S., Esbensen, K. and Geladi, P. (1987) 'PRINCIPAL COMPONENT ANALYSIS', *Chemometrics and Intelligent Laboratory Systems*, 2(1-3), 37-52.

Workman, P., Clarke, P. A., Raynaud, F. I. and van Montfort, R. L. M. (2010) 'Drugging the PI3 Kinome: From Chemical Tools to Drugs in the Clinic', *Cancer Research*, 70(6).

Wu, G. J., Xing, M. Z., Mambo, E., Huang, X., Liu, J. W., Guo, Z. M., Chatterjee, A., Goldenberg, D., Gollin, S. M., Sukumar, S., Trink, B. and Sidransky, D. (2005) 'Somatic mutation and gain of copy number of PIK3CA in human breast cancer', *Breast Cancer Research*, 7(5), R609-R616.

Wu, H., Ding, Z., Hu, D., Sun, F., Dai, C., Xie, J. and Hu, X. (2012) 'Central role of lactic acidosis in cancer cell resistance to glucose deprivation-induced cell death', *Journal of Pathology*, 227(2), 189-199.

Xu, J., Escamilla, J., Mok, S., David, J., Priceman, S., West, B., Bollag, G., McBride, W. and Wu, L. (2013) 'CSF1R Signaling Blockade Stanches Tumor-Infiltrating Myeloid Cells and Improves the Efficacy of Radiotherapy in Prostate Cancer', *Cancer Research*, 73(9), 2782-2794.

Yabushita, S., Fukamachi, K., Tanaka, H., Fukuda, T., Sumida, K., Deguchi, Y., Mikata, K., Nishioka, K., Kawamura, S., Uwagawa, S., Suzui, M., Alexander, D. B. and Tsuda, H. (2013) 'Metabolomic and transcriptomic profiling of human K-ras oncogene transgenic rats with pancreatic ductal adenocarcinomas', *Carcinogenesis*, 34(6), 1251-1259.

Yalcin, A., Clem, B., Makoni, S., Clem, A., Nelson, K., Thornburg, J., Siow, D., Lane, A. N., Brock, S. E., Goswami, U., Eaton, J. W., Telang, S. and Chesney, J. (2010) 'Selective inhibition of choline kinase simultaneously attenuates MAPK and PI3K/AKT signaling', *Oncogene*, 29(1), 139-149.

Yanaka, N. (2007) 'Mammalian glycerophosphodiester phosphodiesterases', *Bioscience Biotechnology and Biochemistry*, 71(8), 1811-1818.

Yang, M., Soga, T. and Pollard, P. J. (2013) 'Oncometabolites: linking altered metabolism with cancer', *Journal of Clinical Investigation*, 123(9), 3652-3658.

Ying, H., Kimmelman, A. C., Lyssiotis, C. A., Hua, S., Chu, G. C., Fletcher-Sananikone, E., Locasale, J. W., Son, J., Zhang, H., Coloff, J. L., Yan, H., Wang, W., Chen, S., Viale, A., Zheng, H., Paik, J.-h., Lim, C., Guimaraes, A. R., Martin, E. S., Chang, J., Hezel, A. F., Perry, S. R., Hu, J., Gan, B., Xiao, Y., Asara, J. M., Weissleder, R., Wang, Y. A., Chin, L., Cantley, L. C. and DePinho, R. A. (2012) 'Oncogenic Kras Maintains Pancreatic Tumors through Regulation of Anabolic Glucose Metabolism', *Cell*, 149(3).

Yun, J., Rago, C., Cheong, I., Pagliarini, R., Angenendt, P., Rajagopalan, H., Schmidt, K., Willson, J. K. V., Markowitz, S., Zhou, S., Diaz, L. A., Jr., Velculescu, V. E., Lengauer, C., Kinzler, K. W., Vogelstein, B. and Papadopoulos, N. (2009) 'Glucose Deprivation Contributes to the Development of KRAS Pathway Mutations in Tumor Cells', *Science*, 325(5947), 1555-1559.

Zablocki, K., Miller, S. P. F., Garciaperez, A. and Burg, M. B. (1991) 'ACCUMULATION OF GLYCEROPHOSPHOCHOLINE (GPC) BY RENAL-CELLS - OSMOTIC REGULATION OF GPC - CHOLINE PHOSPHODIESTERASE', *Proceedings of the National Academy of Sciences of the United States of America*, 88(17), 7820-7824.

Zeisel, S. H. and da Costa, K.-A. (2009) 'Choline: an essential nutrient for public health', *Nutrition Reviews*, 67(11), 615-623.

Zeisel, S. H., Dacosta, K. A., Franklin, P. D., Alexander, E. A., Lamont, J. T., Sheard, N. F. and Beiser, A. (1991) 'CHOLINE, AN ESSENTIAL NUTRIENT FOR HUMANS', *Faseb Journal*, 5(7), 2093-2098.

Zhang, A., Sun, H., Wang, P., Han, Y. and Wang, X. (2012) 'Modern analytical techniques in metabolomics analysis', *Analyst*, 137(2), 293-300.

Zhang, G., He, P., Tan, H., Budhu, A., Gaedcke, J., Ghadimi, B. M., Ried, T., Yfantis, H. G., Lee, D. H., Maitra, A., Hanna, N., Alexander, H. R. and Hussain, S. P. (2013) 'Integration of Metabolomics and Transcriptomics Revealed a Fatty Acid Network Exerting Growth Inhibitory Effects in Human Pancreatic Cancer', *Clinical Cancer Research*, 19(18), 4983-4993.

Zheng, B., Chen, D. and Farquhar, M. G. (2000) 'MIR16, a putative membrane glycerophosphodiester phosphodiesterase, interacts with RGS16', *Proceedings of the National Academy of Sciences of the United States of America*, 97(8), 3999-4004.

Zheng, W., Tayyari, F., Gowda, G. A., Raftery, D., McLamore, E. S., Porterfield, D. M., Donkin, S. S., Bequette, B. and Teegarden, D. (2013) 'Altered glucose metabolism in Harvey-ras transformed MCF10A cells', *Mol Carcinog*.

Zhu, A., Lee, D. and Shim, H. (2011) 'Metabolic Positron Emission Tomography Imaging in Cancer Detection and Therapy Response', *Seminars in Oncology*, 38(1), 55-69.

Zhu, Y., Knolhoff, B. L., Meyer, M. A., Nywening, T. M., West, B. L., Luo, J., Wang-Gillam, A., Goedegebuure, S. P., Linehan, D. C. and DeNardo, D. G. (2014) 'CSF1/CSF1R Blockade Reprograms Tumor-Infiltrating Macrophages and Improves Response to T-cell Checkpoint Immunotherapy in Pancreatic Cancer Models', *Cancer research*, 74(18), 5057-69.

Zoncu, R., Efeyan, A. and Sabatini, D. M. (2011) 'mTOR: from growth signal integration to cancer, diabetes and ageing', *Nature Reviews Molecular Cell Biology*, 12(1), 21-35.